Identification of Epigenetic Factors that will Overcome Therapy Resistance in Triple-Negative Breast Cancer

by

Özlem YEDİER BAYRAM

A Dissertation Submitted to the
Graduate School of Sciences and Engineering
in Partial Fulfillment of the Requirements for
the Degree of

Doctor of Philosophy

in

Molecular Biology and Genetics

KOÇ ÜNİVERSİTESİ

Eylül 8, 2022

Identification of Epigenetic Factors that will Overcome Therapy Resistance in Triple-Negative Breast Cancer

Koç University

Graduate School of Sciences and Engineering

This is to certify that I have examined this copy of a doctoral dissertation by

Özlem YEDİER BAYRAM

and have found that it is complete and satisfactory in all respects,
and that any and all revisions required by the final
examining committee have been made.

Committee Members:

Prof. Tuğba BAĞCI ÖNDER (Advisor)

Prof. Tamer ÖNDER

Assoc. Prof. Şerif ŞENTÜRK

Assoc. Prof. Nathan A. LACK

Assoc. Prof. Adam CRIBBS

Date: 08.09.2022

I dedicate my thesis

to Mert, my lovely little boy
to Sefa, my best friend and husband

to Meltem and Cem, my parents and tireless supporters
and to Gülfem, my sister and sunshine.

ABSTRACT

Identification of Epigenetic Factors that will Overcome Therapy Resistance in Triple-Negative Breast Cancer

Özlem YEDİER BAYRAM

Doctor of Philosophy in Molecular Biology and Genetics

September 8, 2022

Triple Negative Breast Cancer (TNBC) is the most aggressive and recurrent type of breast cancer with a poor prognosis. Due to the lack of expression of hormone receptors (HR) and Her2, TNBC cannot be treated with targeted therapies, leaving chemotherapy as the mainstay treatment. However, acquired resistance to chemotherapy is a major challenge that, in part, causes relapse, which is thought to be driven by coordinated actions of genetic and epigenetic events. In this study, we aimed to elucidate the roles of the full spectrum of epigenetic modifiers in both naïve and chemotherapy resistant TNBC cell lines. For this, we generated an epigenome-wide CRISPR knockout library (EPIKOL) targeting all writers, readers and erasers, as well as the chromatin remodelers and structural subunits of epigenetic complexes. First, we discovered novel epigenetic modifiers that regulate TNBC cell fitness and confirmed the effects of NSL complex members (KANSL2, KANSL3, and KAT8) and SS18L2 on cell growth. Notably, *in vivo* screen with EPIKOL on MDA-MB-231 cell line also revealed SS18L2 as a fitness gene in two different time points of tumor growth.

To generate in vitro models of chemoresistant TNBC, we exposed three different TNBC cell lines to escalating doses of an anthracycline (doxorubicin) or a taxane (paclitaxel, taxol). SUM159PT taxol resistant cells had elevated levels of ABCB1 and showed the characteristics of multidrug resistance. EPIKOL screen and a complementary epigenetic probe library screen in one of the taxol resistant SUM159PT cells in the presence of taxol identified BRPF1, a bromodomain-containing reader, as a taxol sensitizer. Upon BRPF1 inhibition or loss, transcriptome analysis revealed a significant downregulation of ribosome biogenesis pathways and a decrease in ABCB1 expression. Additionally, we demonstrated the binding of BRPF1 to the ABCB1 promoter, possibly regulating its expression in drug resistant state. Collectively, these findings provide a basis for developing combination therapies targeting specific chromatin-based epigenetic factors to counteract TNBC cell viability and chemoresistant phenotype.

ÖZETÇE

Üçlü Negatif Meme Kanserinde Tedavi Direncini Kırabilecek Epigenetik Faktörlerin Belirlenmesi

Özlem YEDİER BAYRAM
Moleküler Biyoloji ve Genetik, Doktora
8 Eylül 2022

Üçlü Negatif Meme Kanseri (TNBC), meme kanseri alt türleri arasındaki en agresif, metastatik ve kötü prognozlu meme kanseri türüdür. Hormon reseptörleri (HR) ve Her2 ifadesinin olmaması nedeniyle, TNBC'de hedefe yönelik tedaviler uygulanamamakta ve kemoterapi ana ve tek tedavi yöntemi olarak devam etmektedir. Bununla birlikte, hastaların büyük bir çoğunluğu kemoterapiye karşı direnç kazanmakta ve tedaviye dirençli tümörler nüksetmektedir. Kemoterapi direnci, genellikle genetik ve epigenetik olayların bir bütün olarak çalışmasıyla oluşmaktadır. Bu çalışmada, epigenetik faktörlerin rollerinin hem kemoterapiye duyarlı hem de dirençli TNBC hücre hatlarında aydınlatılması amaçlanmıştır. Bunun için tüm epigenetik yazıcıları, okuyucuları, silicileri, kromatin yeniden şekillendiricilerini ve epigenetik komplekslerin yapısal alt birimlerini hedefleyen epigenom çapında bir CRISPR knockout kütüphanesi (EPIKOL) oluşturulmuştur. Öncelikle, tedaviye duyarlı TNBC hücre dizilerinde yapılan taramalar sonucunda, NSL kompleks üyelerinin (KANSL2, KANSL3 ve KAT8) ve SS18L2'nin TNBC hücre büyümesi üzerinde etkili olduğunu bulunmuştur. Ayrıca, MDA-MB-231 hücre hattında EPIKOL ile yapılan in vivo taramada da, SS18L2, tümör büyümesini düzenleyen bir epigenetic faktör olarak belirlenmiştir.

Bu tez kapsamında, kemoterapi direncini *in vitro* ortamda modellemek amacıyla, 3 farklı TNBC hücre hattını bir antrasiklin (doxorubicin) veya bir taksanın (paclitaxel, taxol) artan dozlarına maruz bırakılarak kemoterapi dirençli hücreler geliştirilmiştir. SUM159PT taxol'e dirençli hücrelerde ABCB1 ifade seviyelerinin arttığı ve çoklu ilaç direnci fenotipi gösterdikleri belirlenmiştir. Taxol'e dirençli SUM159PT hücrelerinden birinde yapılan EPIKOL ve epigenetik probe kütüphanesi taramaları sonucunda bromodomain'e sahip bir okuyucu olan BRPF1'in taxol direncini kırdığı tespit edilmiştir. BRPF1'in ilaçlarla inhibisyonu veya CRISPR yöntemiyle susturulması üzerine yapılan transkriptom analizi, BRPF1 aktivite kaybının ribozom biyogenezi için gerekli genlerde ve ABCB1 ifadesinde önemli bir azalmaya sebep olduğunu ortaya çıkarmıştır. Ek olarak, ChIP deneyi sonucunda, BRPF1'in ABCB1 promotörüne bağlandığı ve bu sayede ABCB1 ifadesini arttırarak ilaç direncini koruyor olabileceği tespit edilmiştir. Sonuç olarak bu bulgular, TNBC hücre canlılığını ve kemoterapi direncini kıracak epigenetik tabanlı kombinasyon tedavilerinin geliştirilmesine katkıda bulunmaktadır.

ACKNOWLEDGMENTS

I would like to express my gratitude to my supervisor Prof. Tuğba Bağcı-Önder. She was always kind and supportive, even at the most challenging times. Besides my journey with my experiments, she supported me to take part in grant writing and manuscript writing processes which, I believe, are fundamental skills to learn if one wants to pursue an academic career. I am also thankful to her for giving me a chance to be a visiting PhD student in Prof. Weinberg's laboratory, the place that changed my perspective on science. I also thank Weinberg Lab members for their warm welcomes and remarkable memories, especially Yun Zhang for giving me the opportunity to be involved in his wonderful project.

I am sincerely grateful to Prof. Tamer Önder for his guidance in my experiments. His way of scientific thinking, critics, and curiosity shaped me as a scientist. I will take every step in my scientific career by asking myself, 'How would he think?' and 'What would he do?'. I believe the answers will guide me to where I need to be.

I would like to thank my thesis committee member Assoc. Prof. Şerif Şentürk for the fruitful discussions in our meetings. I also would like to thank my thesis defense committee members Assoc. Prof. Nathan Lack and Assoc. Prof. Adam CRIBBS. I also feel honored to collaborate with them on two different projects.

I would like to thank The Scientific and Technological Research Council of Turkey (TÜBİTAK) for the scholarship of Tübitak1003 project (216S461), Koç University Research Center for Translational Medicine (KUTTAM), Graduate School of Health Sciences and Graduate School of Science and Engineering for their financial support during my PhD studies.

As a past member of TBO Lab, Dr. Filiz Şenbabaoğlu was always there for me starting from the first day. She helped me to find my way during my PhD even from the miles apart. I feel lucky to know her. Dr. Ahmet Cingöz was an essential part of my PhD journey, with animal experiments and his valuable friendship.

Ezgi Yağmur Kala and Göktuğ Karabıyık were the fun duo to have around and laugh at the struggles of EPIKOL and PhD together. I have always known that they are

there and ready to help with anything I need, both scientifically and personally. Dr. Ali Cenk Aksu made a huge contribution to my thesis by making the hardest parts easy along the way. I am grateful for his scientific enthusiasm and his friendship.

Beril Esin joined the 'Breast Team' lately; however, her enthusiasm and friendship made it feel like she had been here with me for many years. Watching her grow as a scientist is one of the best feelings. I am also grateful to all members of TBO Lab family, Dr. Alişan Kayabölen, Nareg Pınarbaşı Değirmenci, Ebru Yılmaz, Canan Bayraktar, Beyza Nur Köseoğlu, Mina Küçüktaş and Gizem Doğan Yılmaz, members of TO Lab and Lack Lab, especially Bengül, for their friendship and creating a warm environment to work in the lab.

I cannot thank enough my parents, Meltem and Cem, for their endless love and support, for being a role model to me with their hard work, and for always believing in me. My sister, Gülfem, is the most cheerful person in my life who brings joy whenever I need. They, especially my mom, have sacrificed a lot in the last year of my PhD to make my days easier with a baby boy growing in my belly. This thesis would not have been written without the tremendous help I got from my mother and family.

Lastly, one of my biggest thanks is to my husband, Sefa. He was always supportive and caring. He is a big fan of my research as he rejoiced at all my achievements as if they were his own. I really could not have done any of this without him. He even followed me overseas, being the perfect companion and making my time in Boston memorable. He continues to amaze me as a fresh dad. My lovely little boy, Mert, was my perfect lab mate for nine months and felt every feeling with me during this time. He was the one keeping me sane in the last year of my PhD and during the thesis writing period. I owe him big time.

TABLE OF CONTENTS

LIST OF TABLES

LIST OF FIGURES

ABBREVIATIONS

ABC	ATP Binding Cassette
AR	Androgen Receptor
BC	Breast Cancer
BET	Bromodomain and Extra-Terminal Domain
BRD	Bromodomain
BRPF1	Bromodomain and PHD finger containing Protein 1
ChIP	Chromatin Immunoprecipitation
CSC	Cancer Stem Cell
cPARP	cleaved PARP
CpG	Cystosine-guanine Dinucleotides
CTLA-4	Cytotoxic T Lymphocyte Antigen-4
CRISPR	Clustered Regularly Interspaced Palindromic Repeats
DNMT	DNA methyl transferase
DFS	Disease-Free Survival
DSB	Double-stranded Breaks
dTAG	Degrader TAG
EGFR	Epidermal Growth Factor Receptor
EMT	Epithelial Mesenchymal Transition
EPIKOL	Epigenetic Knockout Library
ER	Estrogen Receptor
FISH	Fluorescence In-Situ Hybridization
HAT	Histone Acetyltransferase
HDAC	Histone Deacetylase
HDR	Homology Directed Repair
HER2	Human Epidermal Growth Factor
HR	Hormone Receptor
IC_{50}	Inhibitory Concentration of 50
IHC	Immunohistochemistry
KMT	Lysine methyltransferase
MOI	Multiplicity of Infection
NHEJ	Non-homologous End Joining

NSL	Non-specific Lethal
NT1	Non-targeting sgRNA-1
PAM	Protospacer Adjacent Motif
PARP	Poly ADP-ribose polymerases
pCR	Pathological Complete Response
PFS	Progression Free Survival
PHD	Plant homeodomain
PR	Progesterone Receptor
PRMT	Protein Arginine Methyltransferase
ROS	Reactive Oxygen Species
RT-PCR	Real Time PCR
sgRNA	single guide RNA
siRNA	Small Interfering RNA
SNH	SS18-N-terminal
SSB	Single-stranded Breaks
SWI/SNF	Switch/Sucrose Non-Fermentable
Tet	Ten-eleven Translocation
TNBC	Triple-Negative Breast Cancer
PDL-1	Programmed Cell Death Ligand 1
TILs	Tumor Infiltrating T Cells

Chapter 1

INTRODUCTION

1.1 Breast Cancer

Breast cancer (BC) is the most common cancer in women worldwide, accounting for almost 30% of female cancers. Although the incidence rate is lower, men may also be diagnosed with BC (Siegel et al., 2021). BC is divided into three subgroups according to the presence of estrogen receptor (ER) or progesterone receptor (PR) and human epidermal growth factor (*ERBB2* or *HER2*). These subtypes are hormone receptor (HR) positive/*ERBB2* negative (HR+/*ERBB2*-), which accounts for 70% of all cases, hormone receptor positive/ERBB2 positive (HR+/*ERBB2*+) which accounts for 15-20% and triple negative which does not express any of the receptors (TNBC) are 15% of all cases. The presence of HR enables endocrine therapy and ERBB2+ tumors can be treated with ERBB2-targeted antibody combined with chemotherapy. However, for TNBC, the only treatment option is chemotherapy (Waks & Winer, 2019).

In 2000, Perou and Sorlie proposed a more detailed molecular classification of BC as a result of gene expression microarray profiling studies (Perou et al., 2000). These subtypes, namely intrinsic subtypes, include Luminal A, Luminal B, Her2/Neu, Basal-like and Normal-like breast cancer (**Figure 1.1**). Luminal A tumors express luminal cytokeratins and they are HR+/*ERBB2*-. Since they have low expression of proliferation related genes, prognosis of patients is good (Yersal & Barutca, 2014). Luminal B tumors also express luminal cytokeratins but the expression of HR is low with variable expression of *ERBB2*. Luminal A type responds to endocrine therapy such as tamoxifen and aromatase inhibitors better than Luminal B and both patient groups receive chemotherapy (Eliyatkin et al., 2015). Her2/Neu tumors have high expression of *ERBB2* and low expression of HR constituting 20% of breast cancers. These patients can be treated with trastuzumab (Herceptin), an *ERBB2*-targeted antibody. Basal like tumors express basal epithelial genes and basal cytokeratins with low or no expression of HR and *ERBB2*. 15%

of breast cancers are basal like and also known as (HR-/*ERBB2*-) (Yersal & Barutca, 2014). This subtype may sometimes be referred as triple-negative breast cancer (TNBC), but they are not exactly synonymous. There is 80% overlap between basal-like and triple-negative tumors (Yersal & Barutca, 2014). Some basal-like tumors may express one of the HR or ERBB2 and not all TNBC tumors exhibit all the molecular characteristics of basal-like tumors. According to the expression of targetable molecules, best prognosis is observed in Luminal A type while the patients with basal-like tumors have the worst prognosis. Lastly, normal breast-like subtype constitute 5-10% of BCs but is poorly characterized and their clinical significance is unknown (Yersal & Barutca, 2014). This molecular classification is also known as Prediction Analysis of Microarray 50 (PAM50) classification since the gene expression of 50 genes is used to identify subtypes (Kensler et al., 2019).

Intrinsic subtypes of breast cancer	
Luminal A	ER+, PR+, HER2−, Ki-67 low
Luminal B	ER+, PR+, HER2−, Ki-67 high ER+, PR+, HER2+, Ki-67 high
HER2-enriched	ER−, PR−, HER2+
Basal-like	ER−, PR−, HER2− Expression of keratins 5 and 17, laminin and fatty acid binding protein 7
Normal-like	ER+, PR+, HER2−, Ki-67 low Genes expressed by adipose tissue and other nonepithelial cell types

Figure 1.1: Intrinsic subtypes of breast cancer. These subtypes were defined by Perou and Sorlie according to the status of hormone receptors and HER2. Figure adapted from (Temian et al., 2018)

1.2 Triple-Negative Breast Cancer

Accurate assessment of triple-negative breast cancer tumors relies on the immunohistochemical (IHC) analysis of ER, PR and *ERBB2*, as well as fluorescence in-situ hybridization (FISH) analysis of *ERBB2*. It is important to accurately determine if a tumor is triple-negative since the patient will not be able to receive targeted therapies. TNBC has the most heterogenous and aggressive tumors, among all types of breast cancer. To better categorize this heterogenous disease and offer more specialized therapies, Lehmann et al. defined six TNBC subtypes (TNBCtype) by using publicly available gene expression profiles of TNBC patients. These subtypes are Basal-like 1 (BL1), Basal-like 2 (BL2), Mesenchymal (M), Mesenchymal stem-like (MSL), Immunomodulatory (IM) and Luminal Androgen Receptor (LAR) (Lehmann et al., 2011). BL1 is characterized by increased expression of cell cycle, cell division and DNA

damage response related genes and high Ki-67 expression. BL2 has elevated growth factor signaling. M and MSL subtypes are enriched in cell motility related pathways. MSL also expresses angiogenesis related genes but unlike M subtype MSL has low expression of proliferation related genes. IM subtype expresses immune antigens and has elevated immune signal transduction pathways. LAR has increased expression of Androgen Receptor (AR), its targets and cofactors (Lehmann et al., 2011).

This classification was made by analyzing surgical tumor specimens likely to have normal or immune cells from the tumor microenvironment. This suspicion led the same group to perform histological and gene expression analysis after laser-capture microdissection on a group of TNBC tumors. Indeed, the analysis revealed that the IM subtype contains tumor infiltrating lymphocytes and MSL subtype includes tumor-associated mesenchymal cells. Therefore Lehmann et al. refined their classification to 4 different subtypes (TNBCtype-4): BL1, BL2, M and LAR in 2016 (**Figure 1.2**). Among these subtypes, BL1 has the greatest pathological complete response (pCR) while the BL2 and LAR has the lowest pCR (Lehmann et al., 2016).

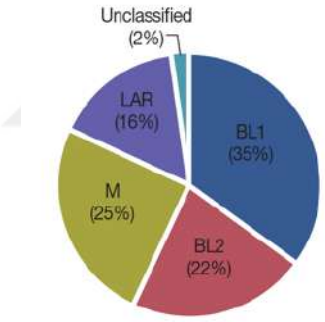

TNBCtype-4	
BL1	Enriched in cell division pathway components and DNA damage response (ATR/BRCA) pathways
BL2	Growth factor signaling (EGF pathway, NGF pathway, MET pathway, Wnt/β-catenin, and IGF1R pathway), glycolysis and gluconeogenesis and expression of myoepithelial markers (TP63 and MME)
M	Genes involved in motility, extracellular matrix, cell differentiation pathways and genes associated with epithelial to mesenchymal transition (EMT)
LAR	Enriched for genes involved in steroid synthesis and androgen/estrogen metabolism, including high levels of androgen receptor (AR) and its downstream targets and coactivators

Figure 1.2: Classification of TNBC tumors by Lehmann et al. In 2016 (TNBCtype-4) and characteristics of these subtypes. Figure adapted from (Temian et al., 2018)

Another classification of TNBC subtypes was made by Burstein *et al.* using RNA and DNA profiling and they also identified 4 different groups: Basal-like immunosuppressed (BLIS), basal-like immune activated (BLIA), mesenchymal (MES), luminal androgen receptor (LAR). Among them, BLIS has the worst and BLIA has the best prognosis in terms of disease free survival (Burstein et al., 2015). The overlap between the classifications from two groups strengthens the acceptance of these four new TNBC subtypes for developing subtype-specific and molecular-targeted therapies against this aggressive type of breast cancer.

TNBC is more commonly seen in younger women aged 20 to 39 years and the likelihood of diagnosed with TNBC decreases with each decade in a woman's life.

Similarly, it is known that breast cancer in younger ages is mostly basal-like. Again, over age 65, tumors of half of the patients are non-basal. Ethnically, incidence rate of TNBC is higher in African American women followed by Hispanic women (Howard & Olopade, 2021; Kumar & Aggarwal, 2016). Some studies associate obesity with only HR+ breast cancers while some showed that most patients diagnosed with TNBC pre-menopausal are obese or overweight (Howard & Olopade, 2021; Kumar & Aggarwal, 2016). Due to the disparity between ethnic groups having TNBC, a genetic predisposition link was investigated. 60-80% of tumors carrying germline *BRCA1* mutations are classified as TNBC. Average age at diagnosis was lower in deleterious *BRCA1, BRCA2* mutant tumors (44-45 years, $p<0.001$) when compared to wild-type TNBC (52 years) (Kumar & Aggarwal, 2016). In some non-hereditary breast cancers, although BRCA1 is intact, BRCA1 pathway might be dysfunctional or its expression might be regulated via epigenetic mechanisms leading to 'BRCAness'. There is an evidence of BRCA1 promoter methylation in rare types of breast cancer (medullary and metaplastic). This phenotype caused a synthetic lethality for PARP inhibitors which explained in detail below. (Foulkes et al., 2010).

TNBC has a poor prognosis compared to other types of breast cancers that have targeted therapy option. TNBC has a high likelihood of recurrence in the first or third year after diagnosis and mostly metastasize to the brain and lungs rather than bones (**Figure 1.3**) (Pogoda et al., 2013). Unfortunately, recurrent-TNBC patients have shorter survival when compared to other recurrent breast cancer subtypes (Kumar & Aggarwal, 2016). After first 5 years, recurrence rate of TNBC decreases rapidly (Foulkes et al., 2010).

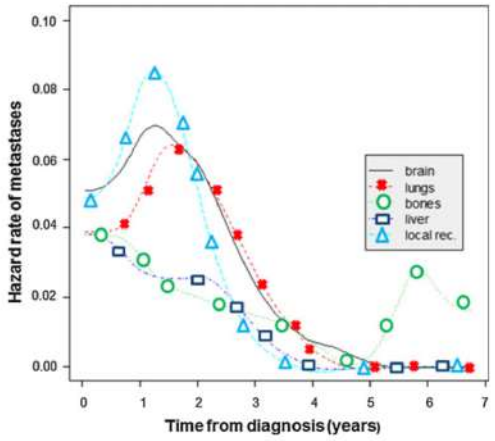

Figure 1.3: Recurrence and metastasis plot of TNBC patients. Figure adapted from (Pogoda et al., 2013)

1.3 Treatment options of TNBC

Lack of hormone receptors and *ERBB2* limits the endocrine and anti-Her2 targeted therapy for TNBC, leaving cytotoxic chemotherapy as the only option. High proliferation rate of TNBC forms a basis for a successful chemotherapeutic approach. They can be applied as neoadjuvant (prior to surgery to decrease the tumor burden) or adjuvant therapy (following surgery to eliminate any remaining cells). Primary chemotherapeutics used in TNBC includes taxanes and anthracyclines. Although patients initially respond to chemotherapy, they exhibit a poorer overall survival (De Laurentiis et al., 2010). This outcome might be explained by the presence of a subset of cells intrinsically resistant to the applied therapy. With new advancements and broader understanding of the molecular details of TNBC, more targeted therapies became available.

1.3.1 Surgery

One of the golden standards of TNBC treatment, as in other subtypes of BC, is surgical removal of small tumors with breast-conserving surgery and larger tumors with mastectomy. If axillary lymph node involvement is evident at the time of diagnosis, axillary lymph node dissection is the standard of care. However, if there is no evidence, sentinel lymph node biopsy can be applied, and dissection is only considered if there is positivity in the biopsy. Following neoadjuvant therapy, clinical practice is to perform sentinel lymph node biopsy to decide if axillary lymph node dissection is required or not (Waks & Winer, 2019).

1.3.2 Cytotoxic Chemotherapy

Early stage TNBC patients that have tumors<0.5 cm (T1a) or tumors between 0.6 and 1 (T1b) have relatively good prognosis and there is no additional benefit of chemotherapy in these patients. However, neo-adjuvant and adjuvant chemotherapy is recommended for TNBC patients with stage I-III disease with tumors greater than 1 cm with or without lymph node metastasis (Gupta et al., 2020). There is no consensus on preferred chemotherapy drug and regimen in neoadjuvant or adjuvant settings. Anthracycline and taxane based neoadjuvant therapy applied to TNBC patients resulted in 30-40% pathological complete response (pCR) (Bianchini et al., 2022). Response rate of TNBC to chemotherapy is higher than any other subtype of breast cancer however the overall survival of patients is the worst in TNBC. This phenomenon is called ‘TNBC paradox’. Patients who did not have pCR are several times more likely to recur and die due to

metastatic disease when compared to patients with HR+ tumors (Nedeljkovic & Damjanovic, 2019). Even though pCR is achieved, only <30% of patients with metastatic BC will survive 5 years after diagnosis. Many different combination strategies were investigated when compared to single-agent therapy to improve the survival rates. Although successful at first, combination therapies caused increased toxicity and did not improve the overall survival (Bianchini et al., 2022).

Taxanes

One of the most frequently used taxane is paclitaxel. It acts as a microtubule stabilizer and arrests cells at prometaphase state of the cell cycle due to the inability of cells forming spindles (**Figure 1.4**). Docetaxel is another drug with the same mechanism of action with a stronger effect on microtubule depolymerization than taxol. The disadvantage of taxol is its high hydrophobicity and low solubility in aqueous solutions. It can be dissolved in polyoxyethylated castor oil (Chremophor EL) however this solvent can cause severe allergies in patients and also restricts the release of taxol resulting in decreased efficacy. As an alternative, albumin-bound paclitaxel (Nab-paclitaxel) does not cause allergic reactions and does not limit the release of paclitaxel, allowing for shorter therapy periods. Basal-like subtypes of TNBC can have four times more remission rate than other subtypes upon taxane treatment since they have high expression of proliferation related genes that allows targeting by antimitotic agents (Yin et al., 2020). Taxane group of drugs are often used as adjuvant therapy.

Figure 1.4: Mechanism of action of paclitaxel. Figure created in biorender.com

Anthracyclines

Anthracyclines are a group of drugs that is used in am wide range of cancers with a more defined dosing schedule as adjuvant therapy. Epirubicin and doxorubicin are examples of anthracyclines. Two main mechanisms of doxorubicin are intercalation into DNA and generation of free radicals (**Figure 1.5**). DNA intercalation by doxorubicin inhibits topoisomerase II activity resulting in extensive DNA damage that ultimately

results in cell death. Doxorubicin is also oxidized forming semiquinone, however it is converted back to doxorubicin due to its instability. During this process reactive oxygen species (ROS) are released. ROS is well known cause of oxidative stress, DNA damage and induction of apoptosis (Thorn et al., 2011). Anthracycline therapy for six months decreased the mortality rate around 38% in younger patients (<50) and 20% in older patients (50-69 years). Although the anthracycline therapy did not cause difference in the response of different BC subtypes, combination of anthracycline and taxane therapies showed greater pCR in Basal-like subtype of TNBC expressing high levels of proliferation related genes (Yin et al., 2020).

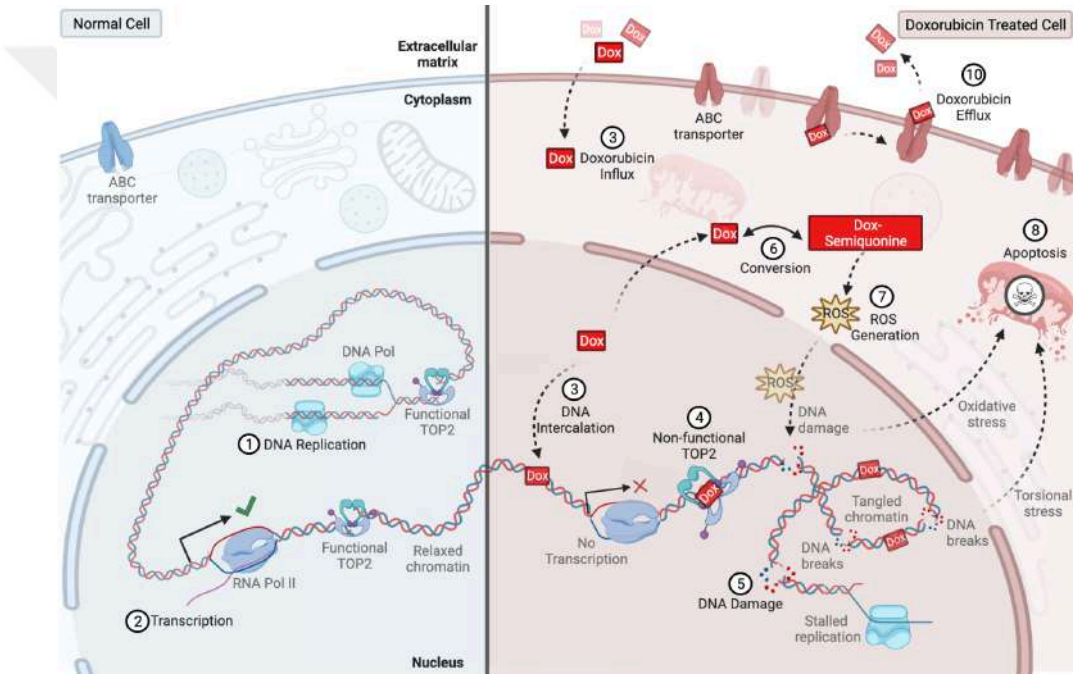

Figure 1.5: Mechanism of action of doxorubicin. Left hand side of the figure shows the DNA replication and transcription in normal cells. Right hand side of the figure shows the effect of doxorubicin on these pathways. Figure created in biorender.com

Platinum-based drugs

Mutant *BRCA1/2* is highly associated with basal-like phenotype and TNBC. BRCA1 is required to repair of double-stranded DNA breaks and its absence may pose a susceptibility to DNA-damaging agents (De Laurentiis et al., 2010). In neo-adjuvant setting, using platinum agents such as carboplatin increased pCR by 10-15% (Poggio et al., 2018). The drawback of carboplatin is its high hematological toxicity levels. The role of carboplatin in adjuvant setting is less clear. In a trial (PATTERN), carboplatin plus paclitaxel treatment has higher 5-year disease-free survival (DFS) when compared to

anthracycline plus taxane treatment (86.5% vs 80.3%, p<0.03). This study lacks the information about the administration of carboplatin in the presence of both anthracyclines and taxane. (Yu et al., 2020).

1.3.3 Targeted therapies

PARP Inhibitors

DNA repair is an important function for maintaining genome integrity. There can be single-stranded breaks (SSB) or double-stranded breaks (DSB). BRCA1 and BRCA2 repairs DSB by homologous recombination. Mutation in these genes or related genes in this pathway increases genomic instability and alterations of BRCA pathway are frequently observed in basal-like or TNBC tumors. Poly (ADP-ribose) polymerases (PARPs) are an important class of DNA repair enzymes. Among them, PARP-1 is essential for SSB repair to recruite base-excision repair proteins to the damaged area. PARP inhibitors such as olaparib and talazoparib were developed against PARP-1. However, using PARP inhibitors alone is insufficient since the DNA repair mechanisms complement each other. PARP inhibitors shows their greatest effect in 'synthetic lethality' format if the cells are deficient in other repair mechanisms such as BRCA1 (De Laurentiis et al., 2010). When PARP-1 is inhibited, SSB could not be repaired and turns into DSB due to replication fork stalling. If BRCA pathway is also dysfunctional, cells cannot tolerate the break leading to chromosome instability and eventually apoptosis (De Laurentiis et al., 2010). In intact DSB repair mechanisms, PARP inhibitors can be combined with DNA damaging agents however toxicity of this combination therapy limits this application. Although median progression free survival (PFS) increased with olaparib when compared to chemotherapy alone (7 months vs 4.2 months), no significant difference was observed in overall survival (Mehanna et al., 2019).

Antibody-drug conjugates

Antibody-drug conjugates are recombinant monoclonal antibodies that are covalently bound to cytotoxic agents. These immunoconjugates can be targeted to cancer cells targeting specific molecules, thereby reducing systemic toxicity. An example is Sacituzumab govitecan that carries a humanized monoclonal antibody targeting TROP2, linked to a DNA topoisomerase-I inhibitor SN-38. TROP2 is highly expressed on the surface of TNBC tumor cells (Lyons, 2019). Another combination includes zinc

transporter (ZIP6 or LIV1) targeting monoclonal antibody and a microtubule-disrupting agent (Bianchini et al., 2022). FDA approved several antibody drug conjugates including ado-trastuzumab emtansin and fam-trastuzumab deruxtecan-nxki for the treatment of Her2+ breast cancer (Tong et al., 2021). Antibody-drug conjugates hold a great promise in terms of targeted therapies. Identifying the threshold of target antigen expression or innovation of linker technologies are required to develop new conjugates.

Immunotherapy

Immunotherapy is one of the most promising therapeutic approaches that is developing rapidly. Around 20% of TNBC patients express Programmed cell death ligand 1 (PDL-1) and tumor infiltrating T cells (TILs) were found in BC tumors. PDL-1 binds to programmed cell death protein (PD-1) and conveys signal to inhibit T cell proliferation. Many different immune checkpoint inhibitors such as pembrolizumab, nivolumab, atezolizumab and durvalumab are being investigated in clinical trials. Some of these drugs such as pembrolizumab, were tried as a single agent and in combination with conventional chemotherapy such as Nab-paclitaxel. It is known that chemotherapy triggers the immunity and taxanes activate the toll-like receptors and dendritic cells. On top of this primed immunity, immune checkpoint blockade generates a robust immune response (Vagia et al., 2020). Another focus is cytotoxic T lymphocyte antigen-4 (CTLA-4) that can be targeted by anti-CTLA-4 antibody (ipilimumab). CTLA-4 binds to CD80 or CD86 molecules to inhibit T cell activation (Lyons, 2019).

Other targets

Epidermal Growth Factor Receptor (EGFR), also known as HER1, is highly expressed in 70-78% of basal-like TNBC offering a targeted approach. It can be targeted by tyrosine kinase inhibitors such as gefitinib and erlotinib, as well as monoclonal antibody cetuximab. Combination of cetuximab with carboplatin increased the PFS when compared to carboplatin alone group (3.7 vs 1.5 months, $p<0.03$) (De Laurentiis et al., 2010). Although pre-clinical data suggests promising results, clinical trials did not obtain expected results. Results showed that, in patients treated with EGFR inhibitors, downstream pathway was still active suggesting that there might be a complementary signaling pathways. Moreover, diarrhea, rash, fatigue and nausea were commonly observed side effects of EGFR inhibition (Yin et al., 2020).

Activation of PI3K/AKT/mTOR pathways are frequently observed in TNBC tumors. It can be through the activation of PIK3CA or AKT1 or loss of PTEN leading to

hyperactivation of AKT pathway which is observed in ~50% of TNBC. AKT inhibitors may be used as combination therapy on top of the paclitaxel (Lyons, 2019).

The LAR subtype of TNBC has luminal-like gene expression and does not respond neoadjuvant therapy as good as the other subtypes. However, it has high expression of Androgen Receptor that can be targeted by bicalutamide and enzalutamide (Kumar & Aggarwal, 2016). AR inhibitors were also tried in combination with PI3K inhibitors (Yin et al., 2020).

Since TNBC is highly proliferative, it needs a developing vasculature system. Vascular endothelial growth factor-A (VEGF) inhibitors and anti-VEGF monoclonal antibody (bevacizumab) were used in combination with first-line chemotherapy and increased the PFS of TNBC patients significantly. It should be noted that FDA withdraw the approval of bevacizumab in BC due to its high toxicity and low efficacy (Kumar & Aggarwal, 2016).

1.4 Chemoresistance in TNBC

Chemotherapy resistance is commonly seen in TNBC than other subtypes of breast cancer especially in metastatic tumors. This causes a significant problem in clinics since the chemotherapy is the only option for TNBC treatment. Resistance to chemotherapy can be divided into two categories: intrinsic or acquired resistance. Intrinsic resistance is characterized by the existence of a subpopulation of cells refractory to therapy due to a pre-existing altered gene expression or cell state. Acquired resistance develops during the therapy due to an epigenetically poised state or acquisition of new mutations. These changes can cause drug inactivation or alteration of the drug targets. Once the cells become resistant to one chemotherapeutic, they often do not respond to other chemotherapeutics as well, known as the ‘multidrug resistance’ phenotype. Common reasons of chemotherapy resistance in TNBC are explained below.

1.4.1 ABC transporters

Transporter mediated drug efflux is one the highly validated cause of therapy resistance. ATP-binding cassette (ABC) transporters pump a wide variety of molecules and compounds out of the cell by utilizing ATP hydrolysis. There are 48 ABC transporters in humans (Dean, 2009). They are expressed in almost all tissues and especially high levels in cells with secretory roles. Role of ABC transporters in therapy resistance of solid tumors including breast cancer is well established. Compared to other subtypes, in TNBC, P-glycoprotein (ABCB1), multidrug-resistant protein-1 (ABCC1/MRP1), breast cancer

resistance protein (ABCG2/BCRP) and multidrug-resistant protein-8 (ABCC11/MRP8) are highly expressed with the first three being most studied ABC transporters (Bai et al., 2021). Increased ABCC1 expression has been linked to the neodjuvant chemotherapy in TNBC while ABCG2 high expression is commonly seen in TNBC cancer stem cells (Britton et al., 2012; Guestini et al., 2019).

There are 2 main approaches to fight against the ABC transporters: inhibition of activity or inhibition of expression. For inhibition of efflux activity, ABC inhibitors were generated. However, first generations of inhibitors were not beneficial since they lacked sensitivity and their toxicity levels were high. Efforts on discovering new inhibitors for ABC transporters are still ongoing. Nonsteroidal anti-inflammatory drugs were used to inhibit ABCC1 and concomitantly epirubicin was applied. This combination showed promising anti-tumor activity in Phase I trials (O'Connor et al., 2007). Combining highly specific ABCB1 inhibitors zosiquidar and tariquidar with anthracyclines or taxanes did not show additional benefit (Holohan et al., 2013). Another approach is to use small interfering RNAs (siRNAs) or microRNAs to silence ABC transporters. These approaches achieve limited benefit because in most cases inhibition of only one transporter is not enough to re-sensitize the cells due to high redundancy among the ABC transporters and inhibition of multiple transporters at once increases the toxicity (Nedeljkovic & Damjanovic, 2019).

1.4.2 Cancer Stem Cells (CSCs)

Cancer stem cells (CSCs) are a rare population in tumors that are CD44+/CD24- and have self-renewal ability (Ma et al., 2014). These cells are often associated with drug resistance, recurrence and metastasis (Shibata & Hoque, 2019). In TNBC, studies showed higher percentages of CSCs compared to other subtypes (Ma et al., 2014; Park et al., 2010). Moreover, the number of CSCs increased upon neoadjuvant chemotherapy. Treatment with gemcitabine or paclitaxel increased ABCB1 expression in CSCs (Nedeljkovic & Damjanovic, 2019). The mechanism behind the evasion of CSCs from therapies is still unclear. First, since they are relatively quiescent, they can escape chemotherapy which acts on highly proliferative cells. Second, CSCs have high expression of ABC transporters, especially ABCG2, even before any therapies (Shibata & Hoque, 2019).

1.4.3 Other pathways

Some chemotherapeutics exert their killing effect through high production of reactive oxygen species (ROS) and DNA damage. However, TNBC is known to have higher levels of ROS at the baseline than other BC subtypes. They further activate Nrf2 to induce transcription of antioxidant genes (Sarmiento-Salinas et al., 2019). DNA repair mechanisms are equally important. An example is the administration of PARP inhibitors to *BRCA1/2* mutant TNBCs as described earlier. *MGMT* is a gene that remove alkyl groups upon DNA damage. Similarly, methylation status of *MGMT* promoter determines the response of TNBC patients to alkylating agent therapy (Bai et al., 2021).

Autophagy is another well-established cause of drug resistance due to its effect on nutrient recycling and inactivation of compounds (Lefort et al., 2014).

Several signaling pathways including NF-κB, PTEN/PI3K/AKT/mTOR, JAK/STAT and receptor tyrosine kinases are associated with the chemotherapy resistance in TNBC. NF-κB signaling is related to TNBC growth since it inhibits apoptosis, regulates inflammatory response and angiogenesis. NF-κB signaling is known to regulate chemoresistance and also becomes upregulated in hypoxia by further contributing to chemoresistance (Fusella et al., 2017).

1.5 Epigenetics

Epigenetics is the heritable changes of gene expression without any alterations in the underlying DNA sequence (**Figure 1.6**). These changes are reversible and occur at chromatin level. The smallest unit of chromatin is the nucleosome composed of two of each H2A, H2B, H3 and H4 histones. Around 147 bp of DNA is wrapped around this histone octamer forming nucleosome structure. Two nucleosomes are separated by 20-50 bp linker sequences that can dynamically change according to the gene expression needs. Linker sequences are more accessible for binding of proteins when compared to DNA wrapped around the histones. Nucleosomes in heterochromatin regions are tightly packed and associated with repressed gene expression while nucleosomes found in a more relaxed conformation in euchromatin regions allowing active transcription (Dawson et al., 2012). DNA packaging around histones is regulated via the covalent modifications on DNA itself or lysine, serine or arginine residues of the histone tails. First, these modifications may change the electrostatic interactions between the nucleosomes and between nucleosomes and DNA resulting in accessibility changes. Second, combination of different modifications on histones, known as ‘histone code’ recruits specific proteins

and regulates distinct biological pathways (Strahl & Allis, 2000). DNA itself can have methyl groups on the special regions called CpG islands at the promoter of the genes and results in gene repression. However, histone tails have different covalent modifications such as acetylation, methylation, phosphorylation, ubiquitination and sumoylation on specific histone residues. Acetylation of histone lysines is often associated with active transcription however the effect of methylation might be residue specific. Methylation of H3 Lysine 4 (H3K4me) is linked to active transcription while H3K9me and H4K20me are linked to transcriptional repression (Esteller, 2008). There are special groups of proteins called epigenetic modifiers that are responsible for addition (writers) or removal (erasers) of these modifications and also the readers that interpret the histone code and recruit required downstream proteins (Dawson et al., 2012).

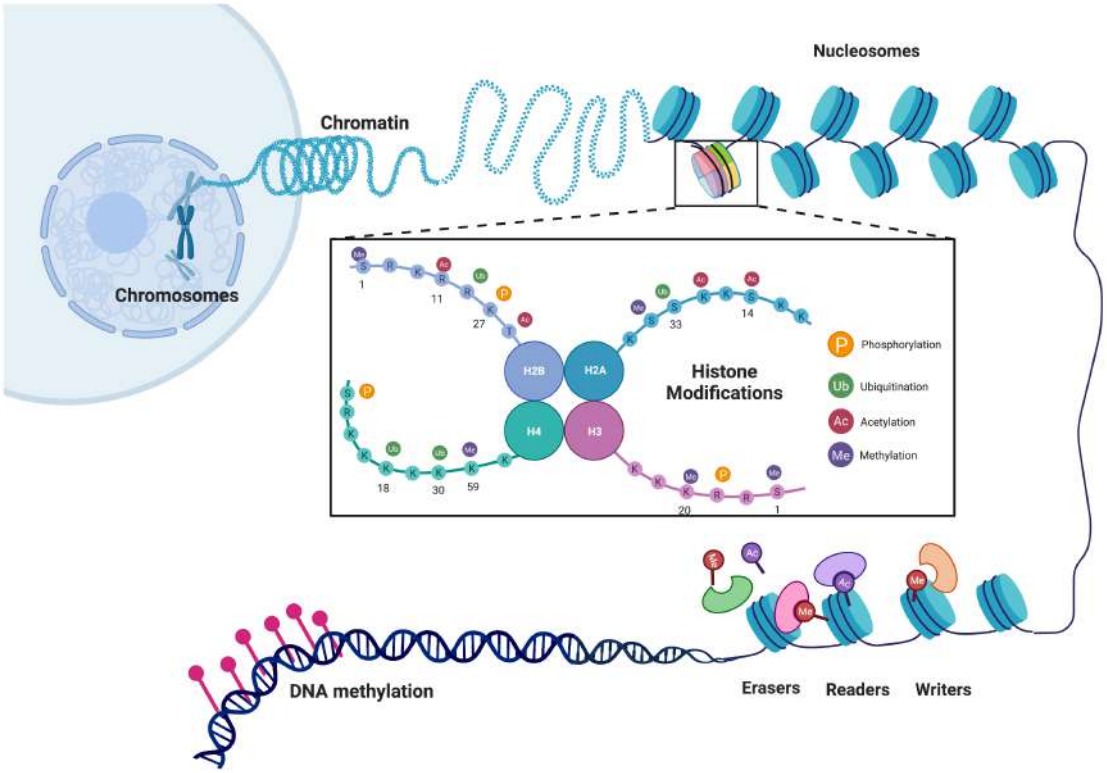

Figure 1.6: Chromatin and epigenetic regulations. Figure created in biorender.com

1.5.1 Writers

Writer epigenetic proteins are responsible for adding methyl groups to DNA or post-translational modifications to histone tails. Enzymes that catalyzes the addition of methyl groups on the cytosine-guanine dinucleotides (CpG) forming 5-methylcytosine (5mC) at the promoter regions of DNA are called DNA methyl transferase family (DNMTs). DNMT family include DNMT1, DNMT3A, DNMT3B and DNMT3L (Li et al., 1992).

For histone methylation, two classes of enzymes add methyl groups to the lysine residues: Lysine methyltransferases (KMTs) and Protein arginine methyltransferases (PRMTs). KMTs may add one (monomethyl), two (dimethyl) or three (trimethyl) methyl groups on the same lysine eventually leading to different outcomes. For example, H3K4me3 is generally found in the promoters of active genes while H3K4me1 is found in active and poised enhancers (Hon et al., 2009). Similarly, functions of PRMT family results in different biological outcomes depending on the location of the added methyl group. All PRMTs first generate ω-N_G-monomethyl arginine by adding a methyl group to one of terminal nitrogen atoms of arginine (MMA). Another methyl group can be added to the same nitrogen atom (N^G-asymmetric dimethylarginine, ADMA) or the other nitrogen atom (N^G-symmetric dimethylarginine, SDMA). PRMTs can work closely with KMTs and DNMTs to regulate the gene expression (Gayatri & Bedford, 2014).

Histone acetyltransferases (HATs, also known as lysine acetyltransferases KATs) are responsible for adding acetyl groups to the lysine ε-amino groups. This negatively charged post-translational modification neutralizes the positive charge on histones thereby decreasing the interaction between DNA and nucleosomes rendering that area more accessible for transcription factors. (Shahbazian & Grunstein, 2007). KATs can be divided into three main groups based on the conservation of sequence: p300/CBP, GNAT (GCN5-related N-acetyl transferase) and the MYST (MOZ, YBF2/SAS3, SAS2, TIP60) families. CBP (KAT3A) and P300 (KAT3B) have significant homologies in their catalytic domain and bromodomain. They have many shared targets as well as the divergent ones. GNAT family includes GCN5 (KAT2A) and PCAF (KAT2B) (Vetting et al., 2005). The MSYT family proteins contain a MYST domain with acetyl-CoA-binding and Zinc finger motifs. This family has 5 proteins with alternative naming: MOF (MYST1/KAT8), HBO1 (MYST2/KAT7), MOZ (MYST3/KAT6A), MORF (MYST4/KAT6B) and TIP60 (KAT5) (Thomas & Voss, 2007). All these MYST family KATs share histone residue targets as well as the protein specific ones as shown in **Table 1.1** (Dawson et al., 2012).

Table 1.1: MYST Family of KATs and their target histone residues

Enzyme	Alternative Names	Histone Substrate
MOF	MYST1/KAT8	H4K16, H4K5Ac, H4K8Ac
HBO1	MYST2/KAT7	H3K14, H4K5, H4K8, H4K12
MOZ	MYST3/KAT6A	H3K23, H3K9, H3K14
MORF	MYST4/KAT6B	H3K23, H4K5, H4K8, H4K12, H4K16
TIP60	KAT5	H2AK5, H4K5, H4K8, H4K12, H4K16

MOF is important for H4K16 acetylation. Its interactions with KANSL2 and KANSL3 in the NSL complex, also regulate the H4K5Ac and H4K8Ac (Radzisheuskaya et al., 2021). HBO1 forms complexes with JADE1/2/3 and together with ING4/5 and EAF6, they are responsible for most of the H4 acetylation. MOZ and MORF forms complexes with Bromodomain and PHD Finger Containing Protein 1 (BRPF1) together with ING5 and EAF6 accessory proteins. Formation of this complex, increases the acetylase activity of MOZ and MORF. TIP60 is the catalytic subunit of NuA4 complex (Biswas & Rao, 2018).

1.5.2 Erasers

Epigenetic modifications are reversible and can be adjusted according to the cells' needs thanks to the 'erasers'. Almost for each modification written by the specific writer enzyme, there is a corresponding eraser enzyme that removes that modification. Ten-eleven translocation (TET) family of proteins are responsible for removing DNA methylation. They convert 5mC to 5hmC by oxidation reaction that generates intermediate products such as 5-formylcytosine (5fC) and 5-carboxylcytosine (5caC). These bases with new modifications are recognized and removed by base-excision repair leading to total removal of methyl mark (Allis & Jenuwein, 2016).

Removal of histone lysine methylations are mediated by the flavin adenine dinucleotide (FAD)-dependent amine oxidases (lysine specific demethylases, LSD, KDM) and jumonji C (jmjC) containing iron- and α-ketoglutarate dependent deoxygenases. Former only removes mono- and di-methylation however latter is able to remove trimethyl groups as well (Black et al., 2012). To date, an equivalent of KDM family has not been identified for arginine methylation that are added by the PRMT family.

Removal of histone acetylation is performed by histone deacetylases (HDACs) and represses the transcription of corresponding gene by increasing the compaction of chromatin. Interestingly, HDACs do not have a DNA binding domain and are recruited to the specific locuses owing to their presence in multi-protein complexes such as Sin3A, NuRD and CoREST (Hayakawa & Nakayama, 2011).

1.5.3 Readers

In order to interpret the histone code, a group of proteins, some with catalytic activities, binds to the histone tails with post-translational modifications and conveys the signal to downstream effector proteins. For example, methylated CpG islands are recognized by the methyl CpG binding proteins (MBPs) to repress the gene expression

(Musselman et al., 2012). For recognition of methylated histones, there are many specific binding domains. These include ankyrin, ATRX-DNMT3-DNMT3L (ADD), bromo-adjacent homology (BAH), chromobarrel, chromodomain, malignant brain tumor (MBT), plant homeodomain (PHD), PWWP, Tudor and WD40 domains. The high number of methylation-recognizing domains shows the importance of methyl mark for cellular processes. Each domain binds to a specific methyl mark or combination of marks. For example, PHD domain binds to H3K4me3 on the active sites and WD40 binds to several different repression related methyl marks. For these bindings, either the modified lysine itself interacts with the binding pocket or the conformational change in the aminoacids surrounding it recruits specific players (Musselman et al., 2014). For methylarginine, Tudor domains are one of the best characterized domains (Gayatri & Bedford, 2014).

Unlike the wide variety of methyl recognizing domains, there are no multiple reader domains that recognize acetylated histones. Acetyl marks found in different locations are recognized rather nonspecifically by bromodomains (BRD), tandem PHD domains and YEATS domain. Bromodomains have a characteristic hydrophobic pocket that can bind to acetylated histones but not unmodified lysines. Bromodomains are divided into 8 groups depending on the sequence and structural similarities (**Figure 1.7**).

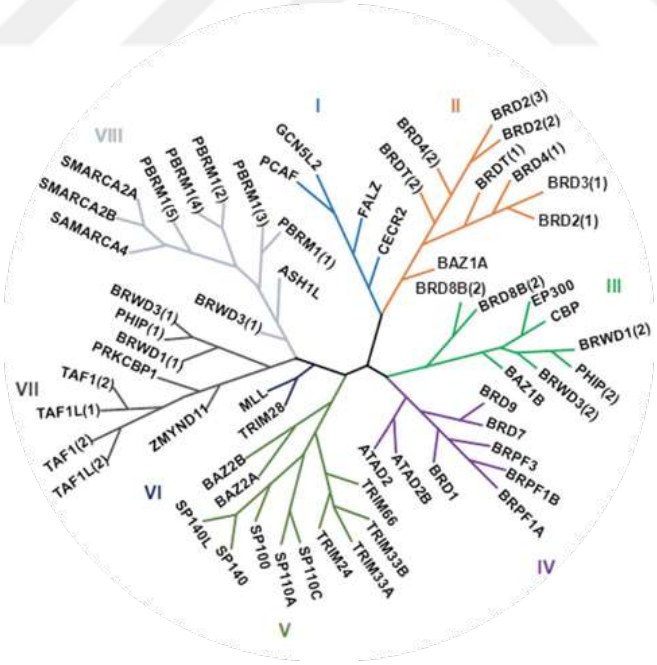

Figure 1.7: Phylogeny of Bromodomain proteins. Figure adapted from (Perez-Salvia & Esteller, 2017)

PCAF in BRD family I recognizes both H3K14ac and H4K8ac, FALZ recognizes H4K16ac. BRD Family II is also called Bromodomain and Extra-Terminal Domain (BET) family. BRD2 and BRD3 bind to H3K14, H4K5 and H4K12. BRD4 has multiple

recognition sites on both H3 and H4. Additionally, BRD4 has been shown to acetylate H3K122 as a novel KAT. BRDT recognizes both H4K5ac and H4K8ac. This family is among the most studied families of BRD due to its implications in cancer. BRD family III includes EP300 and CBP that acts as transcriptional coactivators. BRD family IV contains BRPF proteins and highly studied BRD9. BRD Family V has several proteins with a characteristic tandem PHD and BRD (Biswas & Rao, 2018; Perez-Salvia & Esteller, 2017). BRPF family proteins will be discussed in detail below.

BRPF proteins

Bromodomain- and PHD finger- containing protein 1 (BRPF1) with its paralogs BRPF2 (BRD1) and BRPF3 belongs to the human BRD family proteins class IV. They share 50% sequence identity and are similar in size (BRPF1 1214 aminoacids, BRPF2 1058 aminoacids, BRPF3 1205 aminoacids) (Klein et al., 2014). BRPF1 contains two PHD finger domains linked with a zinc knuckle (PZP module), one bromodomain and a PWWP domain allowing it to recognize different histone marks (**Figure 1.8**).

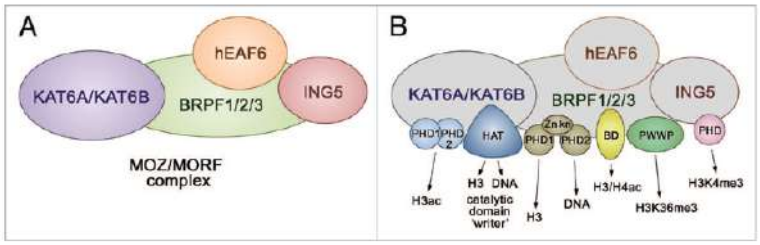

Figure 1.8: MOZ/MORF complex and BRPF1. A. BRPF1/2/3 acts as a scaffold for the association of KAT6A/KAT6B, EAF6 and ING5. **B.** Domains of complex proteins and their functions. Figure adapted from (Klein et al., 2014)

First PHD finger (PHD1) binds to unmodified H3 tail, while the second PHD domain (PHD2) atypically binds to DNA (Yang, 2015). Binding of PHD1 is highly specific that having H3K4me3, H3R2me2 or phosphorylation of T3 or T6 interferes with this binding. Following PZP, BRPF1 has bromodomain that binds to acetylated lysines nonspecifically and a PWWP domain that binds to H3K36me3. PWWP domain is also associated with binding of BRPF1 to mitotic chromosomes (Klein et al., 2014). In addition, BRPF1 contains two enhancer of polycomb (EPC) like motifs that flank its PHD domain. N-terminal EPC-like domain binds to MOZ or MORF while the C-terminal motif binds to ING5 and EAF6. Therefore, BRPF1 acts as a scaffold protein that brings together this tetrameric complex. It also enhances the HAT activities of MOZ and MORF (Yang & Ullah, 2007). HBO1 may also form complexes with BRPF1/2, ING5 and EAF6 (Yang,

2015). BRPF1 determines the substrate specificity of HBO1 in this complex shifting it to H4 from H3 (Yang, 2015; You, Yan, et al., 2015). Another study shows that BRPF1-KAT6 complexes are responsible for H3K23 propionylation in addition to acetylation (Yan et al., 2020). BRPF1 is essential for *Hox* gene expression and during embryonic development of axial skeleton, forebrain, and the hematopoietic system (Klein et al., 2014; You, Zou, et al., 2015). Recently, BRPF1 was identified as a significantly upregulated gene in hepatocellular carcinoma (Cheng et al., 2021).

1.5.4 Chromatin remodeling complexes

Dynamics of chromatin structure are also important for gene expression regulation. Chromatin remodelers are responsible for the accurate distribution and spacing of nucleosomes depending on the transcriptional activity of the specific genomic region. ATP dependent chromatin remodeling complexes were divided into 5 subgroups: SWI/SNF, ISWI, NuRD/Mi2/CHD, INO80, and SWR1. These complexes use ATP to disrupt histone-DNA bonds to slide, dissociate or remove nucleosomes. SWI/SNF complex members were first identified in yeast and extensively studied from that point on. Mammalian homolog of SWI/SNF complex was named as BAF complex and it includes one ATPase either BRM (*SMARCA2*) or BRG1 (*SMARCA4*) as well as BAF155 (SMARCC1), BAF170 (SMARCC2), and BAF47 (SMARCB1) as core members. BAF complex contains BAF250a (ARID1A) or BAF250b (ARID1B) while pBAF contains BAF180 (PBRM1) and BAF200 (ARID2) as additional proteins (Masliah-Planchon et al., 2015). Recently, proteomic analyses identified additional proteins (BCL7A/B/C, BCL11A/B, BRD9 and SYT (SS18)) but these proteins lacked homologous in yeast (Kadoch et al., 2013).

BAF complex and SS18L2

Alterations in BAF complexes have been associated with carcinogenesis. Most studied abnormality about BAF complex is the *SS18/SSX* fusion observed in synovial sarcoma. Normally, with BAF47, SS18 binds to enhancers or promoter of genes to regulate gene expression. However, in synovial sarcoma, SS18 is fused to 78 aminoacids of SSX (Alfert et al., 2019; Masliah-Planchon et al., 2015). SS18/SSX fusion competes with WT SS18 during complex formation leading to eviction and degradation of SS18 and BAF47 (Clark et al., 1994). Interestingly, rescue with BAF47 does not restore the function of BAF complex suggesting that pathogenesis of this fusion is not due to loss of

BAF47 but due to gain of SS18/SSX fusion protein (McBride et al., 2018). This oncogenic fusion protein causes both loss and gain of binding locations of BAF complex. PRC2 complex is found together with BAF complex containing SS18/SSX fusion at the *SOX2* and *PAX3* genes resulting in the loss of H3K27me3 that is enough to increase Sox2 expression (Kadoch & Crabtree, 2013). This new complex can also interact with KDM2B leading to the activation of normally repressed genes (Banito et al., 2018).

SS18 has two homologous genes, *SS18L1* and *SS18L2* (de Bruijn & Geurts van Kessel, 2006) (**Figure 1.9**). Both SS18 and SS18L1 contains a SS18-N-terminal (SNH) domain and a QPGY domain. SS18L2 only contains the SNH domain. QPGY domain seems important for the transcriptional activation while SNH domain is required for interaction with other proteins. It is hypothesized that since SS18L2 lacks QPGY domain, it may be competing with SS18 and SS18L2 for binding to the target regions (de Bruijn & Geurts van Kessel, 2006). SS18L2 is also widely expressed in various tissues (de Bruijn et al., 2001). Apart from this, information about the functions of SS18L2 is very limited leaving it as an uncharacterized gene. A recent study of proximity labeling identified that SS18L2 binds to BAF complex. (Alerasool et al., 2022)

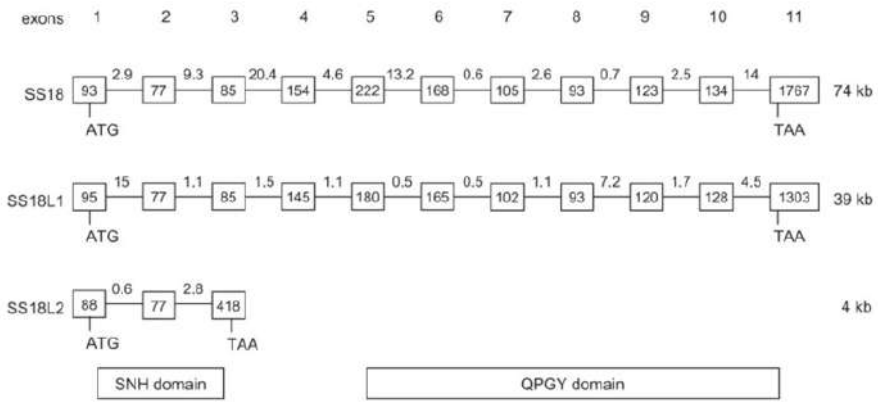

Figure 1.9: Structure and domains of human SS18, SS18L1 and SS18L2 genes. Figure adapted from (de Bruijn & Geurts van Kessel, 2006)

1.6 Epigenetic Regulation in TNBC

Dysregulations in epigenome are highly associated with carcinogenesis and contribute to the heterogeneity of TNBC. A study on TNBC methylome divided TNBC patients into three group based on differentially methylated regions. Group enriched with hypomethylated regions had better survival rates when compared to hypermethylated group. Medium methylated cluster showed the worst prognosis (Stirzaker et al., 2015). Another study analyzed 110 hypermethylated regions in 69 cancer-related genes and proposed a methylation pattern for TNBC (Branham et al., 2012). This pattern was

characterized with hypermethylation of CD44, MGMT, CDKN2B, RB, p73 and hypomethylation of GSTP1, PMS2, MSH2, MLH1, MSH3, MSH6, DLC1, CACNA1A, CACNA1G, TWIST1, and ID4. Interestingly, ID4 is a negative regulator of BRCA1 suggesting a new mechanism for BRCA1 silencing (Branham et al., 2012). Promoter hypermethylation of *BRCA1* is a well-established characteristic of BRCAness observed in TNBC and basal-like tumors exerting a susceptibility against Parp inhibitors, platinum- and anthracycline-based therapies. Moreover, aberrant DNA methylation was observed when metastatic tumors were compared to primary tumors indicating a role in metastasis (Temian et al., 2018).

Subtype analysis performed on TNBC cell lines revealed distinct H3K36me3 profiles on different subtypes of TNBC. Increased or decreased expression of KMTs were also observed in TNBC leading to substantial changes in epigenome (Temian et al., 2018). Similarly, LSD1, lysine specific demethylase that regulate H3K4me and H3K9me demethylation, is highly expressed in ER- tumors leading to increased metastasis (Lim et al., 2010). EZH2, a lysine methyltransferase for H3K27me3 is shown to silence E-cadherin expression by also recruiting DNMT1 to the gene promoter. This shows that several epigenetic modifiers act together to promote EMT (Zolota et al., 2021). 5-azacytidine was approved by FDA to fight against chemoresistance, however its effect in TNBC is inconsistent (Martinez-Useros et al., 2021). Bromodomain containing BET family is another target in TNBC. Several BET inhibitors showed promising results in the treatment of TNBC either alone or in combination with established therapies (Shu et al., 2016). Currently, a new BET inhibitor, ZEN-3694, is in clinical trials for TNBC patients that do not carry germline mutations for *BRCA1/2* (Martinez-Useros et al., 2021).

Breast cancer stem cells are responsible for the aggressiveness of TNBC and recently it has been discovered that cancer stem cells have distinct DNA and histone methylation profiles compared to the normal tumor cells (Li et al., 2018). Another class of epigenetic targets is HDACs known to deacetylate tumor suppressors and contribute to carcinogenesis. The use of several HDAC inhibitors (vorinostat, panabinostat) have been shown to decrease proliferation rates of TNBC cell lines both *in vitro* and *in vivo* (Chalakur-Ramireddy & Pakala, 2018). HDAC inhibitors may also prime cells for immune checkpoint blockade (Temian et al., 2018). A new strategy for HDAC inhibitors is their potential ability to reactivate ER in TNBC for subsequent tamoxifen treatment (Martinez-Useros et al., 2021).

On the other hand, one of the ATPases (*BRG1*) of chromatin remodeling complexes has been shown to have elevated expressions in TNBC. Knockdown of BRG1 impaired tumor formation in vivo and sensitized TNBC cell lines to chemotherapeutics including doxorubicin, paclitaxel and cisplatin (Temian et al., 2018; Wu et al., 2016).

1.7 Epigenetic Regulation of chemoresistance

In recent years, it is well established that genetic alterations are do not adequately explain the chemoresistance phenotype (Gomez-Miragaya et al., 2019). Both epigenetic regulations and transcriptional reprogramming play a significant role in the emergence of therapy resistance. In one study, tumors from 20 TNBC patients were analyzed before and after neoadjuvant chemotherapy. Results showed that resistant clones pre-exist and were selected during neoadjuvant chemotherapy and selected resistant cells were able to produce subpopulations with distinct transcriptomic states (Kim et al., 2018). Another study with TNBC PDX models of residual tumors that are chemotherapy resistant showed altered DNA methylation and increased expression of anthracycline resistant related genes such as SCL25A30 and NNMT (Gomez-Miragaya et al., 2019). Paclitaxel exposed TNBC cells generated chemoresistant subpopulations with distinct H3K27me3 profiles especially on transposable elements and EZH2 inhibitor treatment re-sensitized these cells to paclitaxel (Deblois et al., 2020). The effect of EZH2 inhibitor combination with paclitaxel also confirmed in murine models of TNBC (Lehmann et al., 2021). However, in another study, decrease in H3K27me3 is associated with capecitabine-resistance (Grosselin et al., 2019). Chromatin remodeling mediated by JUN/AP-1 and ARID1A/BAF complexes were located at the CSC gene enhancer regions in TNBC cells. As described earlier CSCs are highly associated with drug resistance (Bhattacharya et al., 2022).

One of the main reasons of chemoresistance in cancers is elevated *ABCB1* expression as described earlier. This gene has two promoters: one major downstream promoter and another minor upstream promoter. CpG islands around exon 1 and exon 2 of *ABCB1* were demethylated upon long term chemotherapeutic or demethylating agent (eg. 5-azacytidine) exposure leading to the increased expression of ABCB1 (Arrigoni et al., 2016). In addition to DNA methylation changes, alterations in active histone marks such as H3K4me2, H3K4me3, H3K9Ac on the promoter of *ABCB1* has been reported. H3K4me2 mark is regulated by MLL1 and this resulted in increased expression of ABCB1 (Huo et al., 2010). This was the first methyltransferase that is linked to one of

the ABC transporters encouraging the studies focusing on epigenetic regulation of multidrug resistance. It is observed that for activation of ABCB1 via histone acetylation is accompanied by ABCB1 hypomethylation. However, effects of histone acetylation are not as established as the effect of DNA methylation on *ABCB1* promoter. In the clinical practice, use of DNMT and HDAC inhibitors together with chemotherapeutics were shown to be successful for locally advanced breast cancer (Chalakur-Ramireddy & Pakala, 2018). However, using these epigenetic inhibitors is not possible in chemoresistant secondary tumors since almost all of these inhibitors were designed to decrease the oncogene activity with DNMT inhibitors or increase the activity of tumor suppressors with HDAC inhibitors. In the case of ABCB1, both drug classes would increase the expression of ABCB1. Therefore, specific therapies need to be established to treat multi-drug resistant cells.

1.8 CRISPR/Cas9 mediated knockout screens

The clustered regularly interspaced short palindromic repeats (CRISPR)–CRISPR-associated protein 9 (Cas9) system has been identified as a bacterial immune system against bacteriophage infection (**Figure 1.10**). In CRISPR locus, there are repetitive sequences (repeats) and in between them there are non-repetitive (spacer) sequences. Cas proteins are also located in Cas operon nearby the CRISPR locus. In front of the Cas operon, trans-activating CRISPR RNA (tracr-RNA) encodes a homologous noncoding RNA to repeat sequences.

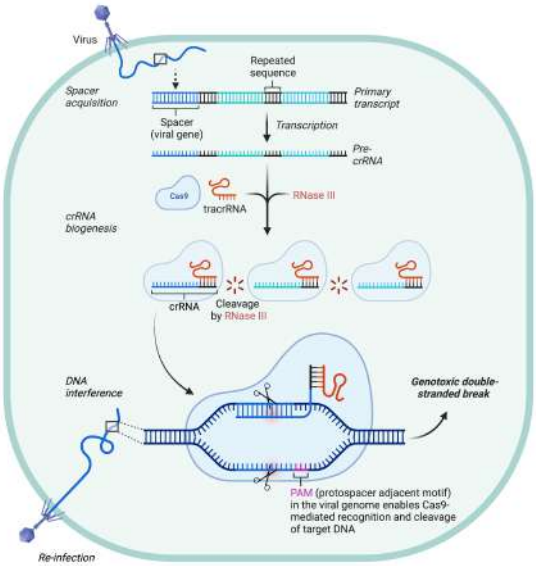

Figure 1.10: CRISPR/Cas system as a bacterial defense mechanism. Figure adapted from biorender.com

When a bacteriophage infects, a new spacer, a part of the phage genome, is incorporated into the CRISPR locus. Later, all repeats together with the spacers are transcribed into a long precursor CRISPR RNA (pre-crRNA). tracrRNA and pre-crRNA anneals together and cleaved by RNaseIII to form mature crRNA. Then nucleases trim the 5' end of crRNAs producing 20 nucleotide long guide sequences. When an infection occurs, these guide sequences bind to Cas proteins and direct it to the foreign organism's DNA to cleave it. Cas proteins also requires a specific sequence called protospacer adjacent motif (PAM) for DNA binding (Jiang & Doudna, 2017; Jinek et al., 2012)

After its discovery, this machinery was adapted to perform RNA guided DNA targeting for various research purposes. For ease-of-use, a chimeric single guide RNA (sgRNA) combining crRNA and tracrRNA was develop that retain the ability to bind to Cas9. By designing 20 nucleotide sgRNAs, any place in genome with a nearby PAM sequence can be targeted with Cas9 and generates double-stranded breaks. These breaks are repaired by two mechanisms: homology directed repair (HDR) or non-homologous end joining (NHEJ). HDR is the precise correction of DNA however it occurs very rarely in cells. NHEJ is the preferred repair system by the cells but it is error-prone and randomly deletes or inserts nucleotides (indels) while repairing. These indels disrupt the gene's open-reading frame resulting a knockout (Ma et al., 2016). Since it is a fast, effective and easy-to use high-troughput approach, it rapidly substituted the RNAi screens (Doudna & Charpentier, 2014; Evers et al., 2016). The generation of multiplexed sgRNA libraries to study gene functions gained momentum after first two successful genome-wide knockout screens (Shalem et al., 2014; Wang et al., 2014). In different biological contexts, essential genes were identified through negative selection screens (Hart et al., 2015; Wang et al., 2015). Although genome-wide screens are effective tools on studying various phenotypes, the library generation and execution of the screens are laborious. In addition, secondary screens with a more focused approach are performed to validate the results of genome-wide screens. Focused libraries allow inclusion of a greater number of sgRNAs targeting a gene compared to genome-wide libraries. Additionally, focused libraries may be useful in scenarios where the starting number of cells are limited as in case of primary cell lines, PDX models or *in vivo* screens (Chen et al., 2015; Manguso et al., 2017; Sanson et al., 2018; Szlachta et al., 2018). To date, various focused sgRNA libraries targeting microRNAs (Kurata & Lin, 2018), kinases (Chen et al., 2019; Tarumoto et al., 2018), nuclear proteins (Szlachta et al., 2018), epigenetic modifiers (Halaburkova et al., 2020;

Henser-Brownhill et al., 2017; Li et al., 2020) or genes belonging to specific pathway such as DNA damage response (Su et al., 2020) were generated.

1.9 Aim of the study

In this thesis, we aimed to identify chromatin regulators of TNBC cell fitness and chemotherapy resistance mainly in three parts.

First, we generated an epigenome-wide CRISPR/Cas9 based knockout library (EPIKOL) to systematically interrogate the functions of epigenetic modifiers in different cellular contexts. After performing quality check analysis of EPIKOL, we performed EPIKOL screens on three TNBC cell lines and one non-malignant cell line to identify TNBC specific chromatin regulators of cell fitness.

Second, we generated taxol- or doxorubicin-resistant TNBC cell lines as models to study chemotherapy resistance in TNBC. We characterized our chemotherapy resistant TNBC cell lines via functional assays and RNA sequencing.

Third, we investigated the epigenetic modifiers that regulate chemotherapy resistance through EPIKOL screens on our taxol- and doxorubicin-resistant TNBC cells. Alternatively, we performed an epigenetic probe library screen on our taxol resistant cells. We validated the effect of candidate genes on chemotherapy resistance through functional assays.

Chapter 2

MATERIALS and METHODS

2.1 Cell Culture

MDA-MB-231, SUM159PT and SUM149PT TNBC cell lines, human mammary epithelial cells (HMLE), and HEK293T cells were kind gifts from Robert Weinberg (MIT, Boston, USA). MDA-MB-231 and HEK293T cells were propagated in DMEM (Gibco, USA) supplemented with 10% fetal bovine serum (Gibco, USA) and %1 Penicillin/Streptomycin (Gibco, USA). SUM159PT and SUM149PT cell lines were propagated in Ham's F12 nutrient mix (Gibco, USA) supplemented with 5% FBS, 5 µg/ml insulin (Sigma-Aldrich, USA), 1 µg/ml hydrocortisone (Sigma-Aldrich, USA) and 10 mM HEPES (Thermo Fisher, USA). HMLE cells were propagated in the MEGM medium (Bierie et al., 2017). Cells were maintained in a humidified incubator at 37ºC with 5% CO_2 level.

2.2 Generation of Epigenetic Knockout Library

Our custom *Epi*genetic *K*nock*o*ut *L*ibrary (EPIKOL) was designed and generated in KUTTAM with the collaborative efforts of three research groups supervised by Prof. Tuğba Bağcı-Önder, Prof. Tamer Önder, and Assoc. Prof. Nathan A. Lack. A list of epigenetic modifiers was curated from the EpiFactors database (Medvedeva et al., 2015). EPIKOL contains 7870 sgRNAs that target 719 epigenetic modifiers, 25 context-specific genes (nuclear receptors, ABC transporters, apoptosis or metastasis-related proteins), 35 essential genes (ribosomal, cell cycle-related) in addition to 80 non-targeting sgRNAs. Each gene in EPIKOL is targeted by 10 sgRNAs used in previously established genome-wide knockout libraries (Doench et al., 2016; Sanjana et al., 2014). In the case of overlapping sgRNAs in these libraries, additional sgRNAs were designed using CCTop and E-CRISP tools (Heigwer et al., 2014; Stemmer et al., 2015). Cloning of sgRNA

oligonucleotides was performed by Dr. Alişan Kayabölen into two lentiviral backbones, lentiCRISPRv2 (Addgene #52961) and lentiGuide-Puro (Addgene #52963).

2.3 PCR amplifications from EPIKOL plasmids

sgRNA distribution in EPIKOL plasmid pools was determined by adding Illumina adapter sequences. 10 ng template DNA were mixed with 0.5 µl Phusion High-Fidelity DNA Polymerase (NEB, USA), 10 µl 5x GC Buffer (NEB, USA), 1 µl dNTP mix (10 mM each) (Thermo Fisher,USA), 2 µl Forward Stagger Mix (10 µM) and 2 µl Reverse Index Primer (10 µM) specific to each backbone and Nuclease-free water (NEB,USA) up to 50 µl. PCR was performed with following conditions: denaturation for 30 s at 98°C, followed by (10 s at 98°C, 15 s at 63°C, 20 s at 72°C) for 16 cycles, final extension for 4 mins at 72°C. PCR products were run on 2% agarose gel and amplicons were extracted from gel using NucleoSpin Gel and PCR clean-up (Macherey-Nagel, Germany) kit according to manufacturer's instructions.

2.4 Viral Packaging, concentration and titration

For lentiviral packaging, 2,5 x 10^6 Hek293T cells were seeded to 10-cm plates. Next day, 2500 ng target plasmid, 2250 ng psPAX2 (Addgene 12260) and 225 ng VSV-G (Addgene 8454) plasmids were mixed in 200 µl serum-free DMEM. DNA mixture was then added to 200 µl serum-free DMEM containing 15 µl Fugene6 (Roche Applied Science). DNA-Fugene mixture was distributed to 10 cm plates as 400 ul drop by drop. After 16 hours, media was changed. Supernatant containing viral particles was collected 48 hours and 72 hours post-transfection and filtered through 45-µm filters. Viruses were either aliquoted directly or concentrated. To concentrate the viruses, supernatants were mixed with PEG8000 in 10% final concentration (Sigma P2139, dissolved in PBS as 50% (w/v)) for overnight at 4°C. Next day, supernatants were centrifuged at 2500 rpm for 20 min at 4°C and pellets were resuspended with PBS as 100x concentrated [23]. Viruses were stored at -80°C until use.

To calculate viral titers, 2x10^5 cells per well in a 6-well plate were transduced with 10, 1, 10^{-1}, 10^{-2} µl virus in the presence of 8 µg/ml protamine sulphate. After 16 hours, media was changed. Next day, cells in each well was transferred to 10 cm plates in the presence of puromycin. Once the puromycin selection of uninfected cells were complete, transduced cells were counted and compared to uninfected/unselected parental controls.

The viral volume that represents 30-50% transduction efficiency was accepted as MOI ~0.3-0.4.

2.5 CRISPR Screens with EPIKOL

EPIKOL in LentiGuide-Puro backbone (Addgene #52963) was used during screens since it has higher viral titer when compared to plentiCRISPR_v2 (Addgene #52961) backbone. Cas9-expressing stable cell lines were generated by transducing the cells with LentiCas9-blast (Addgene #52962) virus at MOI=1. Cells were selected with blasticidin for at least 5 days. Cas9 stable cells were transduced with EPIKOL at low MOI= (0.3-0.4) with 1000x coverage in the presence of 8 µg/ml protamine sulphate. After 16 hours, media were changed. Next day, cells were passaged in the presence of 2 µg/ml puromycin for HMLE, MDA-MB-231, SUM159PT and SUM149PT cells. Following 3 days of puromycin selection, 8 x 10^6 cells were collected to serve as reference point for sgRNA distribution. Rest of the cells were passaged for 15-16 population doublings. At the end, 8 x 10^6 cells were collected and stored at -80ºC. Negative selection screens with EPIKOL were performed as three biological replicates.

2.6 Genomic DNA isolation and Nested PCR

Genomic DNA (gDNA) was isolated by NucleoSpin Tissue kit (Macherey-Nagel, Germany) by following tissue lysis protocol. High quality gDNA serves as template for amplification of sgRNA cassettes that are integrated into genome. For first round of nested PCR (external PCR), input gDNA amount was calculated as 250x coverage of the EPIKOL library which corresponded to 13.2 µg per sample (assuming 6.6 pg DNA per cell). For each sample, 13.2 µg gDNA was divided into four PCR tubes with 3.3 µg gDNA per 100 µl reaction. In external PCR, 3.3 µg gDNA, 1 µl Phusion High-Fidelity DNA Polymerase (NEB, USA), 20 µl 5x GC Buffer (NEB, USA), 2 µl dNTP mix (10 mM each) (Thermo Fisher,USA), 5 µl Forward External Primer (10 µM), 5 µl Reverse External Primer (10 µM) and Nuclease-free water (NEB,USA) up to 100 µl were mixed on ice. PCR was performed with following conditions: denaturation for 3 mins at 95ºC, followed by (25 s at 95ºC, 20 s at 65ºC, 15 s at 72ºC) for 17 cycles, final extension for 3 mins at 72ºC. PCR reactions were then combined. In the second round (internal PCR), NGS (Illumina) adapters (stagger, index and index read primer sequences) were added at the ends of external PCR amplicons. For internal PCR, 5 µl from combined PCR products were used as a template with 5 µl Forward Stagger Mix (10 µM) and 5 µl Reverse Index

Primer (10 μM) in a 100 ul reaction. Thermal cycler conditions were the same as external PCR except that amplification was carried out for 23 cycles instead of 17. Final amplicons from duplicate internal PCRs were run on 2% Agarose gel and bands around 350 bp were extracted using NucleoSpin Gel and PCR clean-up kit according to manufacturer's instructions. All primer sequences are listed in **Table 2.1**. Next generation sequencing was performed at Genewiz (USA) with at least 10 million reads/sample.

Table 2.1: Primer sequences used in nested PCRs of EPIKOL

Primer	**Sequence (5'-3')**
PLG_Ext_Forward	AATGGACTATCATATGCTTACCGTAACTTGAAAGTATTTCG
PLG_Ext_Reverse	CTTTAGTTTGTATGTCTGTTGCTATTATGTCTACTATTCTTTCC
PLC_v2_Ext_Forward	AATGGACTATCATATGCTTACCGTAACTTGAAAGTATTTCG
PLC_v2_Ext_Reverse	TCTACTATTCTTTCCCCTGCACTGTtgtgggcgatgtgcgctctg
Forward_stag1	AATGATACGGCGACCACCGAGATCTACACTCTTTCCCTACACGA CGCTCTTCCGATCT**A**tcttgtggaaaggacgaaacaccg
Forward_stag2	AATGATACGGCGACCACCGAGATCTACACTCTTTCCCTACACGA CGCTCTTCCGATCT**CT**tcttgtggaaaggacgaaacaccg
Forward_stag3	AATGATACGGCGACCACCGAGATCTACACTCTTTCCCTACACGA CGCTCTTCCGATCT**GAC**tcttgtggaaaggacgaaacaccg
Forward_stag4	AATGATACGGCGACCACCGAGATCTACACTCTTTCCCTACACGA CGCTCTTCCGATCT**TCGA**tcttgtggaaaggacgaaacaccg
Forward_stag5	AATGATACGGCGACCACCGAGATCTACACTCTTTCCCTACACGA CGCTCTTCCGATCT**ATCGC**tcttgtggaaaggacgaaacaccg
Forward_stag6	AATGATACGGCGACCACCGAGATCTACACTCTTTCCCTACACGA CGCTCTTCCGATCT**GTCAGA**tcttgtggaaaggacgaaacaccg
Forward_stag7	AATGATACGGCGACCACCGAGATCTACACTCTTTCCCTACACGA CGCTCTTCCGATCT**TGCATCG**tcttgtggaaaggacgaaacaccg
Forward_stag8	AATGATACGGCGACCACCGAGATCTACACTCTTTCCCTACACGA CGCTCTTCCGATCT**CTACGTGA**tcttgtggaaaggacgaaacaccg
Forward_stag9	AATGATACGGCGACCACCGAGATCTACACTCTTTCCCTACACGA CGCTCTTCCGATCT**ACTCGTGAT**tcttgtggaaaggacgaaacaccg
lenticrisprV2_rev (index1)	CAAGCAGAAGACGGCATACGAGAT**CGTGAT**GTGACTGGAGTTC AGACGTGTGCTCTTCCGATCTgggactgtgggcgatgtgcgctct
rev_index2	CAAGCAGAAGACGGCATACGAGAT**ACATCG**GTGACTGGAGTTC AGACGTGTGCTCTTCCGATCTctactattctttcccctgcactgt
rev_index3	CAAGCAGAAGACGGCATACGAGAT**GCCTAA**GTGACTGGAGTTC AGACGTGTGCTCTTCCGATCTctactattctttcccctgcactgt
rev_index4	CAAGCAGAAGACGGCATACGAGAT**TGGTCA**GTGACTGGAGTTC AGACGTGTGCTCTTCCGATCTctactattctttcccctgcactgt
rev_index5	CAAGCAGAAGACGGCATACGAGAT**CACTGT**GTGACTGGAGTTC AGACGTGTGCTCTTCCGATCTctactattctttcccctgcactgt
rev_index6	CAAGCAGAAGACGGCATACGAGAT**ATTGGC**GTGACTGGAGTTC AGACGTGTGCTCTTCCGATCTctactattctttcccctgcactgt
rev_index7	CAAGCAGAAGACGGCATACGAGAT**GATCTG**GTGACTGGAGTTC AGACGTGTGCTCTTCCGATCTctactattctttcccctgcactgt
rev_index8	CAAGCAGAAGACGGCATACGAGAT**TCAAGT**GTGACTGGAGTTC AGACGTGTGCTCTTCCGATCTctactattctttcccctgcactgt
rev_index9	CAAGCAGAAGACGGCATACGAGAT**CTGATC**GTGACTGGAGTTC AGACGTGTGCTCTTCCGATCTctactattctttcccctgcactgt
rev_index10	CAAGCAGAAGACGGCATACGAGAT**AAGCTA**GTGACTGGAGTTC AGACGTGTGCTCTTCCGATCTctactattctttcccctgcactgt
rev_index11	CAAGCAGAAGACGGCATACGAGAT**GTAGCC**GTGACTGGAGTTC AGACGTGTGCTCTTCCGATCTctactattctttcccctgcactgt
rev_index12	CAAGCAGAAGACGGCATACGAGAT**TACAAG**GTGACTGGAGTTC AGACGTGTGCTCTTCCGATCTctactattctttcccctgcactgt

rev_index13	CAAGCAGAAGACGGCATACGAGAT**TTGACT**GTGACTGGAGTTC AGACGTGTGCTCTTCCGATCTctactattctttcccctgcactgt
rev_index14	CAAGCAGAAGACGGCATACGAGAT**GGAACT**GTGACTGGAGTTC AGACGTGTGCTCTTCCGATCTctactattctttcccctgcactgt
rev_index15	CAAGCAGAAGACGGCATACGAGAT**TGACAT**GTGACTGGAGTTC AGACGTGTGCTCTTCCGATCTctactattctttcccctgcactgt
rev_index16	CAAGCAGAAGACGGCATACGAGAT**GGACGG**GTGACTGGAGTT CAGACGTGTGCTCTTCCGATCTctactattctttcccctgcactgt
rev_index17	CAAGCAGAAGACGGCATACGAGAT**CTCTAC**GTGACTGGAGTTC AGACGTGTGCTCTTCCGATCTctactattctttcccctgcactgt
rev_index18	CAAGCAGAAGACGGCATACGAGAT**GCGGAC**GTGACTGGAGTT CAGACGTGTGCTCTTCCGATCTctactattctttcccctgcactgt
rev_index19	CAAGCAGAAGACGGCATACGAGAT**TTTCAC**GTGACTGGAGTTC AGACGTGTGCTCTTCCGATCTctactattctttcccctgcactgt
rev_index20	CAAGCAGAAGACGGCATACGAGAT**GGCCAC**GTGACTGGAGTT CAGACGTGTGCTCTTCCGATCTctactattctttcccctgcactgt
rev_index21	CAAGCAGAAGACGGCATACGAGAT**CGAAAC**GTGACTGGAGTTC AGACGTGTGCTCTTCCGATCTctactattctttcccctgcactgt
rev_index22	CAAGCAGAAGACGGCATACGAGAT**CGTACG**GTGACTGGAGTTC AGACGTGTGCTCTTCCGATCTctactattctttcccctgcactgt
rev_index23	CAAGCAGAAGACGGCATACGAGAT**CCACTC**GTGACTGGAGTTC AGACGTGTGCTCTTCCGATCTctactattctttcccctgcactgt
rev_index24	CAAGCAGAAGACGGCATACGAGAT**GCTACC**GTGACTGGAGTTC AGACGTGTGCTCTTCCGATCTctactattctttcccctgcactgt
rev_index25	CAAGCAGAAGACGGCATACGAGAT**ATCAGT**GTGACTGGAGTTC AGACGTGTGCTCTTCCGATCTctactattctttcccctgcactgt
rev_index26	CAAGCAGAAGACGGCATACGAGAT**GCTCAT**GTGACTGGAGTTC AGACGTGTGCTCTTCCGATCTctactattctttcccctgcactgt
rev_index27	CAAGCAGAAGACGGCATACGAGAT**AGGAAT**GTGACTGGAGTTC AGACGTGTGCTCTTCCGATCTctactattctttcccctgcactgt
rev_index28	CAAGCAGAAGACGGCATACGAGAT**CTTTTG**GTGACTGGAGTTC AGACGTGTGCTCTTCCGATCTctactattctttcccctgcactgt
rev_index29	CAAGCAGAAGACGGCATACGAGAT**TAGTTG**GTGACTGGAGTTC AGACGTGTGCTCTTCCGATCTctactattctttcccctgcactgt
rev_index30	CAAGCAGAAGACGGCATACGAGAT**CCGGTG**GTGACTGGAGTT CAGACGTGTGCTCTTCCGATCTctactattctttcccctgcactgt
rev_index31	CAAGCAGAAGACGGCATACGAGAT**ATCGTG**GTGACTGGAGTTC AGACGTGTGCTCTTCCGATCTctactattctttcccctgcactgt
rev_index32	CAAGCAGAAGACGGCATACGAGAT**TGAGTG**GTGACTGGAGTTC AGACGTGTGCTCTTCCGATCTctactattctttcccctgcactgt
rev_index33	CAAGCAGAAGACGGCATACGAGAT**CGCCTG**GTGACTGGAGTTC AGACGTGTGCTCTTCCGATCTctactattctttcccctgcactgt
rev_index34	CAAGCAGAAGACGGCATACGAGAT**GCCATG**GTGACTGGAGTTC AGACGTGTGCTCTTCCGATCTctactattctttcccctgcactgt
rev_index35	CAAGCAGAAGACGGCATACGAGAT**AAAATG**GTGACTGGAGTTC AGACGTGTGCTCTTCCGATCTctactattctttcccctgcactgt
rev_index36	CAAGCAGAAGACGGCATACGAGAT**TGTTGG**GTGACTGGAGTTC AGACGTGTGCTCTTCCGATCTctactattctttcccctgcactgt
rev_index37	CAAGCAGAAGACGGCATACGAGAT**ATTCCG**GTGACTGGAGTTC AGACGTGTGCTCTTCCGATCTctactattctttcccctgcactgt
rev_index38	CAAGCAGAAGACGGCATACGAGAT**AGCTAG**GTGACTGGAGTTC AGACGTGTGCTCTTCCGATCTctactattctttcccctgcactgt
rev_index39	CAAGCAGAAGACGGCATACGAGAT**GTATAG**GTGACTGGAGTTC AGACGTGTGCTCTTCCGATCTctactattctttcccctgcactgt
rev_index40	CAAGCAGAAGACGGCATACGAGAT**TCTGAG**GTGACTGGAGTTC AGACGTGTGCTCTTCCGATCTctactattctttcccctgcactgt
rev_index41	CAAGCAGAAGACGGCATACGAGAT**GTCGTC**GTGACTGGAGTTC AGACGTGTGCTCTTCCGATCTctactattctttcccctgcactgt

rev_index42	CAAGCAGAAGACGGCATACGAGAT**CGATTA**GTGACTGGAGTTC AGACGTGTGCTCTTCCGATCTctactattctttcccctgcactgt
rev_index43	CAAGCAGAAGACGGCATACGAGAT**GCTGTA**GTGACTGGAGTTC AGACGTGTGCTCTTCCGATCTctactattctttcccctgcactgt
rev_index44	CAAGCAGAAGACGGCATACGAGAT**ATTATA**GTGACTGGAGTTC AGACGTGTGCTCTTCCGATCTctactattctttcccctgcactgt
rev_index45	CAAGCAGAAGACGGCATACGAGAT**GAATGA**GTGACTGGAGTTC AGACGTGTGCTCTTCCGATCTctactattctttcccctgcactgt
rev_index46	CAAGCAGAAGACGGCATACGAGAT**TCGGGA**GTGACTGGAGTT CAGACGTGTGCTCTTCCGATCTctactattctttcccctgcactgt
rev_index47	CAAGCAGAAGACGGCATACGAGAT**CTTCGA**GTGACTGGAGTTC AGACGTGTGCTCTTCCGATCTctactattctttcccctgcactgt
rev_index48	CAAGCAGAAGACGGCATACGAGAT**TGCCGA**GTGACTGGAGTTC AGACGTGTGCTCTTCCGATCTctactattctttcccctgcactgt

2.7 Screen analysis with MAGeCK

To reveal changes in sgRNA counts at the end of EPIKOL screens, MAGeCK algorithm (version 0.5.8) was used (Li et al., 2014). Reads from paired-end fastq files were counted at the sgRNA level and normalized to library size. Three biological replicates were given as individual input files during sgRNA counting. To identify gene level log fold changes, replicates were combined as one output file for each sgRNA. Combined counts were median normalized by using test function and output files were used for downstream data analysis. For visualization, sgRNA counts were normalized as Read Per Million (RPM) and converted to Log_2 values (Breslow et al., 2018; Sanson et al., 2018). To identify significantly depleted genes, $p<0.05$ cutoff was applied to the gene-level analysis. Kernel density estimation (KDE) plots of the Log2 transformed sgRNA counts were plotted with R using the geom_density function in the ggplot2 package. Pearson correlations were calculated and plotted with R using the pairs.panels function in the psych package. Cumulative density plots were plotted with the stat_ecdf function in ggplot2. Epigenetic complex-based gene sets were curated into .gmt files with the information obtained from the Epifactors database and a comprehensive literature review. MAGeCK analysis of screens and generation of plots with R were performed by Ali Cenk Aksu and Ayşe Derya Cavga. Base files of the epigenetic complex-based gene sets were generated by Ali Cenk Aksu via literature review.

2.8 sgRNA cloning

sgRNAs oligos were ordered with specific overhangs (CACCG for 5', CAAA for 3') to have ends compatible with BsmBI digestion. All sgRNAs were listed in **Table 2.2**. Oligos were annealed by adding 1 µl of 100 µM forward and reverse oligos, 1 µl of T4 ligase buffer with ATP and 0.5 µl of T4 Polynucleotide Kinase in total of 10 µl reaction.

Thermal cycler conditions were 37 ºC for 30 mins, 95 ºC for 5 mins ramping down to 25 ºC (5 ºC/min). Annealed sgRNAs were diluted 1/200 with nuclease-free water.

For backbone preparation, 5 µg LentiGuide-Puro was digested with 2 µl of BsmBI for 4 hours at 55 ºC and run on 0.8% agarose gel. Upper band was gel extracted using MN Gel and PCR clean-up kit. 50 ng of digested plasmid and 1 µl of diluted sgRNAs were mixed in the presence of 1 µl T4 Ligase in 11 µl reaction volume. Mixtures were incubated at 16 ºC for 16 hours and transformed into Stbl3 *E. coli* strain.

Table 2.2: sgRNA sequences used in this study

Target Gene	EPIKOL ID	Forward Sequence (5' to 3')	Reverse Sequence (5' to 3')
ARNTL_g1	epikol_v2_372	CTGGACATTGCGTTGCATGT	ACATGCAACGCAATGTCCAG
ARNTL_g2	epikol_v2_378	TTAGAATATACAGAACACCA	TGGTGTTCTGTATATTCTAA
ASH2L_g1	epikol_v2_424	CCATGACTCACCTCACTATG	CATAGTGAGGTGAGTCATGG
ASH2L_g2	epikol_v2_427	GCTCTACCTCACCCAACTGT	ACAGTTGGGTGAGGTAGAGC
BRD3_g1	epikol_v2_785	CGACGTGACGTTTGCAGTGA	TCACTGCAAACGTCACGTCG
BRD3_g2	epikol_v2_788	GAGGAGAGCTCTTCGGACTC	GAGTCCGAAGAGCTCTCCTC
BRD8_g1	epikol_v2_812	AGGAGGTGATTATCCACTTG	CAAGTGGATAATCACCTCCT
BRD8_g2	epikol_v2_814	ATAAGTACCTATATCTCTCC	GGAGAGATATAGGTACTTAT
BRPF1_g4	epikol_v2_872	AGGGTGACTGCAGGCAACGG	CCGTTGCCTGCAGTCACCCT
BRPF1_g5	epikol_v2_874	CCAACCGCCTGACCATCCAA	TTGGATGGTCAGGCGGTTGG
BRPF1_g6	epikol_v2_880	TGAGTACCTAATGGACCGAC	GTCGGTCCATTAGGTACTCA
CDC16_g1	epikol_v2_7577	TGCTCTAGATAACCGAACCC	GGGTTCGGTTATCTAGAGCA
CDC16_g2	epikol_v2_7578	TTACATGGCACCTAGCTGCA	TGCAGCTAGGTGCCATGTAA
CDK1_g1	epikol_v2_1081	ACCCTTATACACAACTCCAT	ATGGAGTTGTGTATAAGGGTG
CDK1_g2	epikol_v2_1090	TTCGTCATCCAAATATAGTC	GACTATATTTGGATGACGAAC
CHAF1B_g1	epikol_v2_1242	AGACTGAGTTTCACTCCCGA	TCGGGAGTGAAACTCAGTCT
CHAF1B_g2	epikol_v2_1248	TTATGTCCAAGGAGTAACCT	AGGTTACTCCTTGGACATAA
CIT_g1	epikol_v2_1405	CCAGCTTGATGTGTCCTGTG	CACAGGACACATCAAGCTGG
CIT_g2	epikol_v2_1408	GCAGCTAAACCAGCTGACCG	CGGTCAGCTGGTTTAGCTGC
DPY30_g1	epikol_v2_1814	CATGGAGCCAGAGCAGATGC	GCATCTGCTCTGGCTCCATG
DPY30_g2	epikol_v2_1817	GATGCTGGAGGGACAAACGC	GCGTTTGTCCCTCCAGCATC
DR1_g1	epikol_v2_1823	AGTAGCATTAAAAAGAAGAA	TTCTTCTTTTTAATGCTACT
DR1_g2	epikol_v2_1825	CAACGATGCTCGAGAGCTGG	CCAGCTCTCGAGCATCGTTG
ELP3_g1	epikol_v2_1938	TATTCCACCCAGTCTTACAC	GTGTAAGACTGGGTGGAATA
ELP3_g2	epikol_v2_1939	TCCGAGCCACCAATTCAACC	GGTTGAATTGGTGGCTCGGA
ELP5_g1	epikol_v2_1951	ACTGCGCCCCTCCCACTCCA	TGGAGTGGGAGGGGCGCAGT
ELP5_g2	epikol_v2_1960	TGGGGAGCAAGTGCATATCC	GGATATGCACTTGCTCCCCA
EXOSC9_g1	epikol_v2_2132	AACTGACACAAATGGGCATG	CATGCCCATTTGTGTCAGTT
EXOSC9_g2	epikol_v2_2140	TTATAGGCAGTCAGATCTCT	AGAGATCTGACTGCCTATAA
FBL_g1	epikol_v2_2221	ACCAACGATGTCAGAGACAT	ATGTCTCTGACATCGTTGGT

FBL_g2	epikol_v2_2225	CCTGTACACTCCCACGACCA	TGGTCGTGGGAGTGTACAGG
GATAD1_g1	epikol_v2_2352	AGAGTAAGCAGGAAATTCAC	GTGAATTTCCTGCTTACTCT
GATAD1_g2	epikol_v2_2354	CGTGACTTGAAATACTCAGA	TCTGAGTATTTCAAGTCACG
GTF3C4_g1	epikol_v2_2445	GCCATTAGCATCGCAACCCA	TGGGTTGCGATGCTAATGGC
GTF3C4_g2	epikol_v2_2449	TGAGAGTAACAAATTGGACC	GGTCCAATTTGTTACTCTCA
HCFC1_g1	epikol_v2_2461	AGCCACTTACTTATTTCCGA	TCGGAAATAAGTAAGTGGCT
HCFC1_g2	epikol_v2_2466	GGACATTCCCATCACTTACG	CGTAAGTGATGGGAATGTCC
HDAC3_g1	epikol_v2_2525	CCCTATGAAGCCCCATCGCC	GGCGATGGGGCTTCATAGGG
HDAC3_g2	epikol_v2_2530	TGGGTCAATGCCAGGCGATG	CATCGCCTGGCATTGACCCA
HINFP_g1	epikol_v2_2626	CGGGACCACATGCGCAACCA	TGGTTGCGCATGTGGTCCCG
HINFP_g2	epikol_v2_2630	TGACTACTTACGATCCAATG	CATTGGATCGTAAGTAGTCA
ING3_g1	epikol_v2_2873	CTTCACGGAAATGCGCGAGA	TCTCGCGCATTTCCGTGAAG
ING3_g2	epikol_v2_2874	GAATTACAGAAATATTAGAG	CTCTAATATTTCTGTAATTC
JADE3_g1	epikol_v2_2976	CCGCGCTCGCCCTACCGGAG	CTCCGGTAGGGCGAGCGCG G
JADE3_g2	epikol_v2_2980	TCAGCATTGCTTGTCCTGAG	CTCAGGACAAGCAATGCTGA
KANSL1_g1	epikol_v2_3032	AATAAGTCTGTTGTATGCTC	GAGCATACAACAGACTTATT
KANSL1_g2	epikol_v2_3036	CTGTACTGAGCTGTAAGAAG	CTTCTTACAGCTCAGTACAG
KANSL2_g1	epikol_v2_3042	ACATGTCCGTAGGAATGCCC	GGGCATTCCTACGGACATGT
KANSL2_g2	epikol_v2_3043	ACTGTGGATCAGACATGGAG	CTCCATGTCTGATCCACAGT
KANSL3_g1	epikol_v2_3052	CAGACTCAAGGTCTCCACAA	TTGTGGAGACCTTGAGTCTG
KANSL3_g2	epikol_v2_3059	TCTCAGCTCGAATCTTCTCC	GGAGAAGATTCGAGCTGAG A
KAT8_g1	epikol_v2_3122	CAATTTCGTAGTTCCCGATG	CATCGGGAACTACGAAATTG
KAT8_g2	epikol_v2_3129	TTGCCCCCCTACCAACGCCG	CGGCGTTGGTAGGGGGGCA A
KDM2A_g1	epikol_v2_3155	CAACATTGAAGATCGGACAC	GTGTCCGATCTTCAATGTTG
KDM2A_g2	epikol_v2_3158	TATGGCAGGGAGTCGTCGCA	TGCGACGACTCCCTGCCATA
KDM8_g1	epikol_v2_3313	CAGAAAGCAAGGGCGGACC A	TGGTCCGCCCTTGCTTTCTG
KDM8_g2	epikol_v2_3319	TGAAAGGCGTGGCTGACCAC	GTGGTCAGCCACGCCTTTCA
KMT2A_g1	epikol_v2_3332	AGAAAGGACGTCGATCGAGG	CCTCGATCGACGTCCTTTCT
KMT2A_g2	epikol_v2_3338	TCAGAGTGCGAAGTCCCACA	TGTGGGACTTCGCACTCTGA
LAS1L_g1	epikol_v2_3427	GATGAACTTAGACTGCTCTA	TAGAGCAGTCTAAGTTCATC
LAS1L_g2	epikol_v2_3429	GTGACGACCATAAGTTGCAG	CTGCAACTTATGGTCGTCAC
MEN1_g1	epikol_v2_3642	CATGCGCTGTGACCGCAAGA	TCTTGCGGTCACAGCGCATG
MEN1_g2	epikol_v2_3644	CCAGGCATGATCCTCAGACA	TGTCTGAGGATCATGCCTGG
MLLT6_g1	epikol_v2_3711	AATCTCAGGAGCGAGCAGCC	GGCTGCTCGCTCCTGAGATT
MLLT6_g2	epikol_v2_3713	AGCTTGCTATGGCATCGTTC	GAACGATGCCATAGCAAGCT
NAT10_g1	epikol_v2_3962	CAACGAGACCCACAAGATCC	GGATCTTGTGGGTCTCGTTG
NAT10_g2	epikol_v2_3968	TGTTCACCCAGATTATCAAG	CTTGATAATCTGGGTGAACA
NIPBL_g1	epikol_v2_4102	CTTTAGCTTGATATGCAACG	CGTTGCATATCAAGCTAAAG
NIPBL_g2	epikol_v2_4108	TATACGAACTAACCTCCATG	CATGGAGGTTAGTTCGTATA
NT1	epikol_v2_7791	ACGGAGGCTAAGCGTCGCAA	TTGCGACGCTTAGCCTCCGT
PAXIP1_g1	epikol_v2_4304	GAGGTCAAGTATTACGCGGT	ACCGCGTAATACTTGACCTC
PAXIP1_g2	epikol_v2_4305	GCACACAAGTTAATCAACCC	GGGTTGATTAACTTGTGTGC

PPP2CA_g1	epikol_v2_4633	AATAAAAGTCATACCTCATG	CATGAGGTATGACTTTTATT
PPP2CA_g2	epikol_v2_4638	GGTATATCTCCTCGAGGAGC	GCTCCTCGAGGAGATATACC
PPP4C_g1	epikol_v2_4643	CGATCAGGATAGCGAACCTG	CAGGTTCGCTATCCTGATCG
PPP4C_g2	epikol_v2_4649	TGGATGTCGCCGCACACCTG	CAGGTGTGCGGCGACATCCA
PRMT1_g1	epikol_v2_4907	GGATGTCATGTCCTCAGCGT	ACGCTGAGGACATGACATCC
PRMT1_g2	epikol_v2_4909	GTGGATGCCAAAGTGTGCGT	ACGCACACTTTGGCATCCAC
PRMT5_g1	epikol_v2_4923	CAGCATACAGCTTTATCCGC	GCGGATAAAGCTGTATGCTG
PRMT5_g2	epikol_v2_4929	TCTTCCATCCGCGTTTCAAG	CTTGAAACGCGGATGGAAGA
PRPF31_g1	epikol_v2_4971	AAGCAAGCCAAAGCTTCAGA	TCTGAAGCTTTGGCTTGCTT
PRPF31_g2	epikol_v2_4975	CTGCGCTCACCTTGACCGTG	CACGGTCAAGGTGAGCGCAG
RBBP4_g1	epikol_v2_5109	TCTTGGAACCCAAATCTCAG	CTGAGATTTGGGTTCCAAGA
RBBP4_g2	epikol_v2_5110	TCTTTGTTGCGATGATACAA	TTGTATCATCGCAACAAAGA
RBBP5_g1	epikol_v2_5114	CCAGATAGATACCACTCCAC	GTGGAGTGGTATCTATCTGG
RBBP5_g2	epikol_v2_5117	GGCAGCAATAGGGTCCACGC	GCGTGGACCCTATTGCTGCC
RBBP7_g1	epikol_v2_5124	CAGGATTACATTCTCCACTT	AAGTGGAGAATGTAATCCTG
RBBP7_g2	epikol_v2_5129	TCTGCGGCATGTAACGAGCA	TGCTCGTTACATGCCGCAGA
RPL11_g1	epikol_v2_7725	GCTGTCCACTGCACAGTTCG	CGAACTGTGCAGTGGACAGC
RPL11_g2	epikol_v2_7728	TGTCCACTGCACAGTTCGAG	CTCGAACTGTGCAGTGGACA
RUVBL1_g1	epikol_v2_7789	GTGAACAAGTACATCGACCA	TGGTCGATGTACTTGTTCAC
RUVBL1_g2	epikol_v2_7790	TCCCCTTCTGCCCAATGGTG	CACCATTGGGCAGAAGGGGA
RUVBL2_g1	epikol_v2_5305	CTCTACCTGCCGAGGCTCCA	TGGAGCCTCGGCAGGTAGAG
RUVBL2_g2	epikol_v2_5310	TGGCTGTGAATGGCGTGTCA	TGACACGCCATTCACAGCCA
SFPQ_g1	epikol_v2_5612	ATGATCGTGGAAGATCTACA	TGTAGATCTTCCACGATCAT
SFPQ_g2	epikol_v2_5616	TCATCCTCCGTGATATCAGC	GCTGATATCACGGAGGATGA
SMARCE1_g1	epikol_v2_5843	ACCAACAGCCGGGTCACGGT	ACCGTGACCCGGCTGTTGGT
SMARCE1_g2	epikol_v2_5847	TATGTAAGCAAGGTACGCGG	CCGCGTACCTTGCTTACATA
SS18L2_g1	epikol_v2_6012	ACTGCACGCACTCGTTCCCG	CGGGAACGAGTGCGTGCAGT
SS18L2_g2	epikol_v2_6014	CCTCAGCCAGTCCGGTACGA	TCGTACCGGACTGGCTGAGG
SUPT16H_g1	epikol_v2_6056	CCCATCCTCCTTTACAGCGA	TCGCTGTAAAGGAGGATGGG
SUPT16H_g2	epikol_v2_6059	TGACGTGTATAACGCTGTCA	TGACAGCGTTATACACGTCA
TOP2A_g1	epikol_v2_6533	ATTCAGTACCAAATTTACTG	CAGTAAATTTGGTACTGAAT
TOP2A_g2	epikol_v2_6539	TGTACGCTTATCCTGACTGA	TCAGTCAGGATAAGCGTACA
TRRAP_g1	epikol_v2_6624	CCACTGGGGATCGTTCAGTG	CACTGAACGATCCCCAGTGG
TRRAP_g2	epikol_v2_6629	TGGTGTCAAGACAATCACGT	ACGTGATTGTCTTGACACCA
USP7_g1	epikol_v2_6962	AGACCACACCAAAAAAGCGT	ACGCTTTTTTGGTGTGGTCT
USP7_g2	epikol_v2_6967	GGCAGTAGAACAGCTCGATG	CATCGAGCTGTTCTACTGCC
VPS72_g1	epikol_v2_6992	CATAAGAAGCGGAAGTGCCC	GGGCACTTCCGCTTCTTATG
VPS72_g2	epikol_v2_6999	TGACGCATAGACTTCCGACC	GGTCGGAAGTCTATGCGTCA
WDR5_g1	epikol_v2_7026	GAACTTCACAAAAGACACGG	CCGTGTCTTTTGTGAAGTTC
WDR5_g2	epikol_v2_7027	GGCACGCACCTTGCTCTGAG	CTCAGAGCAAGGTGCGTGCC

WDR82_g1	epikol_v2_7046	TACCATGTTGGAACACGCAC	GTGCGTGTTCCAACATGGTA
WDR82_g2	epikol_v2_7047	TCTCCGGTCTCCTAACTGCC	GGCAGTTAGGAGACCGGAGA
YEATS4_g1	epikol_v2_7124	AGCTATGGCAATCCTTTAAG	CTTAAAGGATTGCCATAGCT
YEATS4_g2	epikol_v2_7126	CAGCTTTAGCAAATGATACA	TGTATCATTTGCTAAAGCTG

2.9 *Dual Color Competition Assay*

To validate the effects of candidate genes from EPIKOL screens, cell growth competition assays were performed. Cas9-stable cells were transduced with either PGK-H2BmCherry (Addgene #21217) or PGK-H2BeGFP (Addgene #21210) viruses at MOI ~5. mCherry+ cells were transduced with LentiGuide-NT1 viruses, while eGFP+ cells were transduced with viruses carrying sgRNA of interest for selected genes. 2 different sgRNAs per gene were used. Following 3 days of puromycin selection, mcherry or eGFP labeled cells were mixed in a 1:1 ratio and seeded as triplicates to 24-well plates. Next day, images from 9 different positions were taken with a 4x objective in Cytation5 (Biotek, USA) as Day0 measurements. Cells were imaged every 4 days. Number of mCherry+ and eGFP+ cells were counted from images using Gen5 software (BioTek, USA) and each measurement was normalized to Day0 to determine the percentage of eGFP+ cells.

2.10 *Colony formation assay*

To assess long term growth capabilities, cells were seeded in 6-well plates as 750-1000 cells/well for naïve cells depending on the experiment and as 1500 cells/well for resistant cells. For sgRNA containing experiments, cells were seeded after puromycin selection. Next day, drug treatments were performed as indicated in each experiment. 72 hours later, fresh media were given to each well and cells were allowed to grow for 10-14 days. At the end of the incubation period, media were discarded, cells were washed with PBS and fixed with ice-cold 100% methanol for 5 minutes. Methanol was discarded and cells were stained with crystal violet for 15 minutes. Quantification of colonies was performed by using ImageJ.

2.11 *Western Blotting*

For apoptosis markers, cells were collected with the media that they were growing in. For other experiments, media were discarded, cells were washed with PBS, collected and stored at -80 ^{o}C. For whole cell lysate, pellets were dissolved in NP-40 lysis buffer (50mM Tris Buffer pH 7.4, 250mM NaCl, 5mM EDTA, 50mM NaF, 1%NP40, 0.02% NaN3,

1mM PMSF) for 30 mins by vortexing every 10 minutes. For nuclear and cytosolic fractionation, nuclear lysis buffer (20 mM HEPES pH 7.9, 0.4 M NaCl, 1 mM EDTA, 10 % Glycerol, 1x Protease inhibitor) and cytosolic lysis buffer (10 mM HEPES pH 7.9, 10 mM KCl, 0.1 mM EDTA, 0.4 % NP-40, 1x Protease inhibitor) were used. Cells were dissolved in cytosolic lysis buffer for 15 mins on ice and centrifuged for 3 mins at 3000xg at 4 ^{o}C twice and supernatant was collected as cytosolic fraction. Pellets were washed with cytosolic lysis buffer twice, dissolved in nuclear lysis buffer and sonicated on ice (amplitude 40; 2x10 sec). Samples were centrifuged at 15000xg for 5 mins at 4^{o}C and supernatants were collected as nuclear fraction. Protein concentrations were determined by Pierce's BCA Protein Assay Kit (Thermo Scientific, 23225, USA).

50µg protein for each sample were mixed with 4X Laemni sample buffer (Biorad, 1610747, USA) containing 10% beta-mercaptoethanol and incubated at 95°C for 10 minutes. Samples were loaded and run on a 4-12% Mini Protean TGX Precast Gel (Biorad, 456-1044, USA). Proteins were transferred onto PVDF membrane via Bio-RadTrans-Blot® Turbo™ Transfer System (Bio-Rad, USA). The membrane was blocked with 5% non-fat dry milk in TBS-T for one hour at room temperature. Then, membrane was incubated with primary antibodies, overnight on a shaker at 4ºC. Antibodies used in this study were listed in **Table 2.3**. After washing three times with TBS-T, membranes were incubated with HRP-conjugated secondary antibodies diluted 1:10000 in TBS with 5% non-fat dry milk. SuperSignal™ West Femto Maximum Sensitivity Substrate (Thermo Scientific, 34095, USA) were used for signal detection in ChemiDoc XRS+ System (Biorad, USA). C-PARP detection for SS18L2 and NSL complex members was performed by Göktuğ Karabıyık. C-PARP detection upon BRPF1 inhibitors and taxol combination was performed by Dr. Ahmet Cingöz.

Table 2.3: Antibody List

Antibody	**Brand, Cat no**
GAPDH	Abcam ab9485
PARP	Abcam, ab74290
Goat anti-rabbit	Abcam, ab97051
BRPF1	Novus, NBP2-15620
ABCB1	Cell Signaling, E1Y7S
HA	Biolegend, 16B12
H3	Abcam, ab9049
LaminB1	Abcam, ab16048

2.12 Annexin V/Dead Cell Assay

Annexin V staining was performed with Muse® Annexin V & Dead Cell Kit (Luminex, MCH100105) according to the manufacturer's instructions. Briefly, 75 000 cells were collected with their media and centrifuged at 1200 rpm for 5 minutes. After washing with 500 µl of cold PBS with 1% FBS, pellet resuspended in 75 µl of cold PBS with 1% FBS and mixed with 75 µl of Annexin V & Dead Cell Reagent. Samples were incubated at room temperature for 20 minutes and analyzed with Muse Cell Analyzer (Merck, Darmstadt, Germany) with 5000 events per sample. Gates were determined according to parental cells. AnnexinV/Dead cell assay for SS18L2 and NSL complex members was performed by Ezgi Yağmur Kala.

2.13 Cell Cycle Analysis

$1x10^6$ cells were collected and washed with PBS. Pellet was resuspended in 100 µl PBS. Cell suspension was added drop by drop into the freshly prepared, cold 1 ml 70% Ethanol while vortexing for fixation. Samples were kept in -20˚C for 24 hours. 200 µl of fixed cells were washed with PBS twice and were resuspended in 150 µl of Muse Cell Cycle Reagent (The Muse® Cell Cycle Kit (Luminex, MCH100106)). Samples were incubated with the reagent at room temperature for 30 minutes in the dark and run through the Muse Cell Analyzer (Merck, Darmstadt, Germany) with 10,000 events per sample and analyzed with the Muse Cell Analyzer software. Gates were determined according to parental cells. Cell cycle analysis for SS18L2 and NSL complex members was performed by Ezgi Yağmur Kala.

2.14 PIP-FUCCI cell cycle assay

pLenti-CMV-Blast-PIP-FUCCI (Addgene #138715) plasmid was used for the analysis of cell cycle transitions. Cells were transduced with PIP-FUCCI viruses with high MOI for stable expression. Then, cells were transduced with non-targeting sgRNA or sgRNA-X carrying viruses. After puromycin selection, cells were seeded to 6-well plates. Phase contrast and fluorescent images were captured as 2x2 with 10x objectives using Cytation5 (Biotek, USA) for 4 days. Cells expressing PCNA-interacting protein (PIP) degron appeared as green due to fused mVenus fluorescent protein during G1 and G2/M phases (Grant et al., 2018). On the other hand, cells expressing mCherry-Gem_{1-110} appeared as red with increasing intensity during S and G2/M phases. During G2 phase, overlapping double positive signals were more nuclear while during M phase the cells had both

fluorescent signals more diffusely expressed due to the disassembly of the nuclear envelope. G2/M-arrested cells were quantified by counting the mCherry+ cells in mVenus+ population and presented as the ratio of mVenus+ population.

2.15 RNA sequencing and transcriptome analysis

Total RNAs were isolated by using MN Nucleospin RNA isolation kit according to manufacturer's instructions. Library preparation and sequencing for SS18L2 and BRPF1 knockout experiments and BRPF1 inhibitor treatments were performed at University of Oxford (Oxford, UK). Other Parental-Resistant pair samples were sequenced at BGI (Hong Kong). Briefly, single-indexed and multiplexed samples were run on an Illumina Next Seq 500 sequencer using a NextSeq 500 v2 kit (FC-404–2005; Illumina, Can Diago, CA) for paired-end sequencing. Sequencing length was 42 bp. The sequencing data was then aligned to the GENCODE human transcriptome reference (GRCh38) using STAR (Dobin et al., 2013). SALMON was then used to quantify the transcripts for each sample based on the Transcripts Per Million (TPM) method (Patro et al., 2017). DESeq2 was used to identify differentially expressed genes between cells infected with NT1 carrying or SS18L2 sgRNA carrying lentiviruses (Love et al., 2014). For SS18L2 knockout experiment, differentially expressed genes (DEGs) were defined with a threshold for Log_2FoldChange>1 (up-regulated) or Log2FoldChange<-1 (down-regulated) and false discovery rate (FDR)<0.01. For parental-resistant comparisons, (DEGs) were defined with a threshold for Log_2FoldChange>2 (up-regulated) or Log_2FoldChange<-2 (down-regulated) and p<0.001. For drug or sgRNA treated T1-160 cells, DEGs were determined as the genes that have padj<0.05. Gene set enrichment analysis was performed with Log_2FoldChange rank-ordered gene lists by using GSEA software and all available gene sets from MsigDB (Subramanian et al., 2007).

2.16 Quantitative Real Time PCR

1000 ng total RNA per sample was melted with 1 µl of 100 µM random hexamers and 2.5 µl of 2 mM in 16.5 µl final volume. The mixture was incubated at 65 ºC for 5 mins and transferred to ice. For reverse transctiption mixture, 5 µl of 5x First strand buffer, 2 µl of 0.1 M DTT and 0.5 µl of RNAsin were added and samples were incubated at RT for 10 mins. After addition of 1 µl of M-MLV Reverse transcriptase (Invitrogen), samples were incubated at 37 ºC for 1 hour and 70 ºC for 15 minutes for heat-inactivation. Complementary DNAs (cDNAs) were diluted by adding 75 µl of Nuclease-free water. 2

µl of cDNAs were mixed with 10 µl SYBR-Green Master Mix (Roche) and 1 µl of 100 µM primer mix in total of 20 µl reaction volume. Samples were run on a Lightcycler 480 Instrument II (Roche). Following thermal cycler conditions were repeated for 40 cycles: 30 sec at 95 ºC, 30 sec at 60 ºC and 30 sec at 72 ºC. All genes were normalized to GAPDH and relative quantification values were calculated with $2^{-DeltaCT}$ method. List of primers can be found in **Table 2.4**.

Table 2.4: qPCR primer sequences

Target Gene	Forward Sequence (5' to 3')	Reverse Sequence (5' to 3')
SS18L2	AAGAGACTATCCAGCGGCTCC	GCTGGTTGGACTGGCATCTG
BRPF1	CCACACTGAAGATGCAGCCGA	CCGCAGTGCCGTCATCTCTT
ABCB1	ACAGAGGGGATGGTCAGTGT	TCACGGCCATAGCGAATGTT
ABCC1	CCGCTCTGGGACTGGAATG	ATGTAGCCTCGGTCATGTCG
ABCG2	CTGAGATCCTGAGCCTTTGG	AAGCCATTGGTGTTTCCTTG
ABCC3	TATGCCCCCGATGAGGACCA	GACAGGGCACTCAGCTGTCTCA
GAPDH	AGCCACATCGCTCAGACAC	GCCCAATACGACCAAATCC

2.17 In vivo EPIKOL Screen

All in vivo experiments were approved by Koç University Animal Experiments Ethics Committee. Cas9-expressing MDA-MB-231 cells were transduced with Firefly Luciferase (Fluc) expressing lentiviruses. Cells were transduced with EPIKOL at low MOI=(0.3-0.4) with 1000x coverage in the presence of 8 µg/ml protamine sulphate. Following three days of puromycin selection, an initial timepoint pellet was collected as $8x10^6$ cells. Remaining cells in DMEM-10% FBS were mixed with Matrigel (354277, Corning) in 1:1 ratio aiming for $8x10^6$ cells in total of 150 µl per injection. Six 8-weeks old Nude mice were used. Tumor cells were injected subcutaneously into both flanks of each mouse and monitored using IVIS Lumina III (Perkin Elmer, USA) weekly following intraperitoneal 150 µg/g body weight of D-Luciferin injection. At 2- and 4-weeks post-injection, three mice were sacrificed, and tumors were fresh-frozen in liquid nitrogen. Whole tumors were grinded using pestles. Genomic DNAs from homogenized tumors were isolated using NucleoSpin Tissue kit as described above. Nested PCRs for library amplification of 3 out of 6 tumors for each timepoint were performed as described above. 16.5 µg gDNA was used per tumor to account for the gDNA that might be coming from the basement membrane that is covering the tumors.

2.18 *In vivo validation experiments*

MDA-MB-231-Cas9-Fluc cells were infected with either NT1 or SS18L2 sgRNA carrying viruses and selected with puromycin for 3-4 days. After selection, cells were mixed with Matrigel (354277, Corning) in a 1:1 ratio aiming for $4x10^6$ cells in total of 100 µl per injection. Eight Nude mice were injected subcutaneously with tumors carrying NT1 and SS18L2 sgRNA in the left and right flank, respectively. Tumor growth was monitored using IVIS Lumina III (Perkin Elmer, USA) weekly following intraperitoneal 150 µg/g body weight of D-Luciferin injection.

2.19 *Resistant Cell Generation*

Cells were seeded as $2x10^5$ cells/well in 6 well plates. Next day, cells were treated with either IC_{10} or IC_{50} values of drugs for 3 days as starting concentrations. When the cells became confluent under drug treatment, concentrations were doubled. If cells did not look healthy or were too sparse, they were taken into drug free environment until they form colonies. When the cells started to become confluent, last concentration of drug was applied again and procedure was followed as explained above. Alongside, DMSO treated parental cell lines were aged as controls. Drug treatment was continued until significant difference between IC_{50} values of parental and resistant cell lines was obtained.

2.20 *Cell Viability Assay*

Cells were seeded into 96 well black plates as 2000 cells/well for SUM159PT and MDA-MB-231 cell lines, 4000 cells/well for SUM149PT cell line in triplicates for each condition. Next day, cells were treated with corresponding chemical. For IC_{50} determination experiments, Taxol (Paclitaxel, Sigma) and Doxorubicin (Sigma) was serially diluted as 3.16 fold (starting from 10 µM to 0.1 nM). After 72 hours of treatment with indicated chemical, media were discarded, 40 µl media mixed with 4 µl Cell Titer-Glo (Promega) and distributed to each well as 44 µl. Plates were shaken 2 minutes and incubated at room temperature for 8 minutes, luminescence were read by a plate reader (Synergy H1 Reader, Bio-Tek). Results were analyzed by using GraphPad Prism 8. First, drug concentrations were transformed to Log_{10} (concentration). Then non-linear regression function was applied to calculate IC_{50} values by using 'log(inhibitor) vs. response – variable slope (four parameters)'.

2.21 Calcein Assay

Calcein-AM is a membrane permeable dye that is converted to a fluorescent calcein by intracellular esterases. It is also a substrate for P-Glycoprotein (Pgp, *ABCB1*). Increased Pgp expression enhances the efflux of Calcein-AM and decreases fluorescence signal. Cells were seeded as 65 000 cells/well in 24 well-plate. Next day, cells were treated with 10 µM Verapamil for 30 minutes at 37ºC. Calcein-AM was added in final concentration of 125 nM and cells were incubated for another 30 minutes at 37ºC. Images were taken with phase contrast and GFP filters as 2x2 with 10x objective using Cytation5 (BioTek, USA). Quantification of green fluorescence was performed in Synergy H1 Plate Reader (BioTek, USA).

2.22 Epigenetic Probe Library Screen

Chemical probe library targeting wide range of epigenetic modifiers consists of 118 drugs (**Table 2.5)**. Library was a kind gift from SGC, University of Oxford in collaboration with Dr. Udo Oppermann. Cells were seeded as 750 cells/well in 384 well-plates. Next day, cells were treated with epigenetic probes alone or in combination with taxol (2,5 nM for Parental, 300 nM for T1-160 and 500 nM for T2-450). Epigenetic probes were added at 1:1000 dilution in triplicate as in the final concentrations indicated in **Table 2.5**. 72 hours later, cell viability was measured by using CellTiter-Glo and results were normalized to untreated controls.

Table 2.5: List of epigenetic probes in library

No	Source Name	Class/Target	[Working] uM
1	AMI-1	Arginine methyltransferase - PRMT	50
2	SGC707	Arginine methyltransferase - PRMT3	1
3	TP-064	Arginine methyltransferase - PRMT4	1
4	TP-064N	Arginine methyltransferase - PRMT4	1
5	MS049	Arginine methyltransferase - PRMT4, PRMT6	1
6	MS409N	Arginine methyltransferase - PRMT4, PRMT6	1
7	GSK591	Arginine methyltransferase - PRMT5	1
8	LLY-283	Arginine methyltransferase - PRMT5	1
9	MS023	Arginine methyltransferase - Type I PRMTs	1
10	GSK8814	Bromodomains - ATAD2	10
11	GSK8815	Bromodomains - ATAD2	10
12	GSK2801	Bromodomains - BAZ2A, BAZ2B	1
13	BAZ2-ICR	Bromodomains - BAZ2A, BAZ2B	1
14	BAY-299	Bromodomains - BRD1, TAF1	1

15	RVX-208	Bromodomains - BRD2, BRD3, BRD4, BRDT (BET, BD2)	5
16	(+)-JQ1	Bromodomains - BRD2, BRD3, BRD4, BRDT (BET)	1
17	PFI-1	Bromodomains - BRD2, BRD3, BRD4, BRDT (BET)	5
18	I-BET	Bromodomains - BRD2/3/4	1
19	I-BRD9	Bromodomains - BRD9	10
20	TP-472	Bromodomains - BRD9	1
21	TP-472N	Bromodomains - BRD9	1
22	LP99	Bromodomains - BRD9, BRD7	1
23	BI-9564	Bromodomains - BRD9, BRD7	1
24	GSK6853	Bromodomains - BRPF1/2/3	1
25	GSK9311	Bromodomains - BRPF1/2/3	1
26	PFI-4	Bromodomains - BRPF1B	1
27	CBP/BRD4 (0383)	Bromodomains - CBP, BRD4(1)	5
28	NVS-CECR2-1	Bromodomains - CECR2	1
29	NVS-CECR2-C	Bromodomains - CECR2	1
30	I-CBP112	Bromodomains - CREBBP, EP300	1
31	SGC-CBP30	Bromodomains - CREBBP, EP300	1
32	(-)-JQ1 (inactive)	Bromodomains - Negative control	1
33	Bromosporine	Bromodomains - pan-Bromodomain	1
34	OF-1	Bromodomains - pan-BRPF	5
35	NI-57	Bromodomains - pan-BRPF	1
36	GSK4027	Bromodomains - PCAF, GCN5	1
37	GSK4028	Bromodomains - PCAF, GCN5	1
38	L-Moses	Bromodomains - PCAF, GCN5	1
39	D-Moses	Bromodomains - PCAF, GCN5	1
40	SMARCA	Bromodomains - SMARCA, PB1	2.5
41	PB1/SMARCA	Bromodomains - SMARCA, PB1	1
42	PFI-3	Bromodomains - SMARCA2/4, PB1(5)	1
43	TRIM24/BRPF	Bromodomains - TRIM24/BRPF	10
44	GSK864	Dehydrogenase	5
45	5-Azacitidine	DNA methyltransferase (DNMT) -	10
46	5-Azadeoxycitidine	DNA methyltransferase (DNMT) - DNMT1/3	5
47	CXD101	HDAC -	1
48	PCI-24781	HDAC -	10
49	Romidepsin	HDAC -	1
50	Mocetinostat	HDAC -	10
51	CI-994	HDAC - 1,2,3,(8)	1
52	Valproic acid	HDAC - aliphatic acid compounds	1000
53	RGFP966	HDAC - HDAC3	10
54	Rocilinostat	HDAC - HDAC6	10
55	Tubastatin A HCl	HDAC - HDAC6	10
56	PCI-34051	HDAC - HDAC8	5

57	Belinostat	HDAC - hydroxamic acids	5
58	SAHA	HDAC - hydroxamic acids	2.5
59	Trichostatin A	HDAC - hydroxamic acids - Class I & II	0.5
60	Entinostat	HDAC - ortho-amino anilides	0.5
61	EX 527	HDAC - SIRT1	1
62	SRT1720	HDAC - SIRT1 (indirect?) activator	1
63	AGK2	HDAC - SIRT2	10
64	TMP269	HDAC -4, 5, 7 &9	10
65	TMP195	HDAC -4,5,7,9	1
66	Santacruzamate	HDAC 2?	50
67	C646	Histone acetyltransferase (HAT) p300/CBP	1
68	A-485	Histone acetyltransferase (HAT) p300/CBP	1
69	A-486	Histone acetyltransferase (HAT) p300/CBP	1
70	Methylstat (Ester)	Histone demethylase	2.5
71	KDOBA67	Histone demethylase	10
72	KDM5-C70	Histone demethylase - JARID1	10
73	ML324	Histone demethylase - JMJD2E	5
74	(E)-JIB-04	Histone demethylase - Pan JmjC	0.05
75	SGC0946	Histone methyltransferase - DOT1L	7.5
76	GSK343	Histone methyltransferase - EZH2	3
77	UNC1999	Histone methyltransferase - EZH2	1
78	UNC2400	Histone methyltransferase - EZH2	1
79	CPI-360	Histone methyltransferase - EZH2 and EZH1	10
80	CPI-169	Histone methyltransferase - EZH2, EZH1	10
81	UNC0642	Histone methyltransferase - G9a, GLP	1
82	UNC0638	Histone methyltransferase - G9a, GLP	1
83	A-366	Histone methyltransferase - G9a, GLP	2
84	PFI-2	Histone methyltransferase - SETD7	2
85	LLY-507	Histone methyltransferase - SMYD2	1
86	BAY-598	Histone methyltransferase - SMYD2	1
87	PFI-5	Histone methyltransferase - SMYD2	1
88	Chaetocin	Histone methyltransferase - SUV39H1	0.05
89	A-196	Histone methyltransferase - SUV420H1/H2	1
90	K00135	Kinase inhibitor - ATP competitive - PIM	1
91	5-Iodotubercidin	Kinase inhibitor - ATP mimetic - Haspin	1
92	SGI-1776	Kinase inhibitor - Haspin	10
93	CHR-6494	Kinase inhibitor - Haspin	1
94	KDOAM-25a	Lysine demethylases - JARID	1
95	KDOAM32	Lysine demethylases - JARID	1
96	GSK J4	Lysine demethylases - JMJD3, UTX, JARID1B	10
97	KDOPZ-32a	Lysine demethylases - KDM5	1
98	Tranylcypromine	Lysine demethylases - LSD1	20
99	GSK-LSD1 (irreversible)	Lysine demethylases - LSD1	0.5

100	GSK2879552	Lysine demethylases - LSD1	10
101	GSK J5 (inactive)	Lysine demethylases - Negative control	10
102	IOX1 (5-carboxy-8HQ)	Lysine demethylases - pan-2-OG	40
103	KDOOA012000	Lysine demethylases KDM2	1
104	A-395	Methyl Lysine Binder - EED	1
105	A-395N	Methyl Lysine Binder - EED	1
106	UNC1215	Methyl Lysine Binder - L3MBTL3	5
107	OICR-9429	Methyl Lysine Binder? - WDR5	1
108	TDO20824a	Methyl Lysine Binder/tudor domain -Spin1	1
109	TDO20826a	Methyl Lysine Binder/tudor domain -Spin1	1
110	GSK484	Peptidyl arginine deiminase (PAD4)	1
111	GSK106	Peptidyl arginine deiminase (PAD4)	1
112	Olaparib	Poly ADP ribose polymerase (PARP)	1
113	Rucaparib	Poly ADP ribose polymerase (PARP)	10
114	IOX2	Prolyl-Hydroxylases - PHD2 (EGLN1)	10
115	MAZ1805		1
116	MAZ1392		1
117	Bortezomib		0.1
118	Carfilzomib		0.1

2.23 *siRNA experiments*

Cells were seeded as 300 000 cells/well in 6-well plates. Next day, Lipofectamine 3000 (Invitrogen, USA) transfection was performed according to manufacturer's instructions. Briefly, one mixture containing 125 µl optimem with 7.5 µl Lipofectamine 3000 Reagent and another mixture containing 125 µl optimum with 1 pmol of BRPF1 siRNA were prepared and vortexed well. siRNA mixture was added onto Lipofectamine 3000 mixture and incubated for 15 minutes. Final mixture was added to the cells dropwise and 8 hours later fresh media were given. Next day, cells were trypsinized and seeded for cell viability or colony formation assays.

2.24 *Cloning of BRPF1 into dTAG construct*

Coding sequence of BRPF1 was amplified from GFP-BRPF1 plasmid (Addgene #65382) with the addition of N-term SalI and C-term XbaI cut sites by using Phusion polymerase. Later, both the amplified PCR products and the pENTR1A plasmid (Addgene #17398) was cut with SalI and XbaI for 2 hours at 37^{o}C. Ligation reaction was performed overnight at 16^{o}C by using T4 Ligase in 1:1 ratio for insert and backbone. Ligation products was transformed, and colonies were picked for diagnostic digest. Later, successfully cloned plasmids were used for LR Clonase Mix as well as the pLEX-305-C-

dTAG plasmid (Addgene #91798) and transformation was performed to pick plasmids that have BRPF1 insertion.

2.25 ChIP-qPCR

Cells were cross-linked with formaldehyde (37%) and cross-linking was stopped by glycine (2.5 M). The suspension was centrifuged, and pellet was washed with cold PBS twice. The pellet was resuspended in ChIP Lysis Buffer Buffer (10 mM Tris; 1 mM EDTA; 140 mM NaCl; 1% Triton X-100; 0.1% Na-deoxycholate; 1% SDS; 1 mM PMSF; Protease Inhibitor Coctail) and incubated on ice. Samples were sonicated (power setting high) with a Bioruptor Sonicator. The sonicated samples were centrifuged and the supernatant containing the sheared chromatin was collected. Some of the sheared chromatin was separated for the assessment of chromatin shearing. The sheared chromatin is decross-linked and the DNA was isolated following the protocols of the ChIP clean-up kit (Zymo Research) prior to agarose gel electrophoresis. This procedure resulted in DNA fragment sizes of 100-500bp.

Dynabeads protein G magnetic beads were washed with PBS-T, the washed magnetic bead suspension was separated using a magnetic rack. For the pre-clearing of the lysate, the chromatin preparation was incubated with magnetic beads. Anti-HA-Tag Antibody (Biolegend, US) and a non-specific IgG antibody were incubated with magnetic beads. The magnetic bead-antibody complex was incubated with pre-cleared chromatin preparation overnight. The magnetic beads were washed with low-salt buffer (0.1% SDS, 1% Triton-X 100, 2 mM EDTA, 20 mM Tris-HCl, 140 mM NaCl, pH 8.1), high salt buffer (0.1% SDS, 1% Triton-X 100, 2 mM EDTA, 20 mM Tris-HCl, 500 mM NaCl, pH 8.1), LiCl-containing buffer (0.25 M LiCl, 1% IGEPAL-CA 630, 1% deoxycholic acid, 1 mM EDTA, 10 mM Tris, pH 8.1), Tris-EDTA solution, respectively. Elution buffer (1% SDS and 0.1M NaHCO3) was added to the magnetic beads. The DNA was separated with a magnetic rack after 15 minutes of incubation. After incubation with Rnase A, NaCl (5 M), and proteinase K, ChIP samples were isolated by following the ChIP clean-up kit (Zymo Research) protocols.

Primers were designed for regions on the chromatin that are thought to be bound by BRPF1 (with 75-100 bp PCR product) using UCSC Genome Browser (https://genome.ucsc.edu/) and Ensembl Genome Browser (https://www.ensembl.org/index.html) (**Table 2.6**). For the quantitative and simultaneous analysis of immunoprecipitated DNA, qPCR was performed using 2× SYBR green dye

(Roche), with a LightCycler 480 (Roche) device. ChIP qPCR results were calculated by % input method. Input sample represents the amount of chromatin used in ChIP. 50% of the initial chromatin was used as input. For the initial input ratio of 50%, the dilution factor is 2, and since the log 2 base of 2 equals 1, 1 is subtracted from the Ct value of the input DNA.

Table 2.6: List of primers used in ChIP-qPCR

Gene	Forward primer (5' to 3')	Reverse primer (5' to 3')
ABCB1- promoter region -658 bp	AGCCTGGGGCTCCTTTTACT	GGTGGCAAACTCTTCACATCAG
RUNX2-acetylation	GGAAACGGAGGGGTCTGAAC	TAAGAGCTGGTTTCGCCGTC
Chr 12 Gene Desert	TGTACAGGGCCTGGTTACCCACA	AGGAGGGCCTAGCTGGTGTCAT

2.26 Statistical Analysis

Analysis of EPIKOL data was performed by using RRA method in MAGeCK. Unless otherwise stated, P values were determined by two-tailed Student's t-test for all experiments in GraphPad Prism8, *P<0.05, **P<0.01, ***P<0.001.

2.27 Data Availability

EPIKOL screen and SS18L2 Knockout RNA sequencing data are deposited to the NCBI GEO database with the accession number GSE17389.

Chapter 3

RESULTS

3.1 EPIKOL Screens in naïve TNBC cell lines

3.1.1 Representation analysis of EPIKOL

To study the effect of epigenetic modifiers in different cellular contexts, an epigenome-wide pooled CRISPR library was generated with the combined efforts of Bağcı-Önder Lab, Önder Lab and Lack Lab at KUTTAM. Epigenetic Knockout Library (EPIKOL) includes 7870 sgRNAs targeting 719 epigenetic modifiers, 25 context-specific controls and 35 pan-essential genes along with 80 non-targeting controls (**Figure 3.1A**) in two different lentiviral backbones. First, library complexity and sgRNA distribution was assessed by sequencing the plasmid pools. Both libraries in two different plasmids had normal distribution of sgRNAs (**Figure 3.1B**) and they were highly correlated (**Figure 3.1C**).

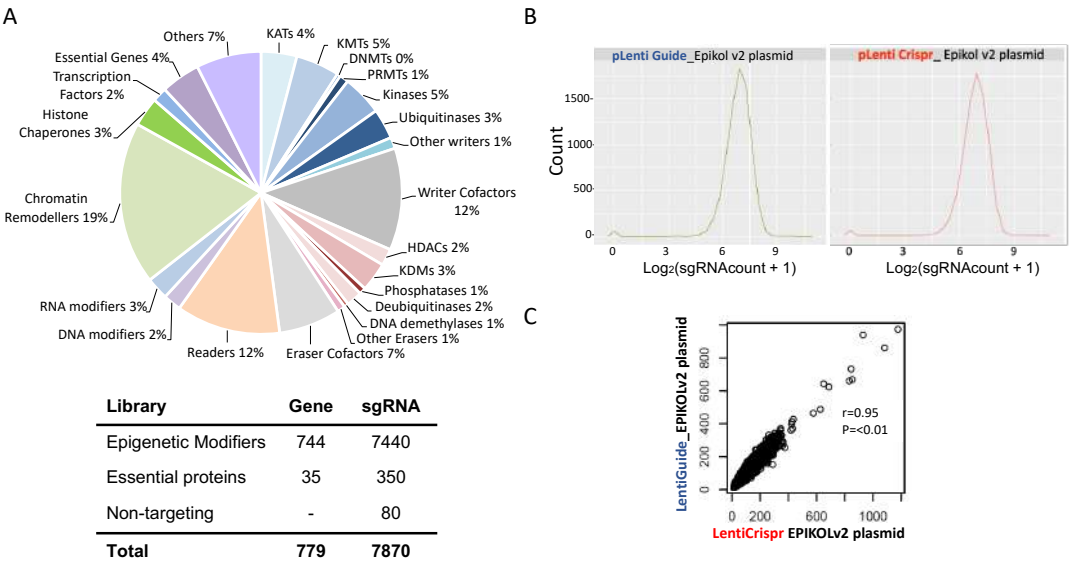

Library	Gene	sgRNA
Epigenetic Modifiers	744	7440
Essential proteins	35	350
Non-targeting	-	80
Total	**779**	**7870**

Figure 3.1: Details of Epigenetic knockout library (EPIKOL). A. Composition of EPIKOL and number of sgRNAs/gene. **B.** Density plots for EPIKOL in LentiGuide or LentiCRISPRv2 backbone. **C.** Correlation plot for two backbones.

Then, viral libraries were produced from LentiGuide_ EPIKOL and transduced into MDA-MB-231 cells. Samples were collected and sequenced following puromycin selection. After transduction, EPIKOL maintained its normal distribution (**Figure 3.2A**) and was highly correlated with the plasmid pool (**Figure 3.2B**) At the end of the screen, significant depletion upon knockout of essential genes were observed, while there was no change in non-targeting controls (**Figure 3.2C**)

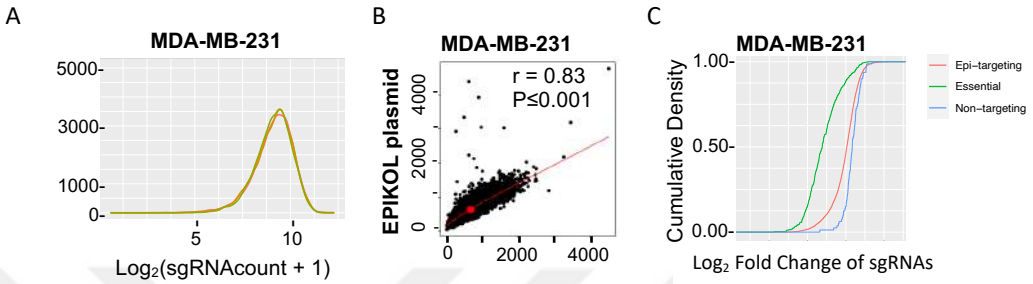

Figure 3.2: Quality check of EPIKOL. A. sgRNA density for MDA-MB-231 cells infected with lentiGuide_EPIKOL virus. **B.** Correlation analysis of plasmid library and samples from EPIKOL-infected MDA-MB-231 cells at initial timepoints. **C.** Cumulative density plots showing differential depletion of sgRNAs targeting essential genes when compared to non-targeting sgRNAs.

3.1.2 In vitro EPIKOL screens on TNBC Cell lines

To uncover the epigenetic modifiers that have role in TNBC cell fitness, negative-selection (drop-out) screens were performed. Three different triple negative breast cancer (TNBC) cell lines MDA-MB-231, SUM149PT and SUM159PT were screened in addition to non-malignant human mammary epithelium cells (HMLE). In each screen, Cas9-expressing cells were transduced with EPIKOL in LentiGuide backbone at low MOI (0.4) to ensure that every cell was infected with only one virus. Coverage of the library was 1000x to prevent introducing bias during the screen. After puromycin selection, initial samples were collected for sequencing. Cells were allowed to grow for extra 2-3 days for completion of the knockouts. Then, cells were cultured for 16 population doublings to determine the essential epigenetic factors for cell fitness (**Figure 3.3**). At the end, samples were collected and sent to next generation sequencing (NGS).

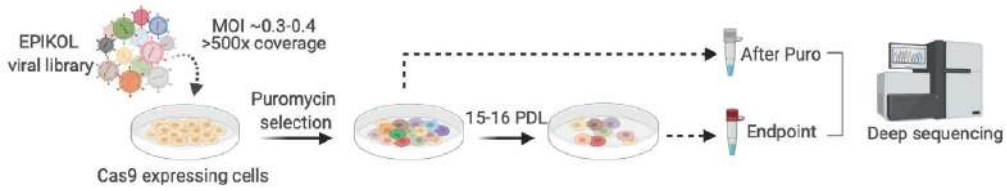

Figure 3.3: EPIKOL screen strategy on naive TNBC cells.

After sequencing, initial quality controls of the screens were performed. Principal Component Analysis (PCA) revealed that all screens in TNBC cells were separated from the control cell line HMLE (**Figure 3.4A**). While biological replicates of each timepoint collected together, initial and final timepoints of the cell lines were separated from each other. Then, we checked Log_2 transformed sgRNA read counts for each sample. As expected, non-targeting sgRNAs were found around the diagonal since they did not have any effect on cells. sgRNAs targeting essential genes were found below the diagonal indicating that they had lower number of read counts at the final timepoint since the cells carrying those sgRNAs were lost from the pool (**Figure 3.4B**).

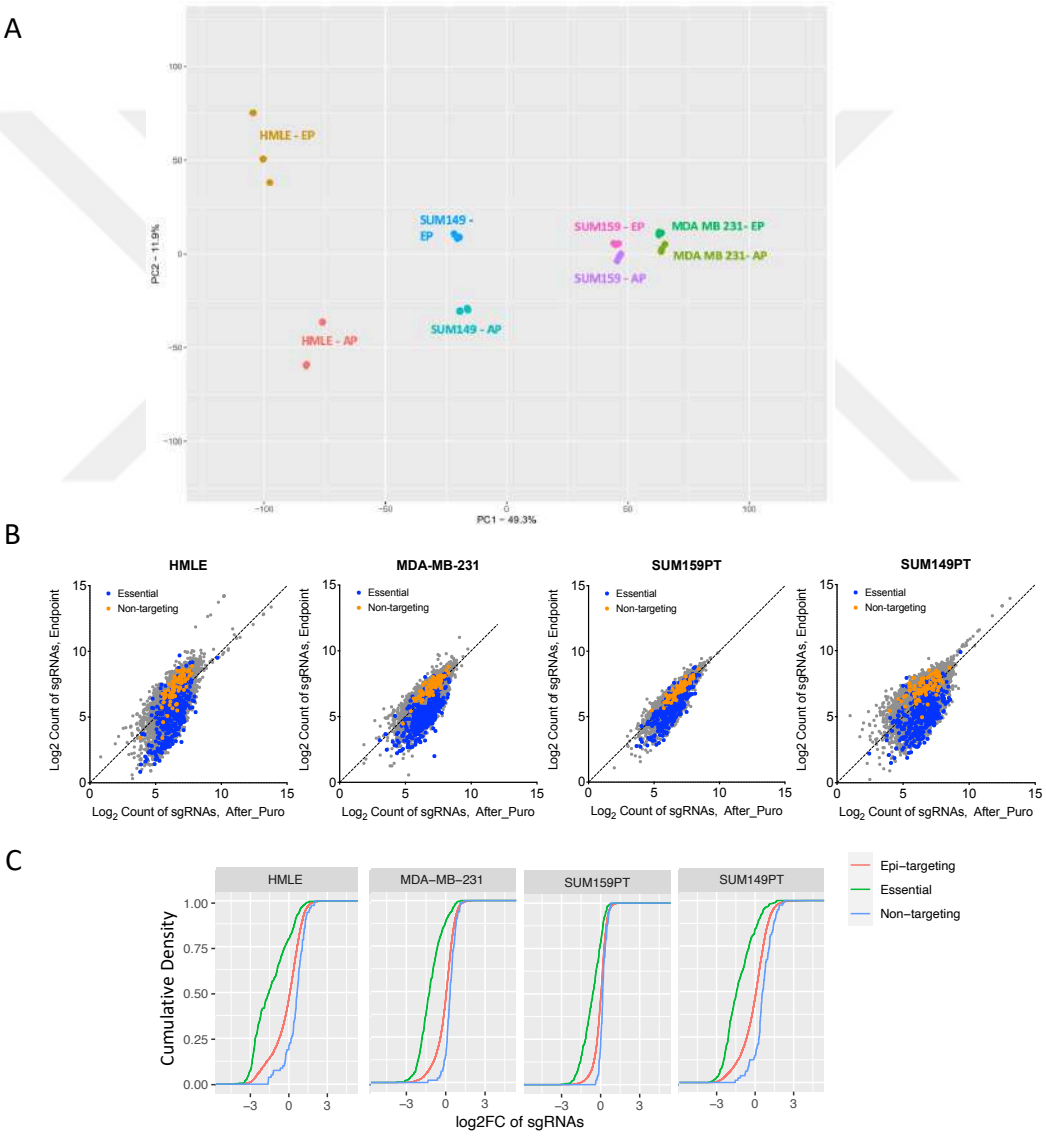

Figure 3.4: Quality control of EPIKOL screens. A. Principal component analysis (PCA) of EPIKOL screens on four different cell line. **B.** sgRNA distributions of EPIKOL screens on TNBC cells. Read counts of initial and final timepoints were normalized as read per million and Log_2 transformed. **C.** Cumulative density of read counts at initial and final time points showing epi-targeting essential and non-targeting sgRNAs.

Similarly, cumulative density plots showed that essential and epi-targeting sgRNAs had lower read counts at final time point when compared to non-targeting sgRNAs. These results indicated that positive and negative controls work as expected during the EPIKOL screens (**Figure 3.4C**).

After these initial quality check of the screens, MAGeCK analysis was performed with median normalization to understand depletions in gene levels. For this, three biological replicates were analyzed together. Almost all essential genes were depleted at the end of the screens while the non-targeting sgRNAs remained unchanged or slightly enriched due to their null effect (**Figure 3.5**). A number of genes were significantly ($p<0.05$) depleted in each screen, HMLE (129), MDA-MB-231 (140), SUM149PT (140) and SUM159PT (98). Among these genes, there were previously known epigenetic modifiers such as PRMT5 (Vinet et al., 2019), HDAC3 (Cui et al., 2018), NPM1 (Malfatti et al., 2019) that regulate TNBC cell fitness serving as positive controls. These results indicated that EPIKOL screens are suitable for the identification of essential epigenetic modifiers of cancer cell fitness.

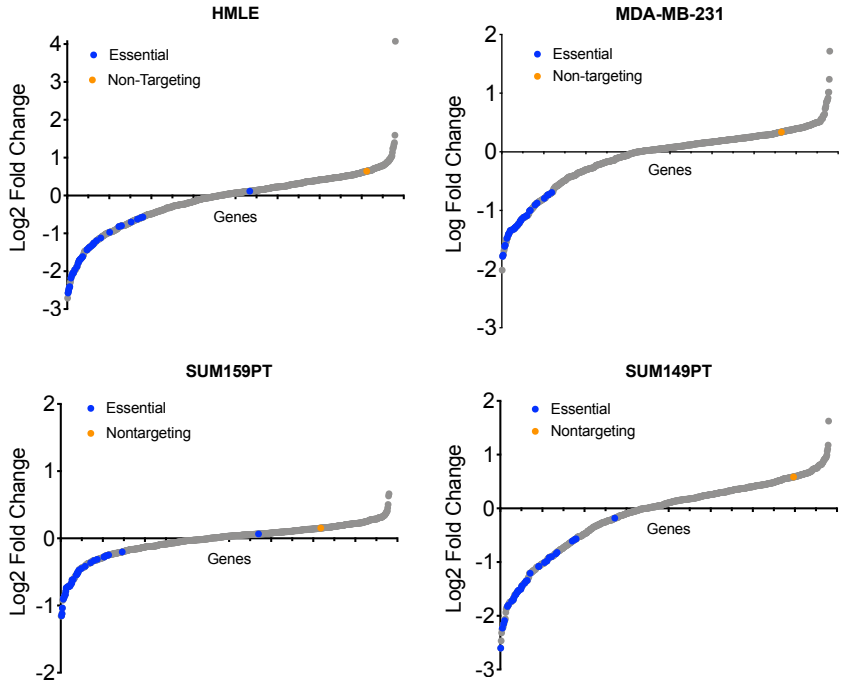

Figure 3.5: Waterfall plots showing gene level depletions in EPIKOL screens after 16 population doublings. sgRNA counts of three biological replicates were used as input for the test function of MAGeCK to reveal depleted genes.

To unravel novel epigenetic modifiers of TNBC cell fitness, genes that were commonly depleted in at least two TNBC cell lines but not in control cell line HMLE were identified (**Figure 3.6A**). From this, 15 genes were found that includes some of the previously known regulators of cancer cell fitness such as UHRF1 (Gao et al., 2017), PELP1

(Zhang et al., 2015) and PRMT1 (Liu et al., 2019). Additionally, to make hit selection process easier, Dr. Ali Cenk Aksu curated epigenetic complex-based gene sets for the genes that are found in EPIKOL to perform Gene Set Enrichment Analysis (GSEA). When MDA-MB-231 EPIKOL screen results were run on GSEA with these newly curated gene sets, several epigenetic modifier complexes such as MLL and COMPASS-like, RNA exosome, Pol2 elongator and NSL were found to be significantly depleted (**Figure 3.6B**).

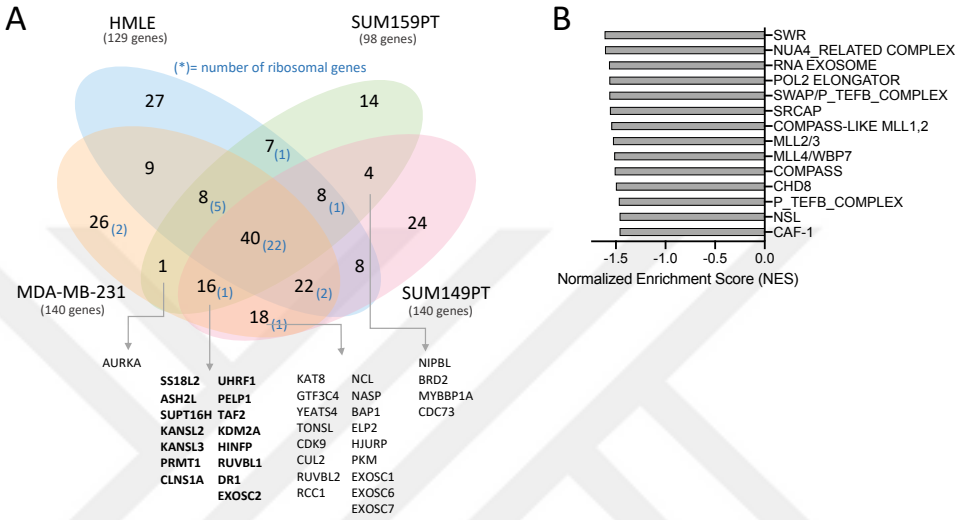

Figure 3.6: Commonly depleted genes in TNBC cells and gene set enrichment analysis of depleted genes. A. Venn diagram shows significantly depleted genes ($p<0.05$) at least in two different TNBC cell line but not in HMLE. 15 genes that are written as bold are depleted in all TNBC cell lines. Blue numbers in parenthesis indicate the number of depleted essential genes in that section. **B.** GSEA analysis of MDA-MB-231 EPIKOL screen results with our custom curated epigenetic modifier gene sets.

Negative rankings, p values and $\log_2$ fold changes of the genes depleted in at least two TNBC cell line were listed in (**Figure 3.7**). These genes have higher negative rankings in HMLE cells with higher p-values indicating that they act specifically on the fitness of TNBC cell lines. In order to validate our screen results, around 40 genes were selected depending on their rankings, p values and commonalities in TNBC cells or they were members of the complexes that are shown in (**Figure 3.6B**). Some of the selected genes were also significantly depleted in HMLE.

3.1.3 Validations of selected hit genes on TNBC Cell lines

For validation experiments, 2 sgRNAs per gene were cloned into lentiGuide backbone. Cas9-stable TNBC cell lines were transduced with either H2B-mCherry or H2B-eGFP viruses for dual-color competition assays.

	MDA-MB-231			SUM159PT			SUM149PT			HMLE		
Gene name	neg|p-value	neg|rank	neg|lfc	neg|p-value	neg|rank	neg|lfc	neg|p-value	neg|rank	neg|lfc	neg|p-value	neg|rank	neg|lfc
RUVBL1	4.93E-06	9	-1.2681	0.028151	84	-0.33415	0.00019231	24	-1.7492	0.30672	272	-0.27871
HINFP	4.93E-06	14	-1.1119	0.039492	89	-0.32195	6.41E-05	16	-1.1825	0.058664	139	-0.75289
SS18L2	5.42E-05	28	-1.1303	0.0064053	45	-0.2988	0.0023028	61	-2.0545	0.10475	177	-0.93795
ASH2L	0.00015286	39	-0.95472	0.01106	55	-0.46822	0.0035158	69	-1.0705	0.27843	264	-0.49674
DR1	0.00042899	49	-0.89452	0.0052022	41	-0.5353	0.020863	115	-0.60154	0.084009	160	-0.52542
TAF2	0.00083333	52	-0.43539	0.027589	83	-0.39133	0.0084566	88	-1.0468	0.23968	250	-0.27448
PELP1	0.0014645	60	-0.85055	0.017017	67	-0.40574	4.93E-06	10	-2.3183	0.088733	166	-0.86348
SUPT16H	0.0015039	61	-1.2189	0.015705	64	-0.43096	6.41E-05	17	-1.8564	0.10209	173	-0.84125
CLNS1A	0.0028748	74	0.14235	0.017214	68	0.0099127	0.028624	120	0.011903	0.35523	293	-0.30404
EXOSC2	0.010843	99	-0.91797	0.014946	63	-0.33348	4.93E-06	3	-1.368	0.10143	172	-0.7132
KDM2A	0.014852	103	-0.81744	0.00029093	12	-0.57385	0.0057939	77	-1.2149	0.61751	396	0.10866
KANSL2	0.026001	117	-0.79885	0.024157	77	-0.39328	0.0018393	53	-1.4002	0.55753	368	-0.1469
UHRF1	0.03179	123	-0.70279	0.013092	58	-0.32654	0.012559	101	-1.0483	0.2258	242	-0.50466
KANSL3	0.039433	129	-0.59969	0.0065828	46	-0.45279	0.00090237	41	-2.2486	0.067372	148	-0.98416
PRMT1	0.046938	138	-0.55997	0.0025838	29	-0.36709	0.0009714	43	-1.5209	0.222	239	-0.60903
EXOSC6	0.00021203	42	-0.7901	0.089078	121	-0.42542	0.016928	108	-0.93679	0.18359	227	-0.66443
TONSL	0.0081509	94	-0.80641	0.19658	183	-0.087145	0.013565	104	-0.74039	0.45097	326	-0.23277
GTF3C4	0.00012327	34	-1.1141	0.26071	197	-0.16404	4.93E-06	5	-1.7789	0.12643	194	-0.77296
CDK9	0.0026085	71	-1.2074	0.18793	179	-0.11172	0.0090483	91	-1.4154	0.14257	202	-0.61889
CUL2	0.028752	120	-0.49495	0.17937	178	-0.16755	0.010084	92	-1.2957	0.16055	216	-0.80706
YEATS4	0.002569	70	-0.87147	0.11097	137	-0.23088	0.0066913	80	-1.211	0.08104	155	-0.38521
EXOSC1	4.93E-06	16	-0.94008	0.080823	117	-0.05632	0.012786	102	-0.72232	0.68685	419	0.033908
PKM	0.0023915	68	-0.78689	0.51449	305	-0.031398	0.049679	140	-0.80898	0.081346	157	-0.61913
RUVBL2	0.013161	101	-1.3338	0.13922	160	-0.30914	0.0087327	90	-1.1984	0.071386	153	-0.77932
RCC1	0.0032495	77	-0.75353	0.34419	227	-0.05565	0.013693	105	-0.95282	0.068052	149	-0.79128
NCL	0.0013067	56	-0.96073	0.059334	107	-0.084656	0.008072	85	-0.90413	0.069344	150	-0.70708
NASP	0.033072	125	-0.60561	0.6184	364	0.017517	0.038516	128	-0.66542	0.31956	282	-0.2213
BAP1	0.0085947	95	-0.8368	0.84323	548	0.13179	6.41E-05	18	-1.817	0.51639	350	0.12746
EXOSC7	0.018585	109	-0.81579	0.50106	294	0.051091	0.012086	99	-0.76419	0.18324	226	-0.01879
ELP2	0.0054882	83	-0.88998	0.46147	274	-0.067739	0.039038	129	-0.68892	0.31299	275	-0.53498
KAT8	0.020577	113	-0.46457	0.13358	158	-0.032634	0.0023718	65	-1.5685	0.051267	131	-0.40913
HJURP	0.040104	131	-0.19635	0.098871	127	-0.1432	0.0032495	68	-1.1976	0.14761	207	-0.81796
AURKA	0.0058235	84	-1.0412	0.011711	56	-0.43689	0.1547	196	-0.4305	0.15986	214	-0.75095
DPY30	0.13521	181	-0.27058	0.009788	53	-0.28356	0.052145	143	-0.78777	0.39489	306	0.39433
NIPBL	0.058023	143	-0.51763	0.019532	70	-0.16533	0.0022239	59	-1.1629	0.10569	179	-0.80944
BRD2	0.89513	489	0.12309	0.039709	90	-0.26285	0.041908	131	-0.70242	0.28668	267	-0.26685
VPS72	0.22141	210	-0.48207	0.053575	101	-0.35867	0.0047781	73	-0.93205	0.06533	146	-0.93364
MYBBP1A	0.16285	194	-0.49397	0.0080128	49	-0.18712	0.049384	139	-1.0017	0.4706	332	-0.18477
CDC73	0.099926	161	-0.51652	0.0041469	38	-0.03932	0.0004783	36	-1.1135	0.22575	241	-0.48531

Figure 3.7: neg|p-value, neg|rank and neg|lfc values of candidate genes for each cell line that were obtained after MaGeCK analysis of EPIKOL screens. Selection of TNBC specific hit genes for further follow-up requires low rank in three TNBC cell line and relatively intermediate ranking in HMLE cell.

H2B-mCherry cells were transduced with Non-targeting sgRNA carrying viruses (NT1) while the H2B-eGFP cells were transduced with sgRNA of interest. Cells were mixed in a 1:1 ratio and followed for 16 days (**Figure 3.8A**). **Figure 3.8B** shows the selected genes, cell lines in which they are significantly depleted, function of the gene and their average depletion scores at day8 and day16. Most significant depletion ratios during the competition assays were observed in MDA-MB-231 cell lines, followed by SUM149PT and SUM159PT. This is in line with the Log2 fold changes observed during EPIKOL screens (Fig5). Positive controls (RPL11, CDC16) and proof of concept genes (TOP2A, PRMT5) showed significant depletions over 16 days. As indicated in the GSEA analysis (Fig6B), the most significantly depleted complex members belong to NuA4 complex (YEATS4, VPS72, RUVBL2), Pol2 Elongator complex (ELP3, ELP5), MLL/COMPASS complex (ASH2L, WDR5, RBBP5), and NSL complex (KANSL2, KANSL3, KAT8). Strong depletions observed in selected genes verified the reliability of our EPIKOL screens.

A

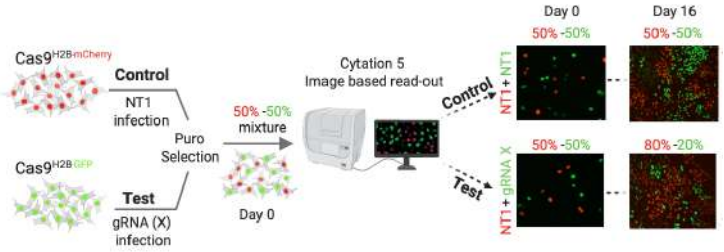

B

Depleted in p<0.05 cut off				gRNA	Function
HMLE	MDA MB 231	SUM159PT	SUM149PT		
				PLGNT1	Non-targeting Mix
+	+		+	CDC16 g1 CDC16 g2	Positive Control (MDA)
+	+	+	+	RPL11 g1 RPL11 g2	Positive Control (MDA and SUM159)
+	+	+	+	TOP2A g1 TOP2A g2	Proof of concept
+	+	+	+	PRMT5 g1 PRMT5 g2	
+	+	+	+	FBL g1 FBL g2	HMT
+	+	+	+	HDAC3 g1 HDAC3 g2	HDAC
+	+		+	WDR82 g1 WDR82 g2	COMPASS (HMT)
+	+			PRPF31 g1 PRPF31 g2	CHD8 (MLL), MLL2/3, MLL4/WBP7
+	+		+	CHAF1B g1 CHAF1B g2	CAF-1
+	+	+	+	SFPQ g1 SFPQ g2	SIN3A Complex
+	+	+	+	ELP3 g1 ELP3 g2	POL2 Elongator (HAT)
+	+		+	ELP5 g1 ELP5 g2	
+	+	+		NAT10 g1 NAT10 g2	HAT activity
+	+	+	+	USP7 g1 USP7 g2	BCOR complex (PcG and PcG like)
+	+	+	+	CDK1 g1 CDK1 g2	
+	+	+	+	PPP4C g1 PPP4C g2	
+	+	+	+	HCFC1 g1 HCFC1 g2	NSL, COMPASS, MLL-HCF, CHD8, MLL2/3, COMPASS-like MLL1,2, MLL4/WBP7
+				KANSL1 g1 KANSL1 g2	NSL, CHD8, MLL2/3, MLL4/WBP7
+	+		+	TRRAP g1 TRRAP g2	SWR, PCAF, TFTC-HAT, NuA4, SAGA, NuA4-related complex, STAGA
+	+	+	+	RBBP4 g1 RBBP4 g2	NuRF, SWI/SNF_Brg1(I), SWI/SNF_Brg1(II), SWI/SNF_Brm, NuRD,
	+	+	+	SS18L2 g1 SS18L2 g2	chromatin remodeling
	+	+	+	KDM2A g1 KDM2A g2	KDM
	+	+	+	ASH2L g1 ASH2L g2	CHD8 (MLL), MLL2/3, COMPASS (HMT)
	+			LAS1L g1 LAS1L g2	CHD8 (MLL) , MLL2/3, MLL4/WBP7
	+	+	+	RUVBL1 g1 RUVBL1 g2	CHD8, Ino80, MLL2/3 (MLL), NuA4 (HAT), SRCAP, SWR
	+	+	+	SUPT16H g1 SUPT16H g2	
	+			EXOSC9 g1 EXOSC9 g2	RNA exosome
	+		+	GTF3C4 g1 GTF3C4 g2	General TF - HAT activity
	+			CIT g1 CIT g2	
		+	+	DPY30 g1 DPY30 g2	COMPASS, Menin-associated_HMT, MLL-HCF, CHD8, MLL2/3, COMPASS-like MLL1,2,
		+	+	RBBP5 g1 RBBP5 g2	COMPASS, Menin-associated_HMT, MLL-HCF, CHD8, MLL2/3, COMPASS-like MLL1,2,
	+		+	KAT8 g1 KAT8 g2	NSL, CHD8, MLL2/3, COMPASS-like MLL1,2, MLL4/WBP7
	+	+	+	KANSL2 g1 KANSL2 g2	NSL
	+	+	+	KANSL3 g1 KANSL3 g2	
	+		+	YEATS4 g1 YEATS4 g2	NuA4, NuA4-related complex, SRCAP
		+	+	VPS72 g1 VPS72 g2	NuA4, NuA4-related complex
	+		+	RUVBL2 g1 RUVBL2 g2	Ino80, SWR, NuA4, NuA4-related complex, CHD8, MLL2/3, MLL4/WBP7, SRCAP
	+			WDR5 g1 WDR5 g2	ATAC, NSL, RING2-L3MBTL2, COMPASS, Menin-associated_HMT, MLL-HCF, CHD8,
	+	+	+	DR1 g1 DR1 g2	ATAC
		+	+	NIPBL g1 NIPBL g2	Histone acetylation
	+	+	+	HINFP g1 HINFP g2	

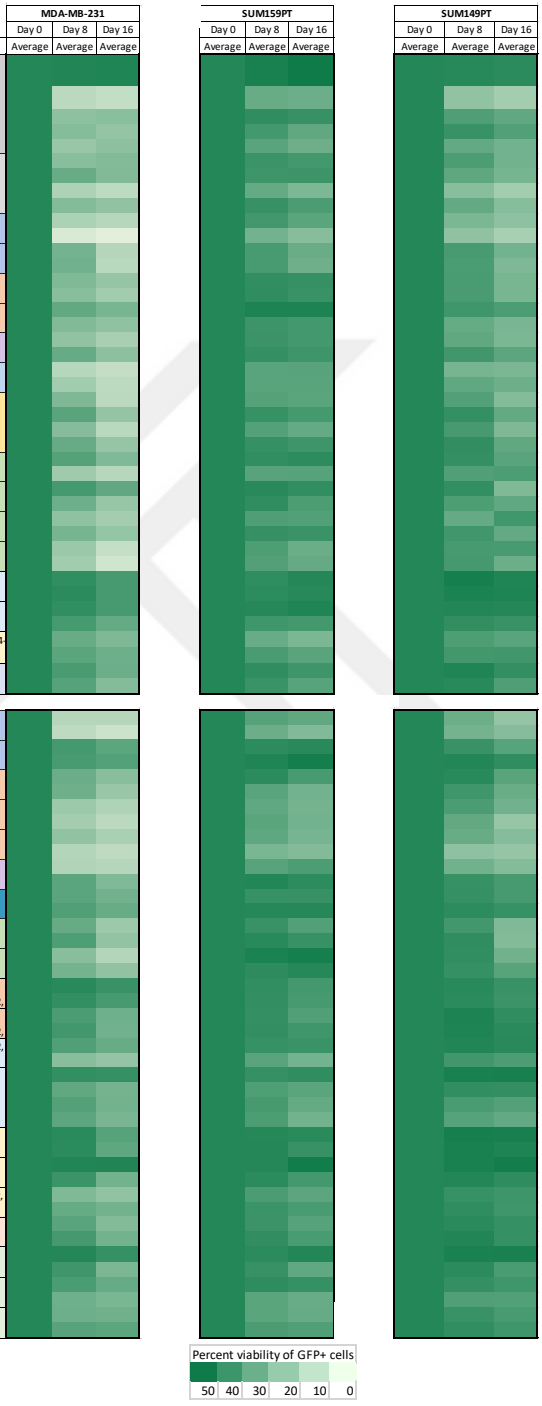

Figure 3.8: Results of dual-color competition assay. A. Schematic of dual-color competition assay. H2B-mCherry and H2B-eGFP labeled cells are transduced with NT1 and sgRNA of interest respectively and mixed in a 1:1 ratio. **B.** Mixtures were followed for 16 days with image-based readout. Day8 and 16 measurements were normalized to Day0.

To further delineate the effects of epigenetic modifiers, we focused on four genes that show strong depletions in MDA-MB-231 cells. Three of these genes were members of *non-specific lethal* (NSL) complex (KANSL2, KANSL3 and KAT8). NSL complex was the only complex that has two members in TNBC specific hits and another member in the cross-section of two cell lines (**Figure 3.6A**). KANSL2 and KANSL3 were structural subunits of NSL complex and they were TNBC specific common hits. KAT8 (MOF, MYST1) was the catalytic subunit of NSL complex that acetylates histone lysine residues and it was significantly depleted in MDA-MB-231 and SUM149PT.

SS18L2 was another candidate gene that does not belong to a complex but showed a very strong depletion phenotype in TNBC cells. SS18L2 is homolog of *SS18* which is associated with chromosomal translocation characteristics of synovial sarcoma. However, information about SS18L2 is very limited and it has not been linked to any cancer in the literature.

In competition assays, all of the four genes showed significant depletions in MDA-MB-231 cells over 16 days (**Figure 3.9A,B**). Similarly, knockouts of selected genes resulted in 70-80% lower number of colonies when compared to NT1 (**Figure 3.9C**). sgRNA against CDC16 was used as a positive control and colony formation capabilities in especially gSS18L2 and gKAT8 samples were comparable to this positive control. Collectively, these results showed that knockout of these four genes decreased the fitness of MDA-MB-231 cells.

To understand the mechanism that cause reduced cell fitness, apoptosis markers were checked. Upon knockout, all candidate genes showed cleavage of PARP (c-PARP) (**Figure 3.9D**) as an indicator of apoptosis. AnnexinV/Dead cell assay also showed increased number of total apoptotic cells at post-transduction (PT) day 9 and 13 upon knockout of four genes (**Figure 3.9E**). Also, knockouts of SS18L2 and KAT8 caused cell cycle arrest in G2/M phase (**Figure 3.9F**). Collectively, these results show that knockout of NSL complex members or SS18L2 have strong effects on the fitness of TNBC cells through apoptosis induction and cell cycle arrest.

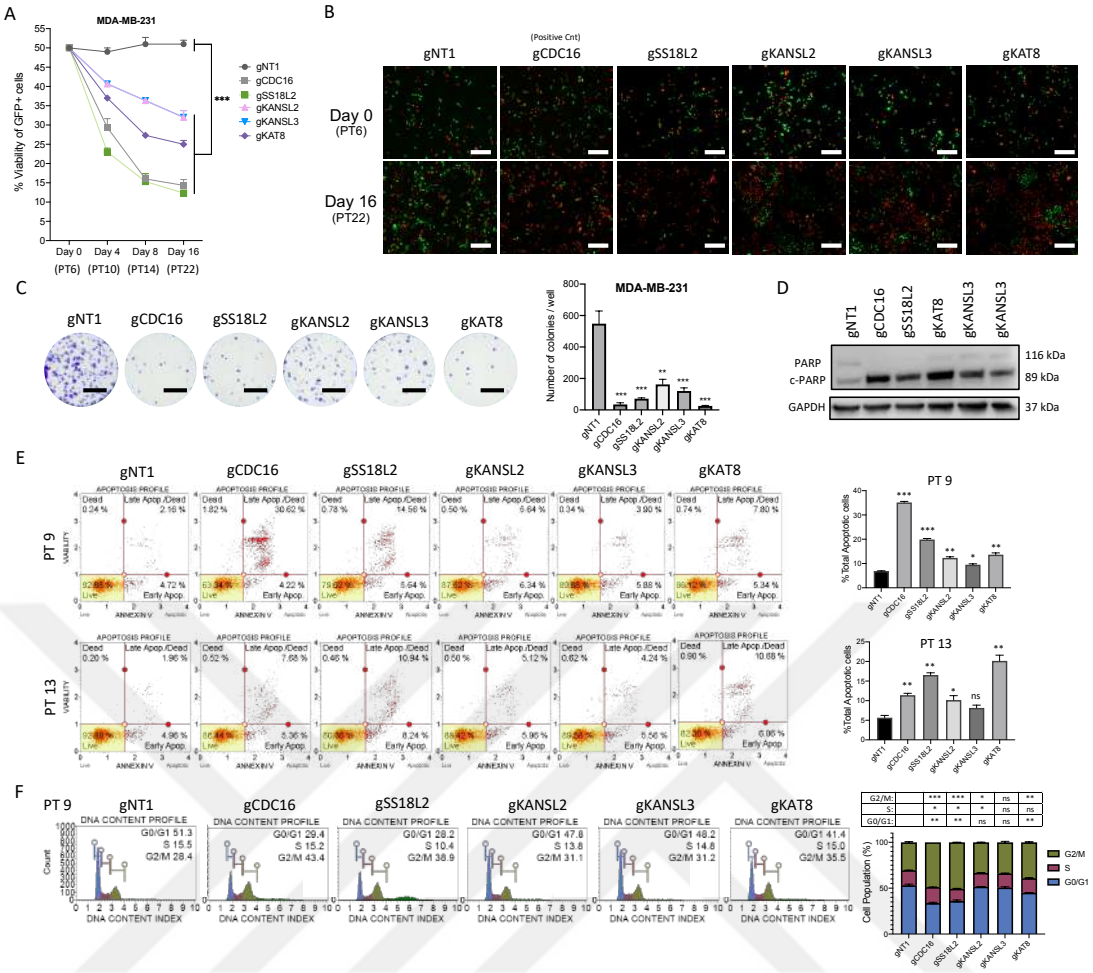

Figure 3.9: Functional assays showing the effects of four hit genes on cell fitness. A. Percentages of GFP+ cells in competition assays upon knockout over 16 days. PT: post-transduction day **B**. Representative images of competition assay on day0 and 16. Scale bar: 200 µm. **C.** Colony formation assay upon knockout of selected genes and its quantification. **D.** Western blot analysis of apoptotic marker c-PARP**. E.** AnnexinV/Dead cell assay showing increased number of early- and late-apoptotic cells at PT9 and PT13. **F.** Cell cycle assay upon knockout at PT9. P values determined by two-tailed Student's t-test in comparison to NT1; *P<0.05, **P<0.01, ***P<0.001

3.1.4 In vivo EPIKOL screen

To assess the efficacy of EPIKOL *in vivo* and reveal the essential epigenetic modifiers in this context, we performed an *in vivo* EPIKOL screen using MDA-MB-231 cells. First, cells were labeled with Firefly Luciferase (Fluc) and transduced with EPIKOL as described earlier. Following puromycin selection, $8x10^6$ cells were mixed with Matrigel and subcutaneously injected into the both flanks of six Nude mice. Tumors from half of the mice were collected 2 weeks after implantation as early tumors while the rest was collected at 4 weeks (**Figure 3.10A**). Three tumors were sequenced for each timepoint. Waterfall plots showed depletion of essential genes while the non-targeting sgRNAs did not show any effect (**Figure 3.10B**). Depletion or enrichment ratios and number of

significantly depleted essential genes were increased from week 2 to week 4. In addition to the positive control essential genes, 10 epigenetic modifiers were identified as commonly depleted in both timepoints (**Figure 3.10C**). 9 out of those 10 genes were also shared with *in vitro* screen results. TFDP1 was identified as an *in vivo* specific cell fitness gene. Depletion of TFDP1 in both week2 and week4 tumors increases its reliability as a true-positive gene rather than a technical artifact of *in vivo* screen. Notably, SS18L2 was among this set of significantly depleted genes.

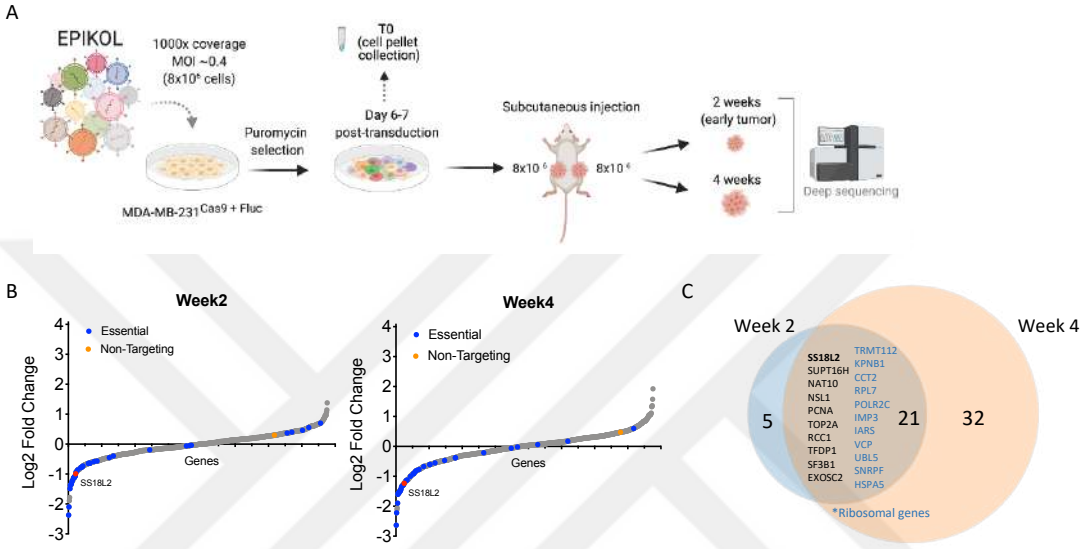

Figure 3.10: *In vivo* EPIKOL screen. A. Workflow. **B.** Gene level waterfall plots for week 2 and 4 tumors. Common hits of EPIKOL screens from week 2 and 4 tumors identified in p<0.05 cutoff.

3.1.4 Validations of in vivo EPIKOL screen

Since SS18L2 was also a hit gene in both timepoints of the *in vivo* screen, effects of its knockout were validated *in vivo*. Fluc expressing MDA-MB-231-Cas9 cells were infected either with non-targeting sgRNA (NT1) or SS18L2 targeting sgRNA and injected subcutaneously into the flanks of eight nude mice (**Figure 3.11A**). Normalized bioluminescence intensities of tumors showed that the tumors carrying SS18L2 sgRNA did not grow in vivo when compared to NT1-tumors (**Figure 3.11B,C,D**).

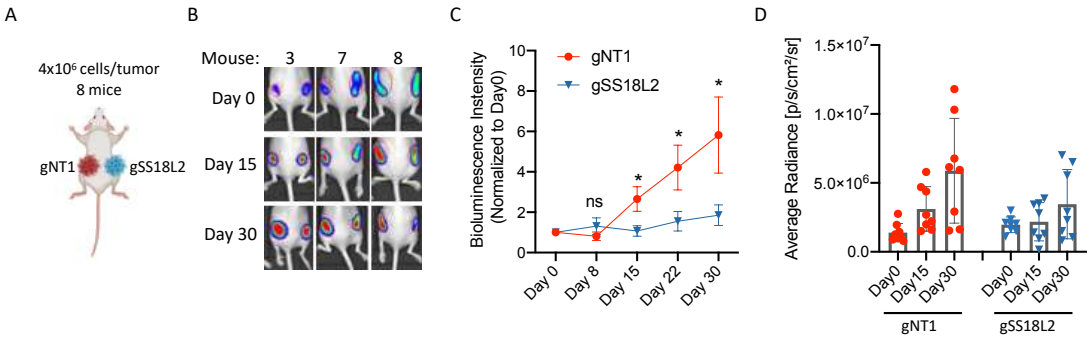

Figure 3.11: Effect of SS18L2 knockout *in vivo*. A. Schematic of in vivo validation experiment. **B.** Representative images of tumors carrying NT1 or SS18L2 sgRNA. C.

Bioluminescence intensity graph showing the growth of individual tumors. (n=8/group) D. Average radiance of control sgRNA or SS18L2 sgRNA carrying tumors.

3.1.5 Immunohistochemistry analysis of SS18L2 in human breast cancer

To assess the expression level of SS18L2 on human samples, a tissue microarray containing mostly TNBC samples (BR1509, Biomax, USA) was stained in Vancouver Prostate Centre (Vancouver, BC, Canada). Dr. Sonia Kung scored the samples and digital scores over 0.1 was considered positive. 80% of TNBC cores had moderate to strong SS18L2 expression (109 out of 132 cores) indicating a relationship between SS18L2 expression and TNBC (**Figure 3.12**).

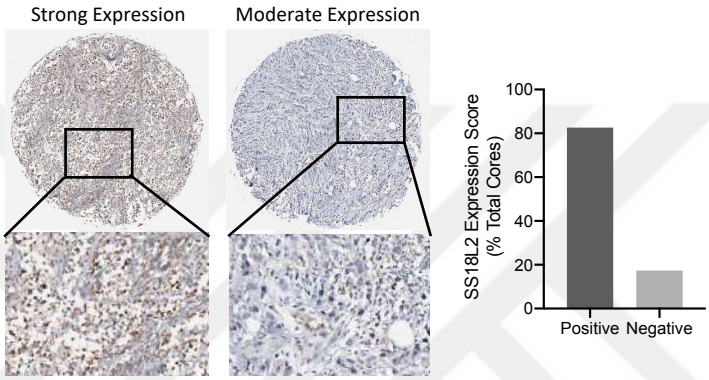

Figure 3.12: SS18L2 staining on breast tissue microarray. Representative images of breast tissue microarray for strong and moderate expression of SS18L2. Graph shows the percentages of SS18L2 positive cores.

3.1.6 Transcriptome analysis of SS18L2 knockout MDA-MB-231 cells

To understand the transcriptomic changes caused by the knockout of SS18L2 on MDA-MB-231, cells were infected with either NT1 sgRNA or SS18L2 sgRNA. Samples were collected on day 6 post-transduction and sent to RNA sequencing (Oxford, UK). SS18L2 knockout resulted in 1283 upregulated and 255 downregulated genes (**Figure 3.13A**). As an internal control, average expression of SS18L2 in all three replicates were significantly downregulated when compared to control samples (**Figure 3.13B**). GSEA revealed a number of negatively enriched pathways related to cell cycle with significant normalized enrichment scores (**Figure 3.13C**). Although the number of upregulated genes were much higher than the downregulated genes, upregulated genes did not significantly overlap with any particular pathway, indicating that the major effect of SS18L2 knockout is downregulation of a specific group of cell cycle related genes. Similarly, biological processes analysis from the Molecular Signature Database (MsigDB) revealed that downregulated genes upon SS18L2 knockout significantly

overlapped with cell cycle, mitosis, chromosome organization and segregation related gene sets (**Figure 3.13D**).

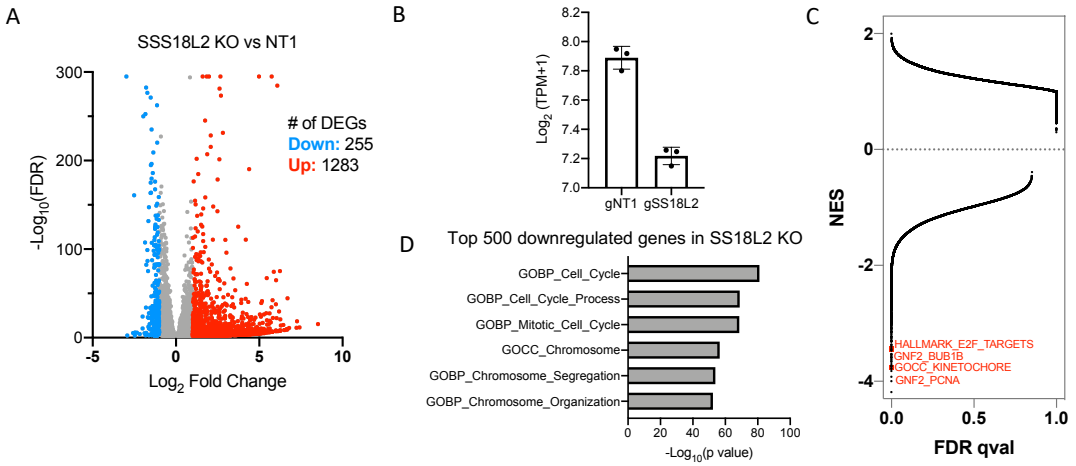

Figure 3.13: Transcriptome analysis of SS18L2 knockout on MDA-MB-231 cells. A. Volcano plot showing upregulated and downregulated genes. Genes that have Log2FoldChange>1 or Log2FoldChange<-1 and false discovery rate (FDR)<0.01 were defined as differentially expressed genes (DEGs). **B.** Transcript per million (TPM) counts of SS18L2 in SS18L2 knockout and control samples. **C.** Normalized enrichment score and FDR-qval results of gene set enrichment analysis (GSEA) of all genes for all gene sets available from MSigDB v7.5. Some of the negatively enriched pathways related to cell cycle were highlighted. **D.** Top 6 biological processes enriched in downregulated genes upon SS18L2 knockout. P values were calculated by hypergeometric test. Top 500 most downregulated genes were used during the analysis.

3.1.7 Effects of SS18L2 knockout on cell cycle progression

First, genes that were significantly downregulated in SS18L2 knockout samples were validated with Real Time PCR (RT-PCR) (**Figure 3.14A**). Significantly downregulated genes mostly belong to late G2/M related gene sets or master regulators of cell cycle progression such as DREAM complex. All of the selected genes showed significantly lower expression when compared to control. To validate the effect of downregulated genes on cell cycle phase transitions, we conducted a time-lapse PIP-FUCCI fluorescence imaging for 72 hours. For this, cells were labeled with PIP-FUCCI construct which expresses green signal in G1 and G2/M phases and red signal in S and G2/M phases. The overlap of both green (mVenus) and red (mCherry) signals is an indication of G2/M phase (**Figure 3.14B**). SS18L2 knockout cells had increased number of double positive cells starting from 24 hours (post-transduction day6) when compared to NT1 samples indicating that those cells were arrested in G2/M phase in the absence of SS18L2 (**Figure 3.14B,C**). Also, number of cells in SS18L2 knockout samples were significantly lower than the control cells and knockout cells resembled to senescence cells morphologically. Altogether, these data showed that SS18L2 might be regulator of cell cycle progression in TNBC cells.

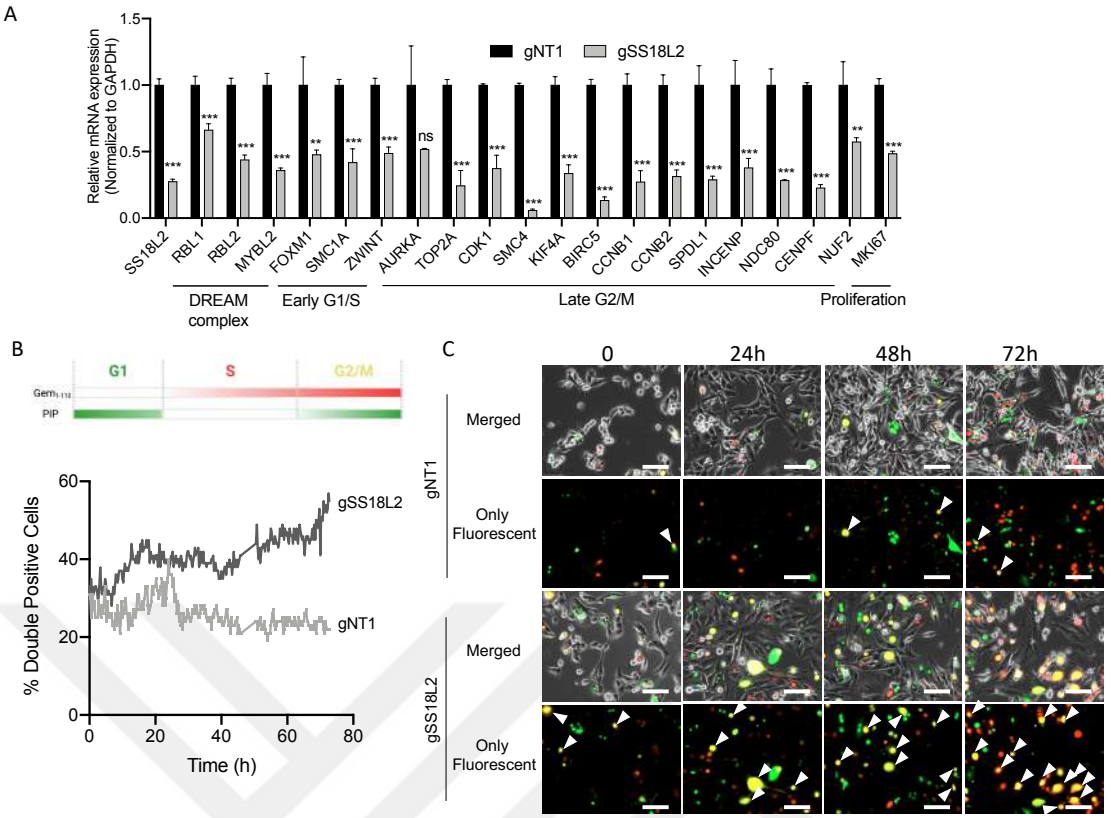

Figure 3.14: Effect of SS18L2 on cell cycle. A. QPCR validation of selected hit genes from RNA sequencing on NT1 or SS18L2 knockout MDA-MB-231 cells. **B.** Color scheme for PIP-FUCCI assay. Gem_{1-110} is fused to mCherry and PIP is fused to mVenus. Coexpression of Gem and PIP forms double positive cells as an indication of G2/M phase.

Since SS18L2 is a homolog of SS18, we also checked the effects of SS18 and SS18L1 on cell cycle in TNBC. Unlike SS18L2, knockout of SS18 and SS18L1 were able to form colonies (**Figure 3.15A**) and they were not arrested at G2/M checkpoint (**Figure 3.15B**).

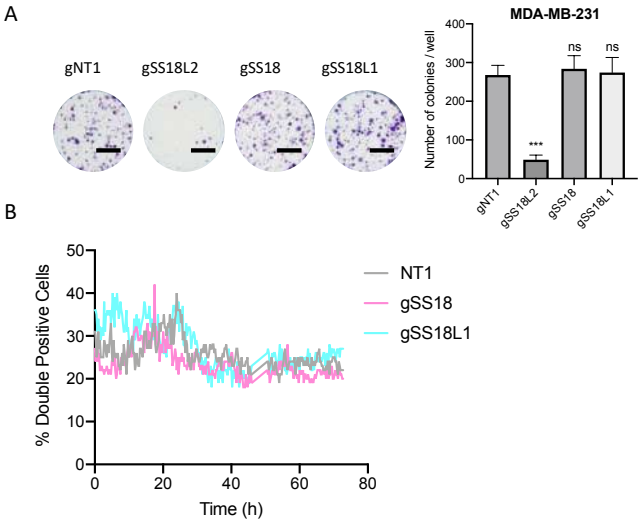

Figure 3.15: Effects of SS18 and SS18L1 knockout on TNBC. A. Colony formation assay upon SS18 and SS18L1 knockout on MDA-MB-231 cells. **B.** PIP-FUCCI assay for 72 hours.

3.2 Generation and Characterization of Chemotherapy Resistant TNBC cell lines

3.2.1 Generation of Chemotherapy Resistant cell lines

Determination of IC50 of chemotherapeutic agents

As starting step of resistant cell generation, the concentration that kills half of the population (IC_{50}) was determined in each cell for each drug (**Figure 3.16**). IC_{50} values of Doxorubicin was higher in each cell line when compared to Taxol.

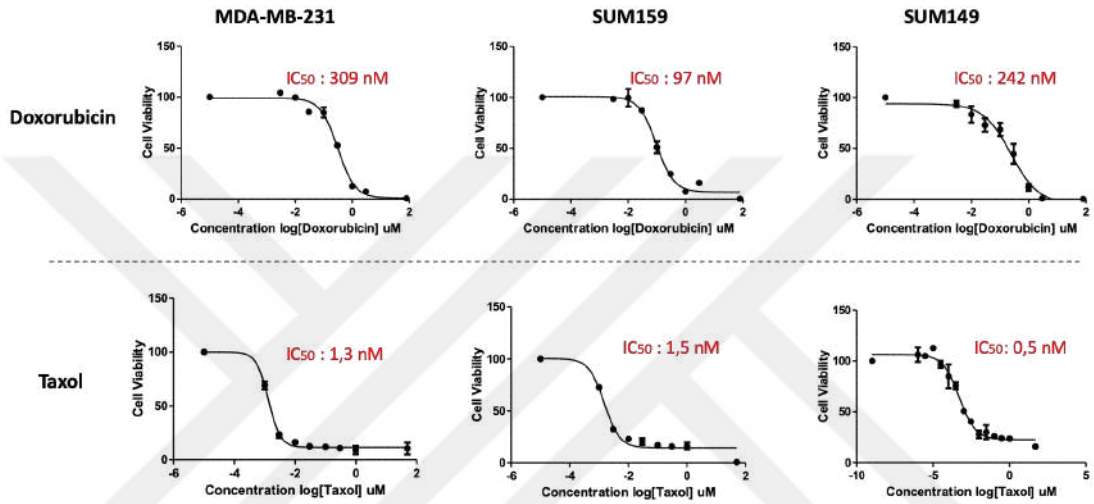

Figure 3.16: IC_{50} values of Doxorubicin and Taxol on TNBC cell lines.

Generation of drug-resistant TNBC cell lines

TNBC cells were seeded on 6-well plates as $2x10^5$ cells and treated with IC_{50} or IC_{10} concentrations of drugs. Dose escalation method for resistant cell generation was used and drug concentrations were increased once cells start to become confluent in the presence of drug (**Figure 3.17A**). During long-term treatment with escalating doses of chemotherapeutic agents, IC_{50} values of drug-treated cells and parental cells (aged alongside the resistant cells in the presence of DMSO) were measured and cells showing increased IC_{50} were cryo-preserved periodically. Resistant cells were named as shown in (**Figure 3.17B**) and cell were always maintained in the final dose of drug.

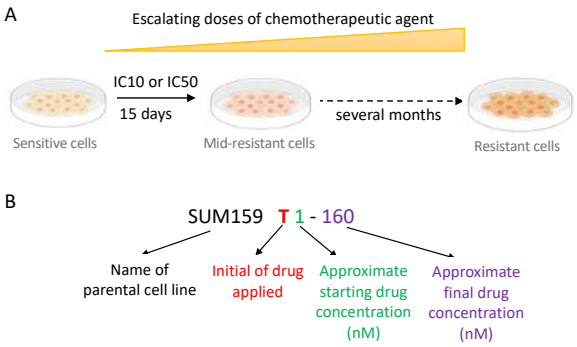

Figure 3.17: Chemotherapy resistant cell generation. A. TNBC cells were treated with either IC10 or IC50 concentrations of taxol or doxorubicin. When cells become confluent under drug treatment, concentration of drugs were doubled. Before increasing the concentration, current concentration was applied at least for 15 days. When the IC50 values of resistant cells significantly differed from the starting concentration, process is finished, and cells were always cultured in the last concentration of the drug. **B.** Resistant cell lines were named as explained.

We were able to select at least two different taxol-resistant subpopulations from all TNBC cell lines (**Figure 3.18**). Duration of resistance development and the degree of resistance differed in each cell line, however, all cells showed significant increase in IC_{50} values when compared to parental cells. Morphology of the cells were changed over time. MDA-MB-231 and SUM159PT cells became more elongated while the SUM149PT cells became more cubical upon being resistant. Although colony formation rates were lower in resistant cells, all cells were able to form colonies in the presence of drug while the parental cells cannot.

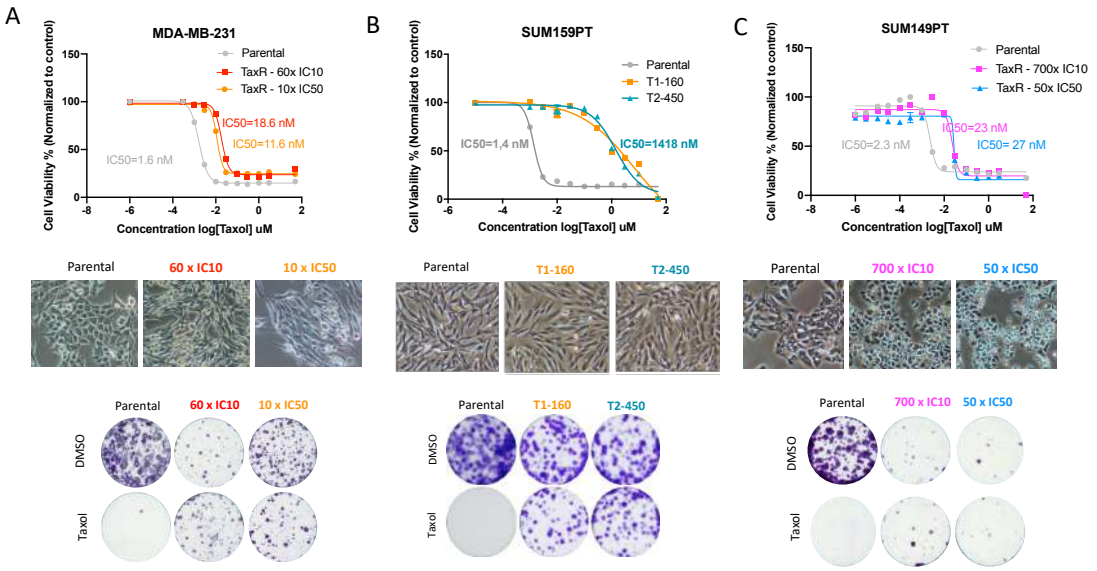

Figure 3.18: Taxol resistant TNBC cell lines. Morphology and colony formation capabilities of **(A.)** Taxol resistant MDA-MB-231 cells, **(B.)** Taxol resistant SUM159PT cells and **(C.)** Taxol resistant SUM149PT cells.

On the other hand, only SUM159PT cells developed doxorubicin resistant subpopulations (**Figure 3.19**). Their morphology was also changed to more elongated cells and they had giant cells resembling senescent cells.

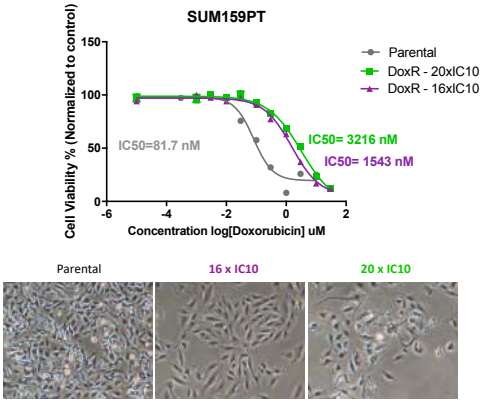

Figure 3.19: Doxorubicin resistant SUM159PT cells and their morphology.

3.2.2 Characterization of SUM159 Taxol resistant cells

In downstream functional assays and screens, SUM159 Taxol resistant cells (T1-160 and T2-450) were used. First, to characterize the resistant cells, their growth capabilities were measured by Cell Titer Glo. It was shown that resistant cells grow significantly slower than the parental cells (**Figure 3.20A**). Similar to the colony formation assay, live cell microscopy showed that resistant cells can grow in the presence of taxol however parental cells cannot grow (**Figure 3.20B**).

Alternatively, T1-160 and T2-450 cells were labeled with H2B-mCherry and mixed with H2B-eGFP positive parental cells. Mixtures were treated with taxol for 3 days. At the end, only mCherry positive resistant cells were able to propagate in the presence of taxol (**Figure 3.20C**).

Cell cycle analysis showed that parental cells arrest in G2/M phase when treated with the taxol dose in which the resistant cells can grow (**Figure 3.21**). These results are in line with the literature since it is known that taxol causes cell cycle arrest at G2/M phase due to its microtubule stabilizing effect.

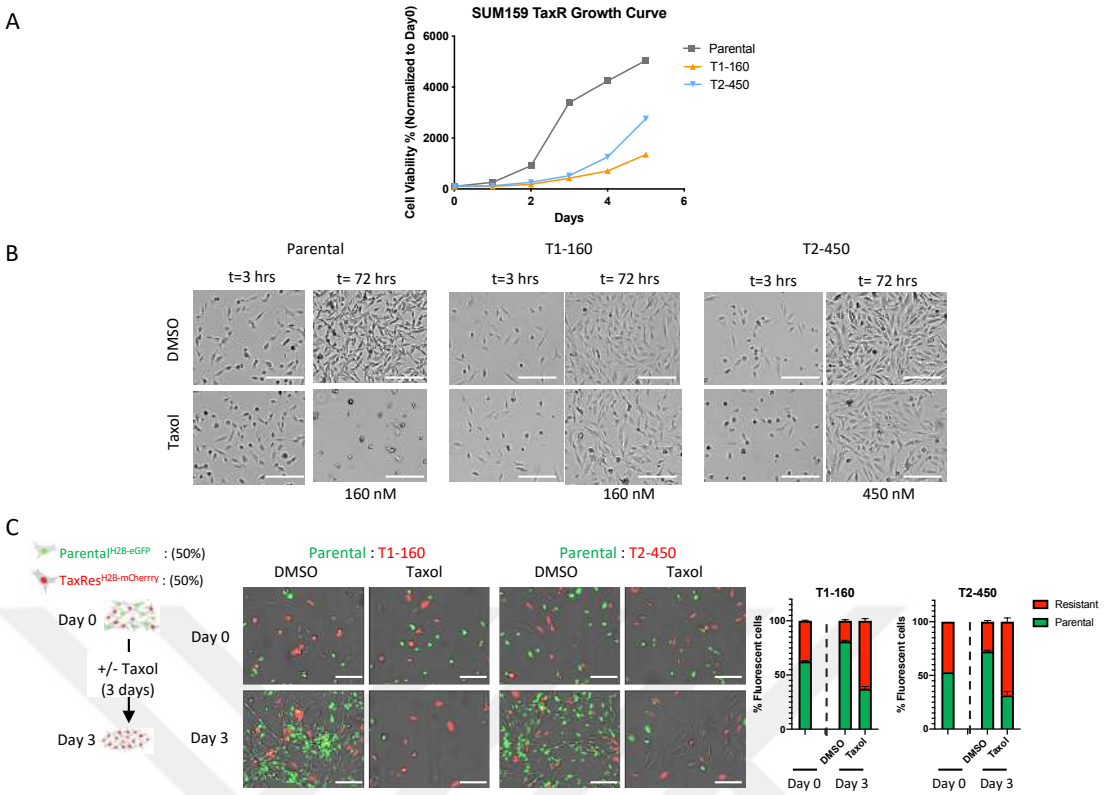

Figure 3.20: Growth characteristics of SUM159 Taxol resistant cells. A. Growth curve of Parental and Taxol resistant SUM159PT cells (T1-160 and T2-450). **B.** Live cell imaging of taxol resistant SUM159PT cells in the presence of taxol for 72 hours. Taxol doses were indicated below images. **C.** Competition assay of parental and resistant cell mixtures in the presence of taxol. For Parental:T1-160 mixture 160 nM taxol was used. For Parental:T2-450 mixture 450 nM taxol was used.

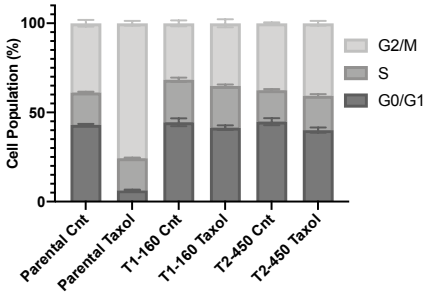

Figure 3.21: Cell cycle analysis in the presence of Taxol. Parental cells were treated with 160 nM taxol. Resistant cells were treated with either 160 nM or 450 nM Taxol.

3.2.3 Cell death mechanism upon taxol treatment

To understand the mechanism in which the parental cells die upon taxol treatment while the resistant cells can grow, we performed AnnexinV/Dead Cell assay (**Figure 3.22A**). When parental cells were treated with 160 nM Taxol, number of early and late apoptotic cells significantly increased. There was no difference in resistant samples in the absence or presence of taxol. Similarly, cleaved-PARP (c-PARP) was only observed in taxol treated parental cells and cleavage of caspase-3 (c-caspase3) was more prominent

in this sample (**Figure 3.22B**). These results indicated that the cell death mechanism of parental cell upon taxol treatment was apoptosis.

Alternatively, α-tubulin staining showed that resistant cells are morphologically bigger in size when compared to parental cells (**Figure 3.22C**). Upon taxol treatment, no change was observed in resistant cells whereas the parental cells become rounded. α-tubulins of parental cells shrinked in taxol treated samples when compared to DMSO sample.

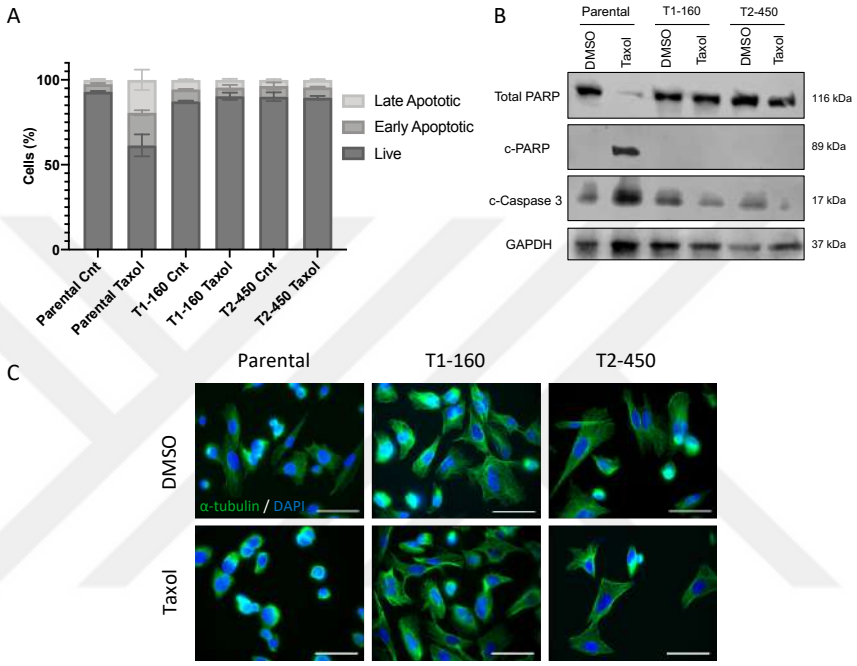

Figure 3.22: Apoptosis induction upon taxol treatment. A. AnnexinV/Dead cell assay in the presence of Taxol. Cells were either treated with DMSO or Taxol (Parental: 160 nM, T1-160: 160 nM, T2-450: 450 nM) for 24 hours. **B.** Western Blot analysis of the cells shown in (A.) for Total PARP, cleaved-PARP (c-PARP), cleaved-caspase3 (c-Caspase 3) and GAPDH as loading control. **C.** Immunofluorescence staining with α-tubulin (green) and DAPI (blue) in the presence of DMSO or Taxol (Parental: 160 nM, T1-160: 160 nM, T2-450: 450 nM) for 4 hours. Scale bar: 50 µm

3.2.4 Cross-resistance of SUM159 Taxol resistant cells

We wondered whether the taxol resistant Sum159 cells were resistant to drugs other than taxol and performed cell viability measurement in the presence of Vincristine and Doxorubicin (**Figure 3.23**). Vincristine destabilizes microtubules and leads to cell death especially during cell division. Doxorubicin has a different mechanism of action and it blocks topoisomerase II leading to DNA breaks and cell death. Both resistant cells were significantly resistant to vincristine since it has a similar mechanism of action to taxol. Although the resistance to doxorubicin was not as prominent, difference from the parental cells was clear.

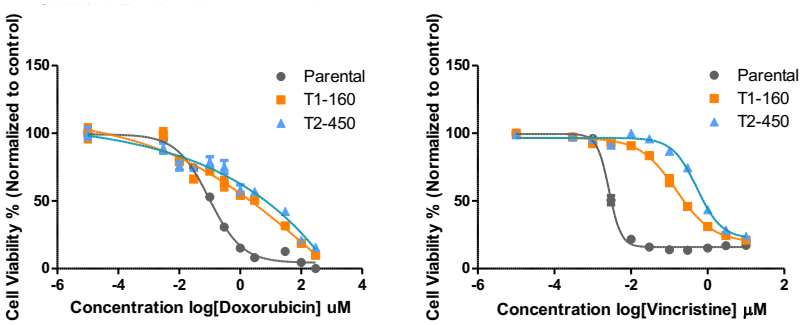

Figure 3.23: Cross-resistance of SUM159 taxol resistant cells. Cell viability response of resistant cells to increasing doses of doxorubicin and vincristine was compared to parental after Cell-Titer Glo assay.

3.2.5 Transcriptome analysis of resistant cells

In order to reveal transcriptomic changes occurred during resistance generation, taxol resistant MDA-MB-231 cells (TaxR 60xIC10), SUM159PT cells (T1-160 and T2-450), SUM149PT cells (TaxR 700xIC10) and doxorubicin resistant SUM159PT cells (DoxR 16xIC10) were sent to RNA sequencing. For detailed analysis of transcriptomic changes of resistant cells, we mainly focused on taxol resistant SUM159PT cells (T1-160 and T2-450). Details of RNA sequencing of other resistant cells were presented in Appendix.

RNAseq revealed many significantly upregulated or downregulated genes in both T1-160 and T2-450 cells (**Figure 3.24A**). Gene set enrichment analysis (GSEA) was performed with the ranked gene list without any cutoff and FDR qval<0.05 was used to interpret significantly enriched pathways. Some of these gene sets were labeled in **Figure 3.24B**. In T1-160 cells, number of significantly negatively enriched gene sets was more than positively enriched ones. Cell adhesion related gene sets were positively enriched. Interestingly, gene sets related with oxidative phosphorylation and electron transport chain were significantly negatively enriched. This might indicate that these resistant cells became more glycolytic when compared to parental. In T2-450 cells, number of significantly positively enriched gene sets was more than negatively enriched ones. Many gene sets related to inflammatory response and complement system were positively enriched.

Later, we performed overlap analysis only with the significantly downregulated or upregulated genes (LFC>2 and pval<0.001) using Gene Ontology (GO) gene sets in Molecular Signatures database (MsigDB). In T1-160 cells, adhesion, movement and cell to cell signaling related pathways overlapped with both upregulated and downregulated genes, however, overlap with upregulated genes was more significant (**Figure 3.24C**). In T2-450 cells, downregulated genes did not overlap with any particular pathway (**Figure**

3.24D). Upregulated genes, similar to the T1-160 cells, overlapped with cell adhesion, movement and cell to cell signaling related pathways. These results suggest that although T1-160 and T2-450 cells share several transcriptomic changes, they have significant differences in terms of gene sets that are positively or negatively enriched.

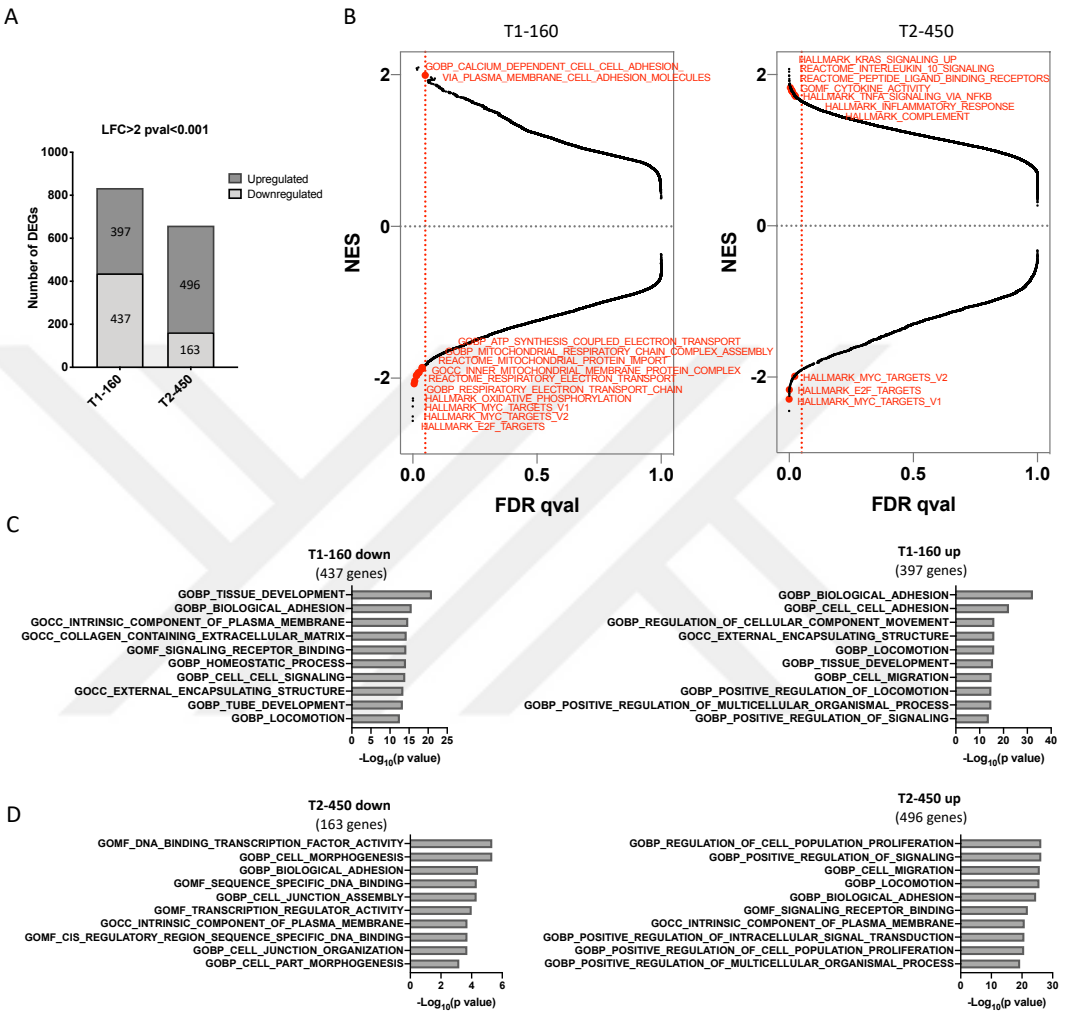

Figure 3.24: Transcriptome analysis of SUM159PT taxol resistant cells. A. Number of differentially expressed genes (DEGs) in T1-160 and T2-450 cells. **B.** GSEA plots showing negatively or positively enriched gene sets when all genes were analyzed together in ranked list format without a cutoff. Red dashed line indicates FDR qval<0.05 **C.** Overlap analysis of T1-160 cells with MSigDB GO gene sets with the genes in LFC>|-2| and p<0.001 cutoff. **D.** Overlap analysis of T2-450 cells with MSigDB GO gene sets with the genes in LFC>|-2| and p<0.001 cutoff.

When we checked the most upregulated and downregulated genes in both cell lines, we observed that *ABCB1* was the most significantly upregulated gene (**Figure 3.25A**). ABCB1 is one of the members of ABC transporter family that is highly associated with the drug resistance. Previous cross-resistance results of SUM159 taxol resistant cells also supports the presence of multidrug resistance phenotype. Therefore, we showed the

expressions of all ABC transporters as heatmap (**Figure 3.25B**). We then checked the mRNA expression levels of several ABC transporters that are known as highly associated with taxol resistance (**Figure 3.25C**). In line with the RNA-seq, ABCB1 was highly upregulated in both resistant cells and no upregulation was observed in the expression levels of other ABC transporters. High expression of ABCB1 was also confirmed with western blot (**Figure 3.25D**). Interestingly, when SUM159 taxol resistant cells were grown in the absence of taxol for 3 months (holiday), resistance level of T1-160 cells reverts back to the parental cell levels (**Figure 3.25E**). Although the resistance level of T2-450 cells did not return to the parental cell levels, it decreased to the levels of the T1-160 cells. When we checked the mRNA expression level of ABCB1 upon 1 month of drug holiday, we observed that the ABCB1 mRNA expression decreased to the parental cell levels in both resistant cells (**Figure 3.25F**). Although the relationship between taxol resistance and ABCB1 is well established in the literature, decrease of ABCB1 expression and loss of resistance upon drug holiday implies an epigenetic regulation which is not fully understood.

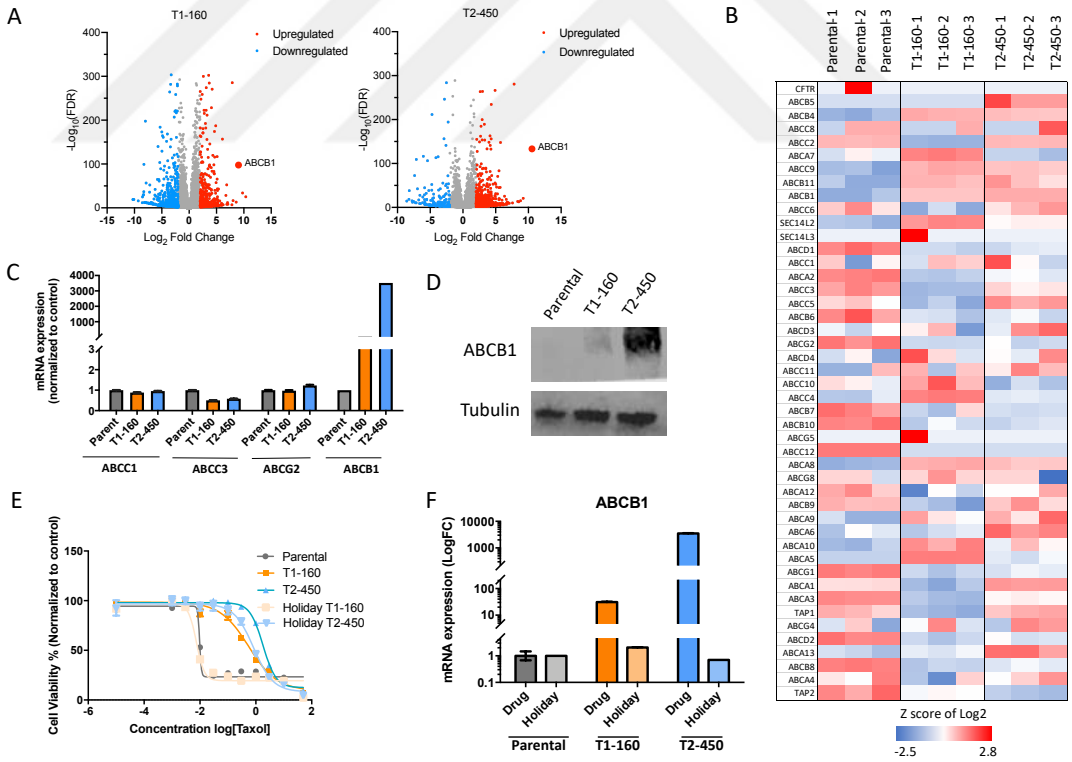

Figure 3.25: ABCB1 is highly upregulated in SUM159 Taxol resistant cells. A. Volcano plot of Log_2Fold Changes of differentially expressed genes (cutoff is LFC>|-2| and p<0.001). **B.** Heatmap showing the expressions of all ABC transporters. **C.** RT-PCR validation of selected ABC transporters in both resistant cells. **D.** Western blot showing overexpression of ABCB1 **E.** Cell viability response of SUM159 taxol resistant cells to taxol after 3 months of drug holiday. F. mRNA expression levels of ABCB1 upon 1 months of drug holiday.

Since copy number increase of ABCB1 at the genomic level is highly associated with chemotherapy resistance, we checked the copy number of ABCB1 by performing qPCR with a specific primer for genomic DNA (**Figure 3.26A**). As expected, increased copy number of ABCB1 and ABCB4 was detected in both resistant cells with more prominent effect on T2-450 cells as an indication of a non-epigenetic adaptation event. Later, we wondered the mRNA expression of other genes in the ABCB1 locus and checked the expressions from RNA-seq data (**Figure 3.26B,C**). The genes closer to the ABCB1 have higher expressions and the expressions decline if a gene is relatively distant to ABCB1. This result suggests that ABCB1 locus with the closest genes amplified in the genome. It should be noted that ABCB1 CNV is around 20-fold of a normal cell however mRNA expression goes up to the thousand folds indicating that there is an additional mechanism that regulate ABCB1 expression.

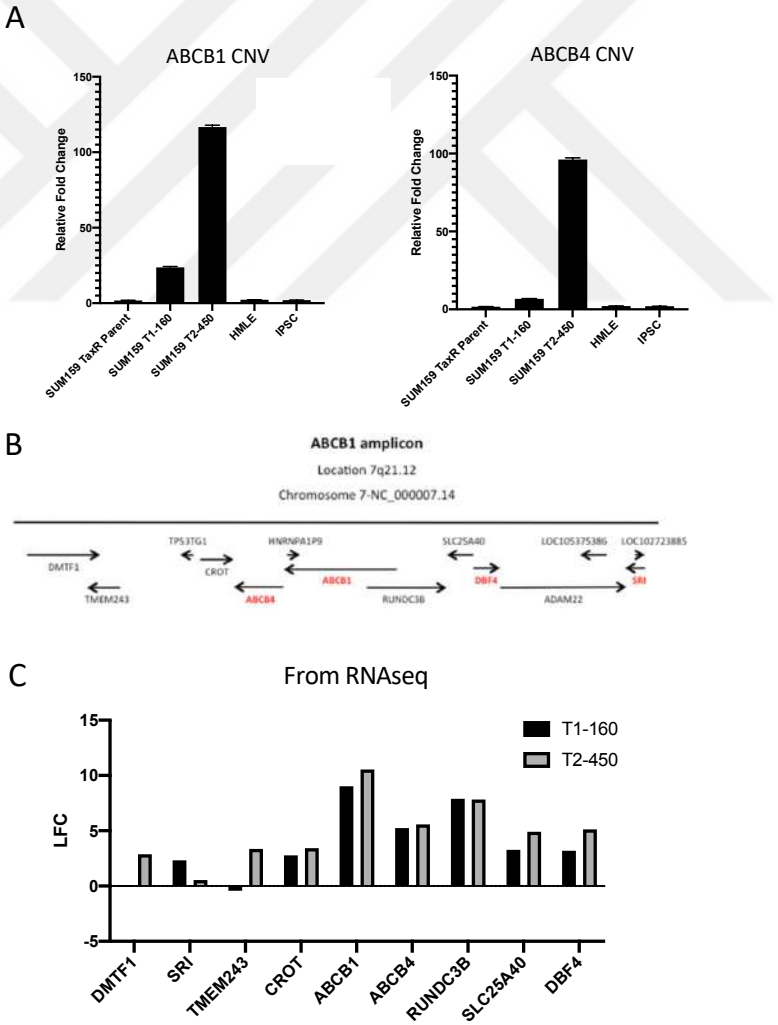

Figure 3.26: Copy number variation (CNV) analysis in Taxol resistant cells. A. Copy numbers of ABCB1 was compared to an IPSC cell line with known karyotype. **B.** Genes found in ABCB1 amplicon. Figure adopted from (Genovese et al., 2017) **C.** LogFoldChanges of other genes found in ABCB1 locus in the RNAseq.

3.2.6 Multidrug resistance phenotype of SUM159 Taxol resistant cells

To check if the taxol resistance can be reverted by ABCB1 knockout, cells were transduced with viruses containing an ABCB1 targeting sgRNA. Efficiency of knockout was confirmed by western blotting (**Figure 3.27A**). Colony formation abilities in the presence of taxol of both resistant cells were completely impaired upon ABCB1 knockout (**Figure 3.27B**). Similarly, cell viability response of resistant cells against taxol was similar to the parental cells upon ABCB1 knockout (**Figure 3.27C**).

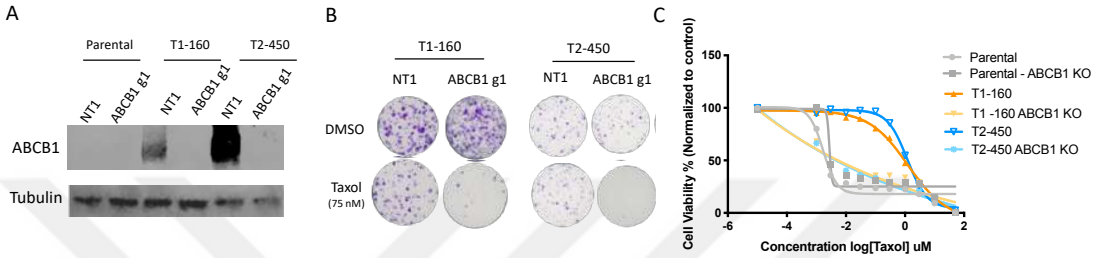

Figure 3.27: ABCB1 Knockout on SUM159 Resistant cells. A. Western blot showing efficient knockout of ABCB1. **B.** Colony formation assay upon ABCB1 knockout in the presence of taxol. **C.** Cell viability assay for ABCB1 knockout cells in response taxol.

As a complementary approach, several different ABCB1 inhibitors were tried (**Figure 3.28**). Verapamil is a calcium channel blocker and inhibits several proteins in ATP-binding cassette (ABC) transporter family. It is known as a first-generation ABC transporter inhibitor. Elacridar is a second-generation ABC inhibitor and binds only to 2 -3 ABC proteins. Zosiquidar is a third generation ABC inhibitor that specifically binds to ABCB1 (P-gp) with high affinity. Although all inhibitors reverted the taxol resistance of T1-160 and T2-450 cells almost to the parental level, Zosiquidar shows the strongest effect possibly due to its high affinity binding to ABCB1.

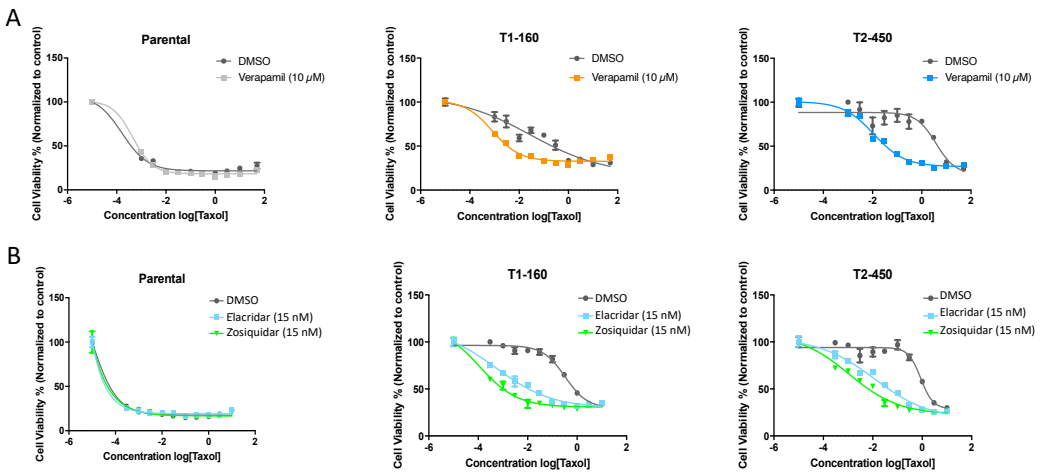

Figure 3.28: ABC transporter inhibitors on Taxol resistant SUM159PT cells. A. Effect of verapamil on cell viability. **B.** Effect of more targeted ABC transporter inhibitors on cell viability of taxol resistant cells.

Alternatively, calcein assay was performed to asses ABCB1 activity. Calcein-AM is a cell permeable dye that become fluorescent upon cleavage by esterases inside the cell. It is also a substrate of ABCB1 that can be used as an indicator of ABCB1 activity. Calcein assay showed that calcein can stay inside the parental cells and become fluorescent while the resistant cells pump it out remaining non-fluorescent (**Figure 3.29**). However, in line with the cell viability results, resistant cells also become fluorescent in the presence of verapamil indicating the blocked activity of ABCB1.

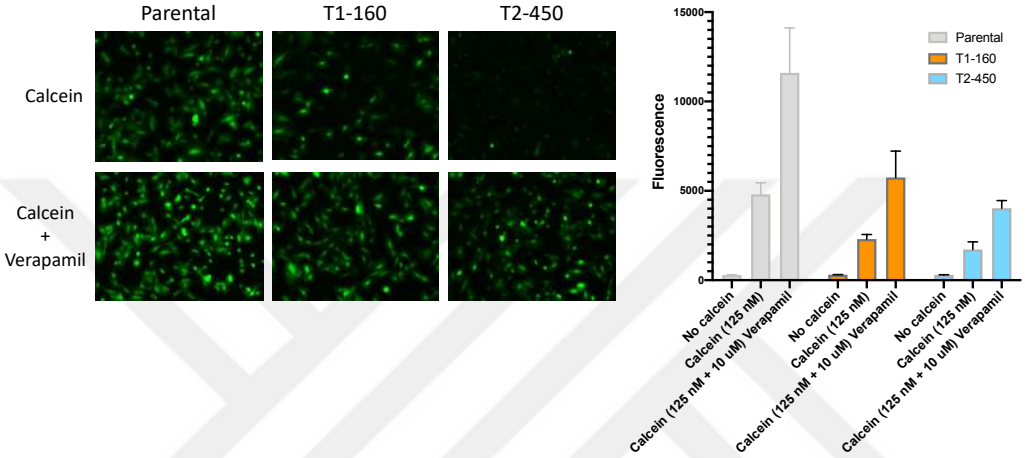

Figure 3.29: Calcein assay on SUM159 taxol resistant cells. Representative images of calcein assay on T1-160 and T2-450 SUM159 taxol resistant cells and its fluorescence readout.

3.3 Epigenetic knockout and probe-library screens on resistant cells

To reveal epigenetic regulators of chemotherapy resistance, we utilized two complementary approaches. First, we performed an EPIKOL screen on T1-160 cells in the absence and presence of taxol and validated several hits through functional assays. Second, we performed an epigenetic probe-library screen on T1-160 and T2-450 cells to understand common regulators in two different taxol resistant SUM159PT cells. Finally, we focused on one hit gene that is found as a result of two different screening methods.

3.3.1 EPIKOL screen on SUM159 Taxol resistant T1-160 cells

EPIKOL screens were performed on chemoresistant TNBC cell lines. First, EPIKOL viral library was transduced into resistant cells and infected cells were selected with puromycin (**Figure 3.30A**). Then, cells were divided into two groups and one group was treated with the drug concentration that the cells were normally cultured. Other group was treated with DMSO as control. After NGS, drug treated samples were compared to the DMSO treated group to reveal epigenetic modifiers whose loss revert resistance.

In T1-160 cells, significantly depleted genes in the presence of taxol were shown as a volcano plot (**Figure 3.30B**). Several positive control genes such as ABCB1 and ABCG2 were depleted upon taxol treatment validating the reliability of the EPIKOL screen on resistant cells. Members of COMPASS/MLL complex and SWI/SNF complex as well as histone ubiquitination related genes were among the most significantly depleted genes.

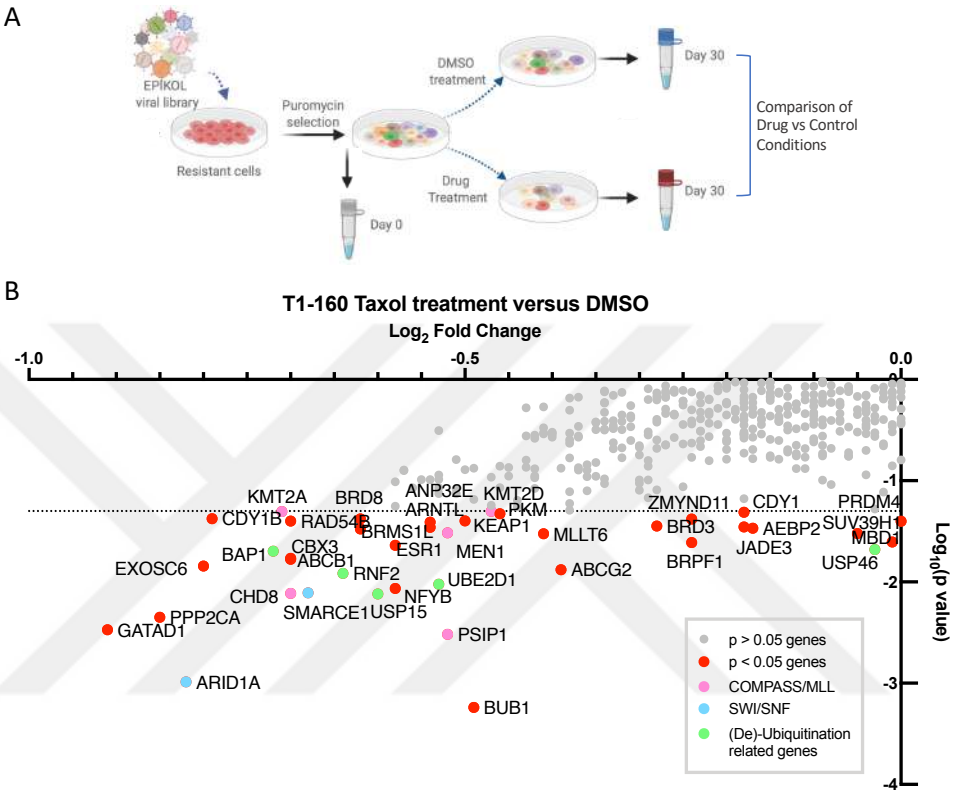

Figure 3.30: EPIKOL screen on resistant cells. A. Workflow of drug resistance screens. **B.** EPIKOL screen results on T1-160 cells. Volcano plot shows Log_2 Fold changes of depleted genes and corresponding p-values in taxol treated T1-160 samples when compared to DMSO.

Validation of candidate genes with competition assays

Different group of genes were selected for further validation with dual-color competition assays (**Figure 3.31A**). First group includes hit genes from T1-160 Taxol vs DMSO comparison (**Figure 3.31B**). Second group includes hit genes from Taxol vs After puro sample comparisons. Almost all of the selected genes were differentially depleted in taxol treated group when compared to DMSO treated group and NT1 control. KMT2A, MEN1, BRD8, CHD8, BRPF1 was among the most significantly depleted genes upon taxol treatment. Except KDM8, all genes selected in second group showed significant depletion upon taxol treatment. reaching to the levels of positive controls such as ABCB1 and RPL11. These results showed that EPIKOL screens can successfully identify drug resistance related genes.

A

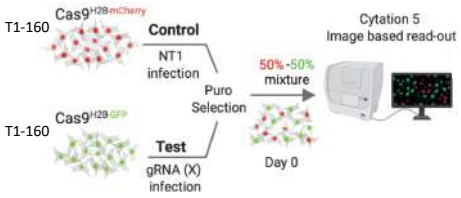

B

		Day 0		Day 4		Day 8		Day 12		Day 16		Day 24	
		- Tax	+ Tax	- Tax	+ Tax	- Tax	+ Tax	- Tax	+ Tax	- Tax	+ Tax	- Tax	+ Tax
1st Group	ARID1A g1	50	50	57	50	58	47	67	52	67	51	71	55
	ARID1A g2	50	50	54	50	55	46	62	51	62	51	65	56
	GATAD1 g1	50	50	55	49	57	42	66	42	66	38	70	42
	GATAD1 g2	50	50	55	48	57	41	67	42	67	37	71	44
	SMARCE1 g1	50	50	61	49	69	48	85	58	85	56	90	63
	SMARCE1 g2	50	50	55	46	61	36	73	29	74	25	81	29
	KMT2A g1	50	50	58	51	62	41	72	41	72	34	75	36
	KMT2A g2	50	50	62	54	69	48	83	52	82	44	88	53
	MEN1 g1	50	50	59	50	64	45	79	44	78	35	84	29
	MEN1 g2	50	50	58	49	62	40	76	33	75	23	81	16
	ARNTL g1	50	50	56	52	57	49	66	54	65	52	68	57
	ARNTL g2	50	50	56	52	57	50	66	55	65	55	68	59
	BRD8 g1	50	50	55	48	55	44	64	48	64	43	68	43
	BRD8 g2	50	50	54	49	55	45	65	46	65	36	68	30
	MLLT6 g1	50	50	55	50	56	48	66	53	65	51	68	57
	MLLT6 g2	50	50	55	50	56	48	65	55	65	53	68	57
	BRD3 g1	50	50	56	52	56	50	64	55	64	54	67	58
	BRD3 g2	50	50	56	52	56	49	64	55	64	53	66	57
	PPP2CA g1	50	50	56	50	57	45	67	46	66	40	70	39
	PPP2CA g2	50	50	54	49	55	44	64	48	64	43	67	48
	CHD8 g1	50	50	54	50	56	45	64	47	64	41	67	34
	CHD8 g2	50	50	54	49	54	44	63	47	63	42	66	37
	BRPF1 g4	50	50	55	52	55	48	63	48	62	43	67	43
	BRPF1 g5	50	50	55	52	55	48	64	49	64	44	66	47
	BRPF1 g6	50	50	54	51	55	48	62	50	62	45	65	46
	JADE3 g1	50	50	59	54	62	52	72	57	72	53	76	59
	JADE3 g2	50	50	55	53	57	50	65	55	65	53	68	57
	KAT7 g1	50	50	55	48	56	39	68	36	68	33	72	33
	KAT7 g2	50	50	54	50	55	45	63	48	63	47	66	53
	MEAF6 g1	50	50	54	50	55	45	64	35	64	40	67	45
	MEAF6 g2	50	50	54	50	55	47	64	50	64	49	67	58
	ING5 g1	50	50	55	51	56	47	63	50	63	48	65	54
	ING5 g2	50	50	56	51	57	48	65	53	64	52	67	56
2nd Group	ING3 g1	50	50	50	44	59	38	76	33	76	25	91	20
	ING3 g2	50	50	51	48	54	42	65	42	64	35	71	34
	RBBP7 g1	50	50	55	50	56	45	64	44	64	39	66	39
	RBBP7 g2	50	50	54	49	54	43	63	41	62	33	65	23
	PRMT1 g1	50	50	52	47	53	42	63	42	62	38	66	39
	PRMT1 g2	50	50	45	40	36	25	40	12	43	7	56	5
	KDM8 g1	50	50	55	51	57	49	64	54	64	53	67	58
	KDM8 g2	50	50	55	51	57	50	64	54	64	52	66	58
	PAXIP1 g1	50	50	52	49	54	46	60	42	61	30	65	15
	PAXIP1 g2	50	50	52	50	54	47	61	47	62	41	66	38
	RPL11 g1	50	50	41	37	46	29	60	27	61	24	71	24
	RPL11 g2	50	50	30	26	35	19	54	13	60	9	73	7
	ABCB1 g	50	50	54	43	56	27	63	11	63	6	66	5
	NT1 mix	50	50	55	51	56	49	64	55	64	53	67	56
	Parental	50	50	56	52	56	49	65	55	65	54	68	59

Figure 3.31: Dual color competition assay with candidate genes from T1-160 EPIKOL screen. A. Schematic of dual color competition assay. After mixing eGFP+ and mCherry+ cells, mixtures were divided into two and either treated with 160 nM Taxol or equivalent volume of DMSO. Cells were imaged every four days**. B.** Results of competition assay as a heat map.

3.3.2 Epigenetic probe-library screen on SUM159 Taxol resistant cells

As an alternative approach to knockout screen, we utilized a chemical probe library that targets epigenetic proteins. Epigenetic probe library was a kind gift from Udo Oppermann (Oxford, UK) (**Figure 3.32A**). First, SUM159PT Parental and Taxol resistant cells were seeded on 384-well plates and next day treated with indicated dose of taxol and epigenetic probe library. IC20-30 concentration of taxol was aimed during the screen for both of the resistant cells. However, dose selection was based on the cell viability results of 96-well plate and selected concentrations of taxol affected the cells in 384-well plate more than expected. After 72 hours of incubation, cell viability was measured using Cell-

Titer Glo. Results were normalized to DMSO control of each cell line (**Figure 3.32B**). Waterfall plot of the screen results shows effect of epigenetic probes only (grey dots) and effect of epigenetic probe and taxol combination (colored dots) (**Figure 3.32C,D,E**). For combination treatment, taxol dose that gives 50-80% cell viability was aimed for each cell to better show the effect of combination. Both in T1-160 and T2-450 screens, several epigenetic probes showed synergistic effects with taxol. These include LLY-507, OF-1, TRIM24/BRPF, SGC-CBP30, CBP/BRD4, SIRT1720, GSK343, GSK8814, GSK864, AGK2, K00135, UNC1999, UNC2400 and PFI-4. According to their functions, most of these probes inhibit bromodomain containing proteins (**Figure 3.32F**). Importantly, two of these probes (SGC-CBP30 and CBP/BRD4) targets CREB-binding protein (CBP) which has a histone acetyltransferase and acts as a reader through its bromodomain. Three of these probes (OF-1, TRIM24/BRPF and PFI-4) inhibit the Bromodomain and PHD Finger Containing (BRPF) family proteins which are the scaffold subunits of several histone acetyltransferase complexes. In addition, bromodomain inhibitors did not show any effect on parental cells (selected drugs were labeled) (**Figure 3.32C**).

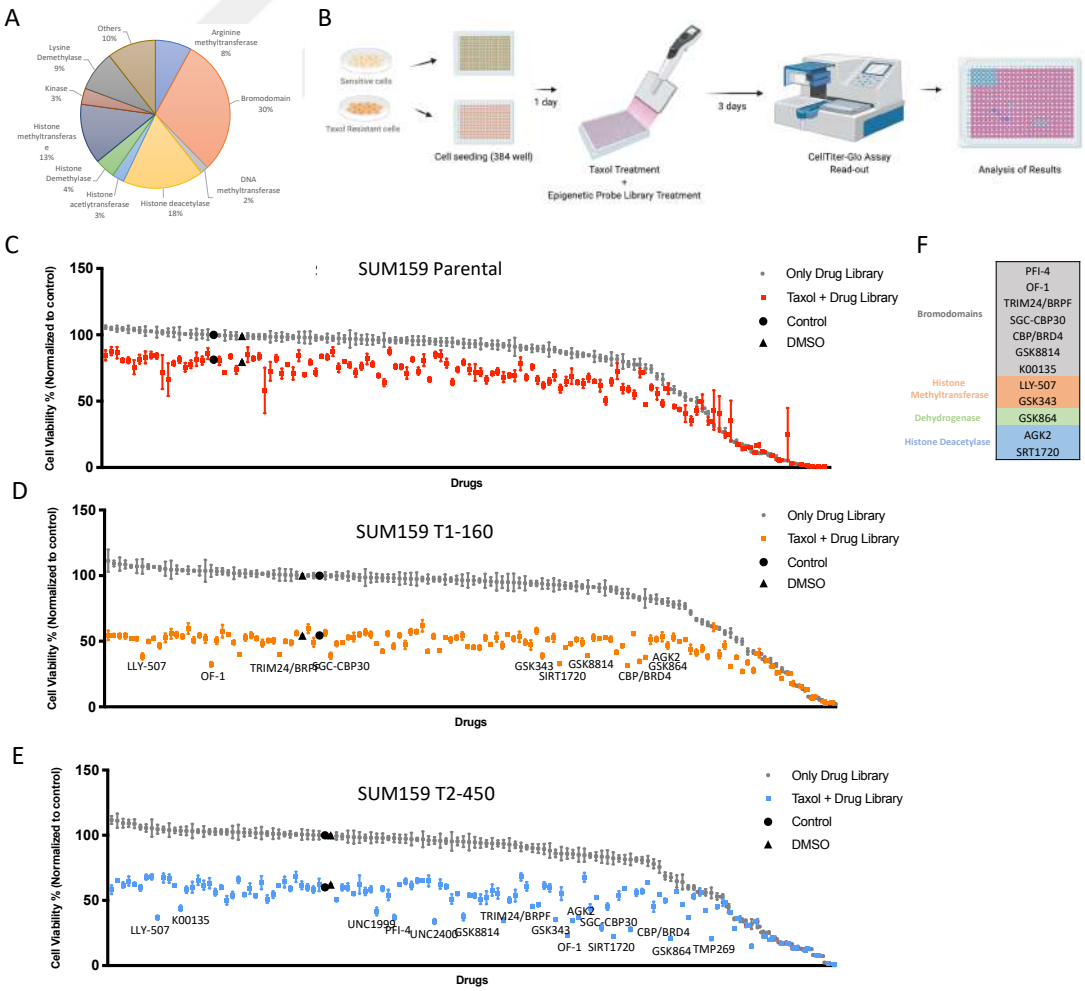

Figure 3.32: Chemical probe library screen on Taxol resistant SUM159PT cells. A.

Composition of Epigenetic chemical probe library. **B.** Chemical screen schematic. Cells were seeded to 384 well plates as 750 cells/well and next day treated with Taxol (Parental: 1.5 nM, T1-160: 300 nM, T2-450: 500 nM) and 1x concentration of epigenetic probe library. After 3 days, cell viability was measured with Cell-Titer glo. **C.** Results of chemical probe screen on SUM159PT Parental cells. Grey dots represent the effect of **Figure 3.32 Figure Legend Continues:** epigenetic probes alone. Colored dots show the changes in cell viability when Taxol was combined with a given epigenetic probe. **D.** Results on SUM159PT T1-160 cells. **E.** Results on SUM159PT T2-450 cells. F. Different groups of epigenetic modifiers that were identified as a hit in both taxol resistant cell screens.

Notably, through EPIKOL screens and epigenetic probe library screens on SUM159PT taxol resistant cells, we identified same protein (BRPF1) as a common hit which reverts taxol resistance. As a result, we focused on BRPF1 with functional assays to reveal the mechanism that causes taxol resistance in TNBC.

3.3.3 Validation of the effect of BRPF1 on SUM159PT Taxol resistant cells

BRPF1 Knockout

As a result of EPIKOL screen on T1-160 cells, BRPF1 was identified as a candidate gene that reverts resistance upon knockout (**Figure 3.33**). Counts of BRPF1 targeting sgRNAs were only decreased in taxol treated group during the screen (**Figure 3.33A**). This sensitizer effect was also confirmed during the competition assay where the -taxol samples were very similar to NT1 control while the +taxol samples significantly differed (Fig26). **Figure 3.33B** shows representative images and its quantification from competition assay as well as ABCB1 as a positive control.

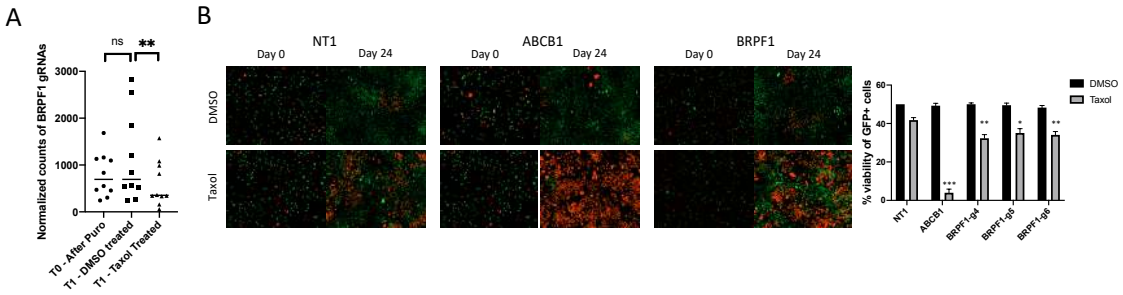

Figure 3.33: Competition assay for validation of the effect of BRPF1 knockout. A. Normalized counts of 10 BRPF1 targeting sgRNAs in initial (After Puro) and final timepoints (DMSO and Taxol treatment). **B**. Representative images of competition assay showing preferential depletion of ABCB1 or BRPF1 knockout cells from the population in the presence of Taxol and its quantification.

To further validate the effect of BRPF1 knockout, we first checked the knockout efficiency with western blot. **Figure 3.34A** shows total clearance of BRPF1 with three different sgRNAs. These sgRNAs were selected from the most depleted sgRNAs during EPIKOL screen. Although BRPF1 knockout affected colony formation in DMSO control

group, its effect was more prominent upon taxol treatment with very few colonies (**Figure 3.34B**).

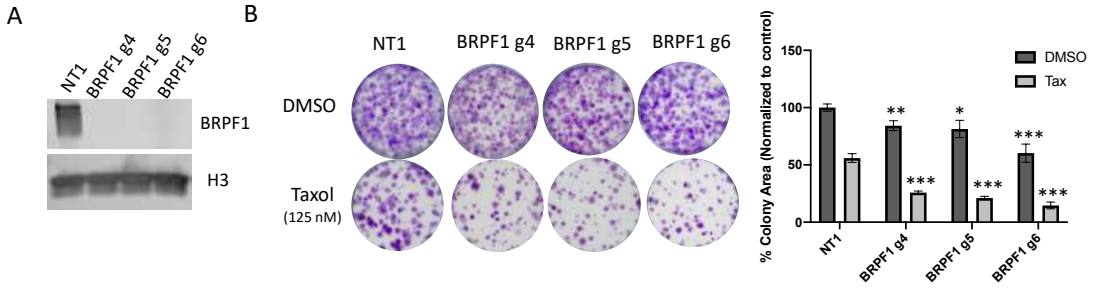

Figure 3.34: BRPF1 knockout on T1-160 cells. A. Western blot of BRPF1 knockout samples with BRPF1 antibody. **B.** Colony formation assay upon BRPF1 knockout in the presence of taxol and its quantification.

BRPF family contains three members which are BRPF1, BRPF2 (BRD1) and BRPF3. Although all of these proteins were targeted by EPIKOL, in T1-160 screen, only BRPF1 was identified as a taxol sensitizer. No change was observed in BRPF2 and BRPF3 sgRNAs during the screen. To confirm that the taxol sensitizer effect is only specific to BRPF1, colony formation assay was performed on T1-160 and T2-450 cells with 2 sgRNAs per gene (**Figure 3.35**). In T1-160 cells, BRPF1 knockout cells could not form colonies in the presence of taxol confirming previous results. We did not observe a significant change in BRPF2 and BRPF3 knockout cells in DMSO or Taxol conditions when compared to NT1 control. Interestingly, in T2-450 cells, BRPF1 knockout alone was enough to reduce number of colonies. Upon taxol treatment there was no differential change in BRPF1 knockout T2-450 cells. Similarly, no sensitizing effect was observed in BRPF2 and BRPF3 knockout T2-450 cells. These results showed that, BRPF1 acts as a sensitizer in T1-160 cells and is essential for fitness of T2-450 cells. This also shows that the two chemotherapy resistant subpopulation of the same cell line (SUM159PT) may be evolved with different resistance mechanisms.

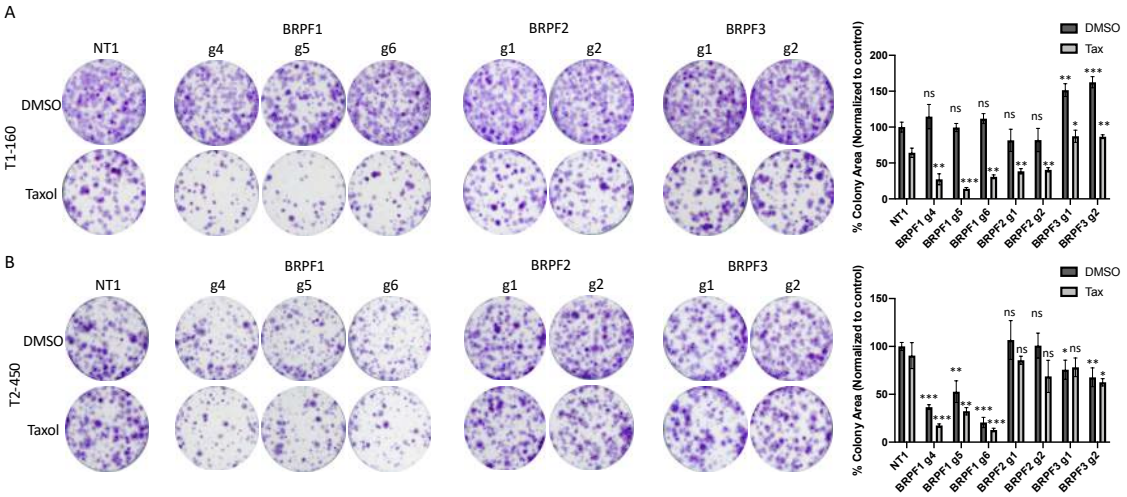

Figure 3.35: Effects of BRPF1, BRPF2, BRPF3 knockouts on T1-160 and T2-450 Taxol resistant cells. A. T1-160 cells. **B.** T2-450 cells

BRPF1 Silencing with siRNA

To further characterize the effect of BRPF1 loss, we utilized RNA silencing approach. siRNA against BRPF1 lead to significant reduction in BRPF1 mRNA in T1-160 cells (**Figure 3.36A**). Similar to the knockout experiments, siBRPF1 samples formed colonies in control conditions with a slight reduction in colony numbers but could not form colonies upon taxol treatment (**Figure 3.36B**). Loss of BRPF1 lead to significantly lower IC_{50} of taxol in T1-160 cells (**Figure 3.36C**). Altogether, these results confirmed that BRPF1 regulates chemotherapy resistance in T1-160 cells.

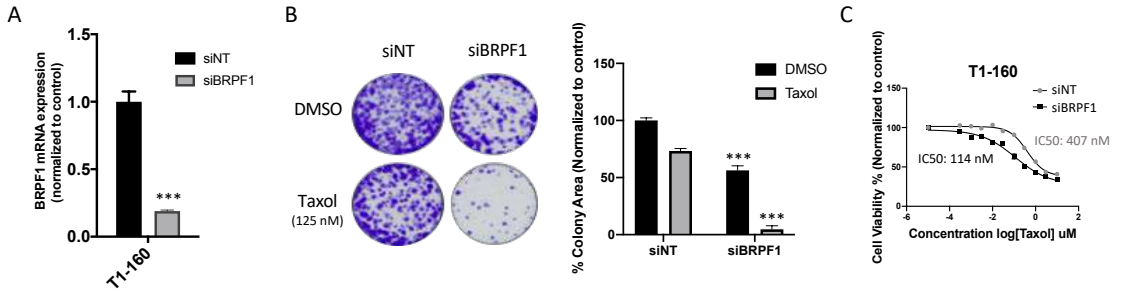

Figure 3.36: BRPF1 siRNA on T1-160 cells. A. BRPF1 mRNA expression level upon siRNA treatment. **B.** Colony formation assay upon BRPF1 silencing in the presence of taxol and its quantification. **C.** Cell viability response of siBRPF1 samples when compared to siNT in the presence of taxol.

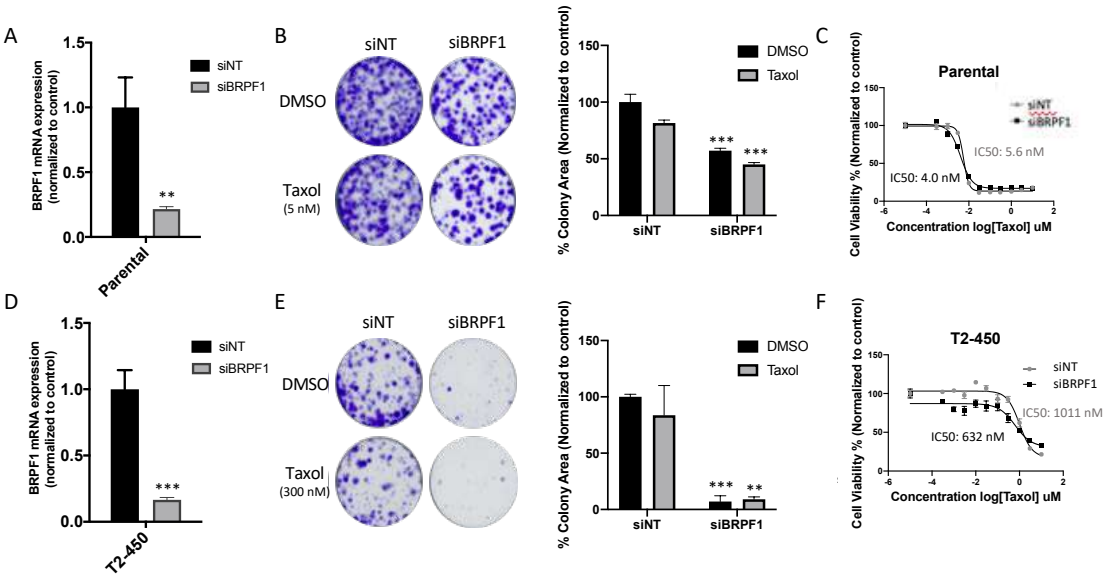

Figure 3.37: BRPF1 siRNA on SUM159PT Parental and T2-450 cells. A. BRPF1 mRNA expression level upon siRNA treatment. **B.** Colony formation assay upon BRPF1 silencing in the presence of taxol and its quantification. **C.** Cell viability response of siBRPF1 samples when compared to siNT in the presence of taxol.

BRPF1 loss in parental SUM159PT cells reduced colony numbers in control conditions but did not cause a differential effect upon taxol treatment (**Figure 3.37A,B**). IC_{50} values of taxol did not significantly changed in parental cells upon BRPF1 loss (**Figure 3.37C**). In T2-450 cells, we observed a similar phenotype to knockout samples where the BRPF1 loss leads to significant decrease in colony numbers in control conditions without further effect upon taxol treatment (**Figure 3.37D,E,F**).

BRPF1 inhibitors on SUM159PT resistant cells

Chemical probe library screen on SUM159PT cells revealed several different groups of epigenetic probes that can revert resistance to taxol (**Figure 3.32**). Interestingly, one group was bromodomains and three of these inhibitors target BRPF bromodomain family. To further validate the effects of BRPF inhibitors, we treated SUM159PT taxol resistant cells with PFI-4 (BRPF1-B specific) and OF-1 (pan-BRPF) (**Figure 3.38**). These inhibitors have different chemical structures and therefore strengthens the observed results (**Figure 3.38A**). In parental SUM159PT, inhibitors did not further affect cell viability. However, in T1-160 and T2-450 cells, both inhibitors significantly decrease cell viability in a concentration dependent manner (**Figure 3.38B**).

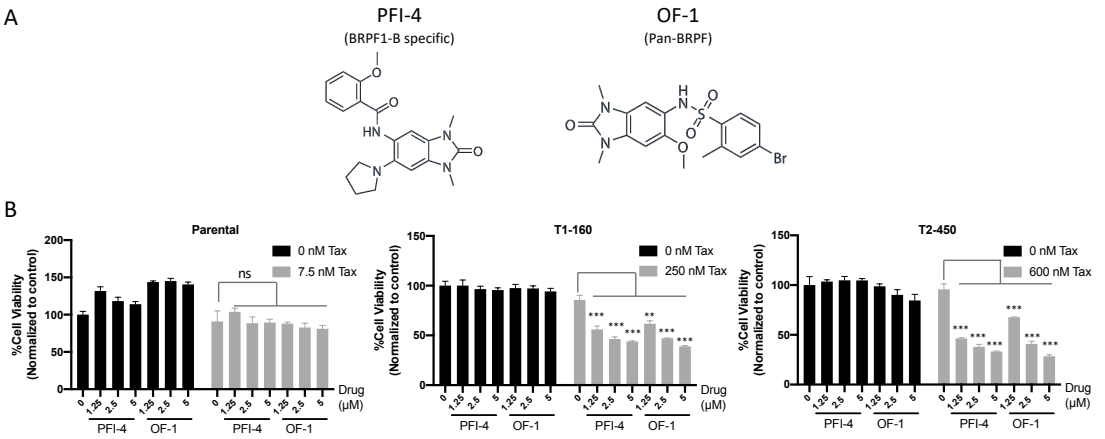

Figure 3.38: Effect of PFI-4 and OF-1 on SUM159PT taxol resistant cells. A. Chemical structure of PFI-4 and OF-1. PFI-4 specifically targets BRPF-1 and OF-1 is a pan-BRPF inhibitor acting against BRPF1/BRPF2/BRPF3. **B.** Cell viability response of combination treatment with taxol.

There are additional chemical inhibitors of BRPF family which are not present in our chemical probe library. These are GSK5959 and GSK6853 (both BRPF1 specific), Ni-42 and Ni-57 (pan-BRPF, mostly targeting BRPF1) and Bay299 (BRPF2 specific). In parental SUM159PT cells, none of the inhibitors showed synergistic effect similar to the PFI-4 and OF-1 results (**Figure 3.39A**). In T1-160 cells, BRPF1 specific inhibitor GSK5959 significantly decreased cell viability in combination with taxol without an effect in GSK5959 only treatment (**Figure 3.39B**). In T2-450 cells, GSK5959 decreased cell viability both alone and in combination with taxol (**Figure 3.39C**). The effect of GSK5959 was in line with the BRPF1 knockout or silenced samples. BAY299 also slightly decreased cell viability on its own and in combination treatment in every cell line. We did not observe a significant change in cell viability in other inhibitors.

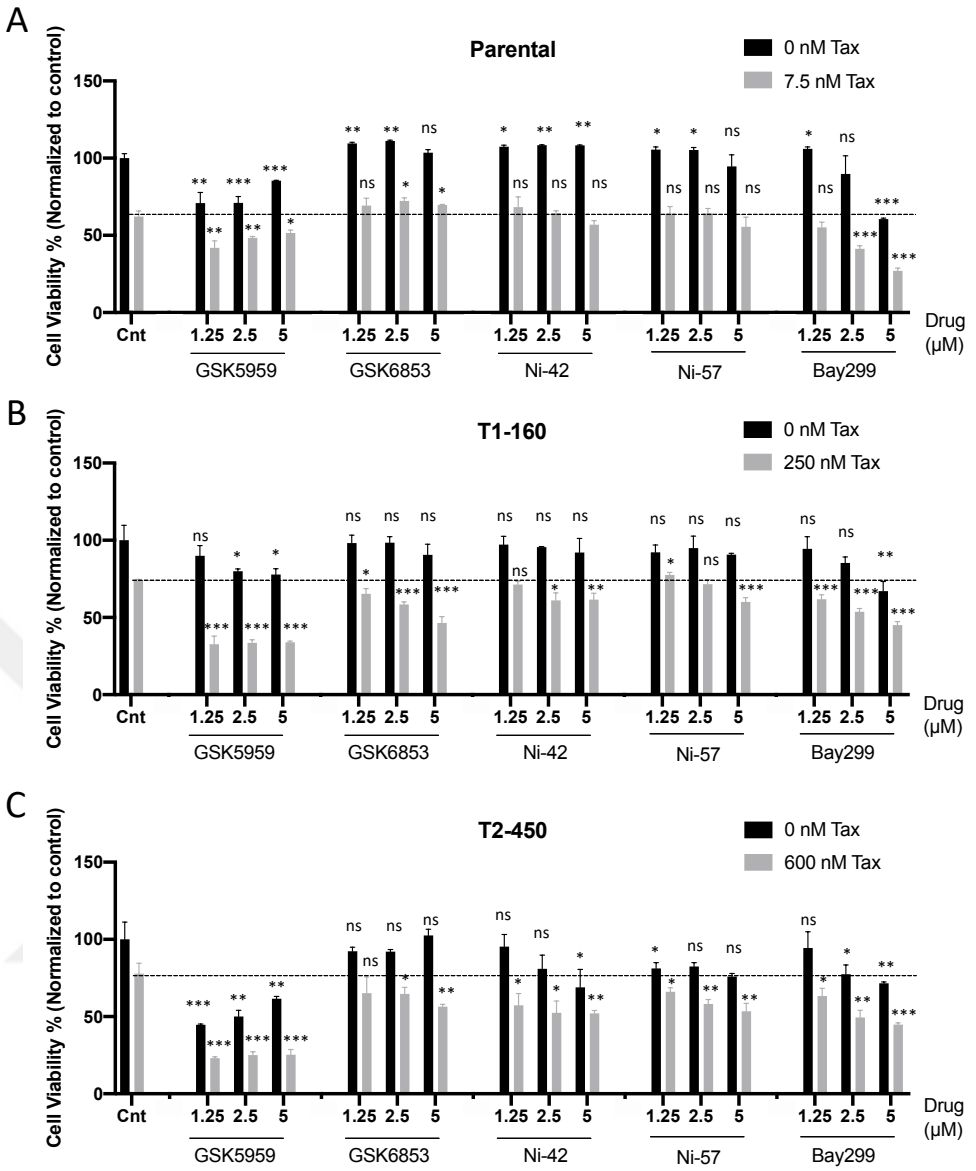

Figure 3.39: Cell viability results of BRPF1 inhibitors that are not found in chemical probe library. A. SUM159PT parental and **B. and C.** taxol resistant cells.

We further characterized the two inhibitors (PFI-4 and OF-1) that we identified during epigenetic probe library screen with additional functional assays. Live cell imaging of combination treatment in SUM159PT parental and taxol resistant cell lines showed that the cells can propagate in the presence of BRPF1 inhibitors alone (**Figure 3.40A**). However, in combination with taxol, resistant cells die while the parental cells are not affected. Notably, OF-1 shows a slight toxic effect on parental and T2-450 cells. Colony formation assay of combination treatment clearly showed the sensitizer effect of BRPF1 inhibitors with almost no colonies (**Figure 3.40B**).

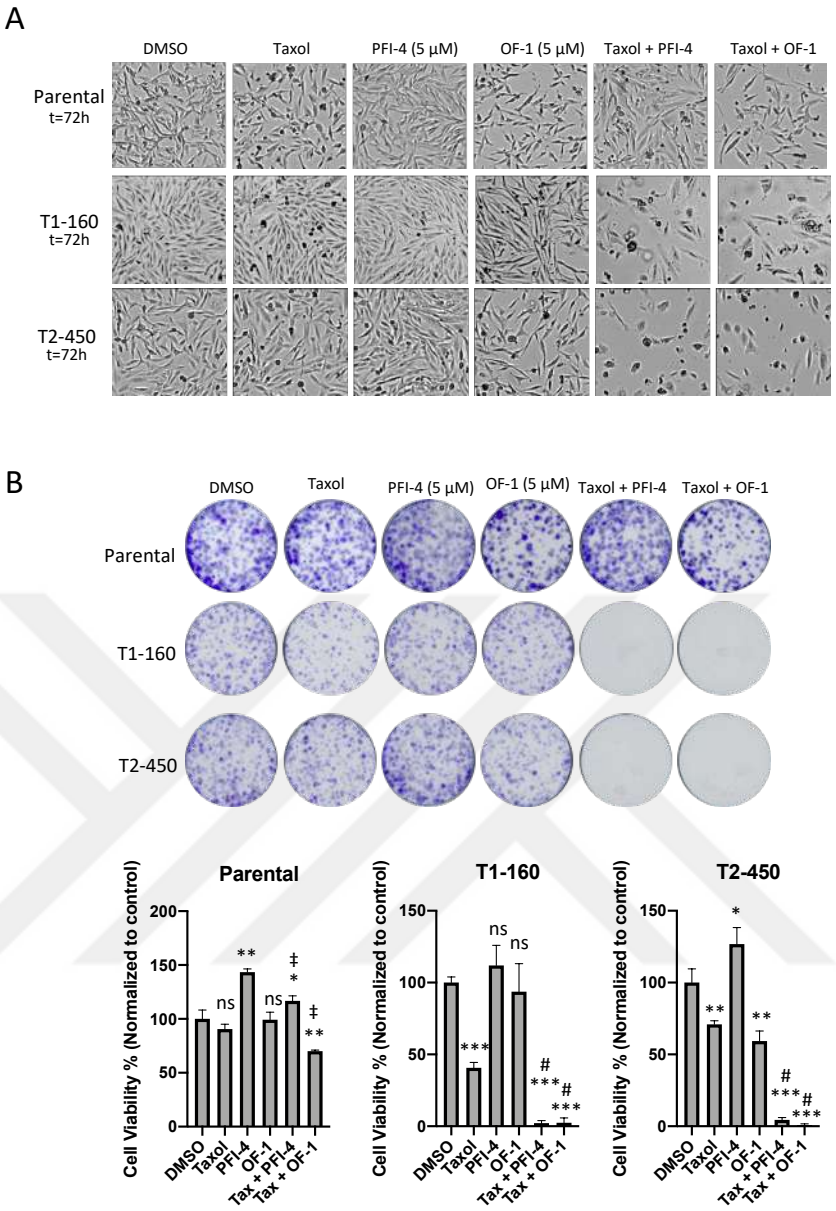

Figure 3.40: Combination of BRPF1 inhibitors and Taxol. A. Representative images of live cell microscopy in the presence of DMSO, Taxol (10 nM for Parental, 200 nM for T1-160 and 500 nM for T2-450), PFI-4 (5 µM), OF-1 (5 µM) and their combination with Taxol. **B.** Clonogenic assay results of Taxol (3 nM for Parental, 125 nM for T1-160 and 300 nM for T2-450) and BRPF1i (5 µM each) combinations with quantification. Asterisks indicate p values when compared to DMSO control ($p<0.05$ *, $p<0.01$ **, $p<0.001$ ***). ‡ indicates $p<0.01$ and # indicates $p<0.001$ when compared to Taxol.

To understand the mechanism of death upon combination treatment with BRPF1 inhibitors, we checked PARP cleavage (c-PARP) by western blotting. In parental cells, we observed c-PARP in taxol and combination treated samples possibly due to taxol. In resistant cells, c-PARP was only present after combination treatment showing apoptosis induction in these cells (**Figure 3.41A**). Then, immunofluorescence staining was performed with α--tubulin antibody to observe morphological changes upon combination

treatment in T1-160 cells. Only in samples treated with taxol and BRPF1 inhibitors, dead cells with apoptotic-body like structures were observed (**Figure 3.41B**).

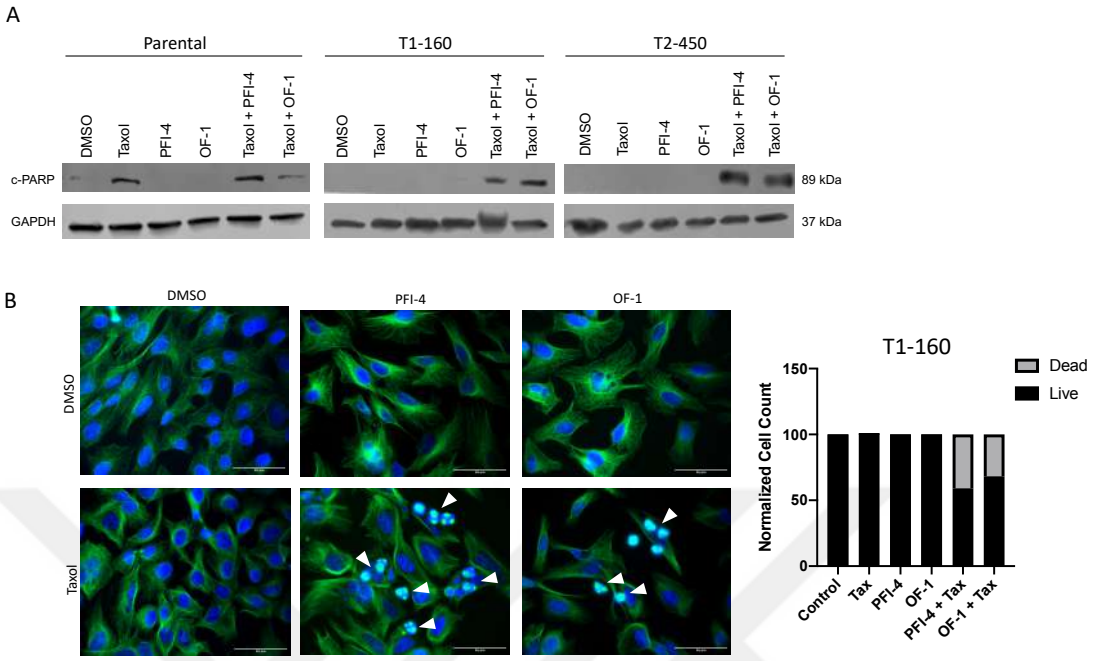

Figure 3.41: Cell death mechanism of combination treatment. A. Western Blot anaylsis for cleaved-PARP (c-PARP) and GAPDH as loading control. **B.** Immunofluorescence staining with α-tubulin (green) and DAPI (blue) in the presence of Taxol (160 nM) and/or BRPF1 inhibitors (5 µM each) for 16 hours. Scale bar: 50 µm

Transcriptome analysis upon BRPF1 loss

To examine transcriptomic changes upon BRPF1 loss, we sent BRPF1 knockout and BRPF1 inhibitor treated samples to RNA sequencing (RNAseq). For this, T1-160 cells were treated with 5 µM of PFI-4 or OF-1 for 72 hours and cell pellets were collected. For knockout experiment, cells were transduced with two different sgRNAs and cell pellets were collected 12 days post-transduction. Both inhibitors induced gene expression changes, but it was more prominent in OF-1 treated samples (**Figure 3.42**). In BRPF1 knockout samples, sgRNA #5 induced more changes when compared to sgRNA #6. Then, we analyzed commonly upregulated and downregulated genes in knockout or inhibitor treated samples and showed with Venn diagrams. Interestingly, commonly upregulated genes did not overlap with any particular pathway while the commonly downregulated genes significantly overlapped with ribosome biogenesis related pathways in both groups (**Figure 3.42**).

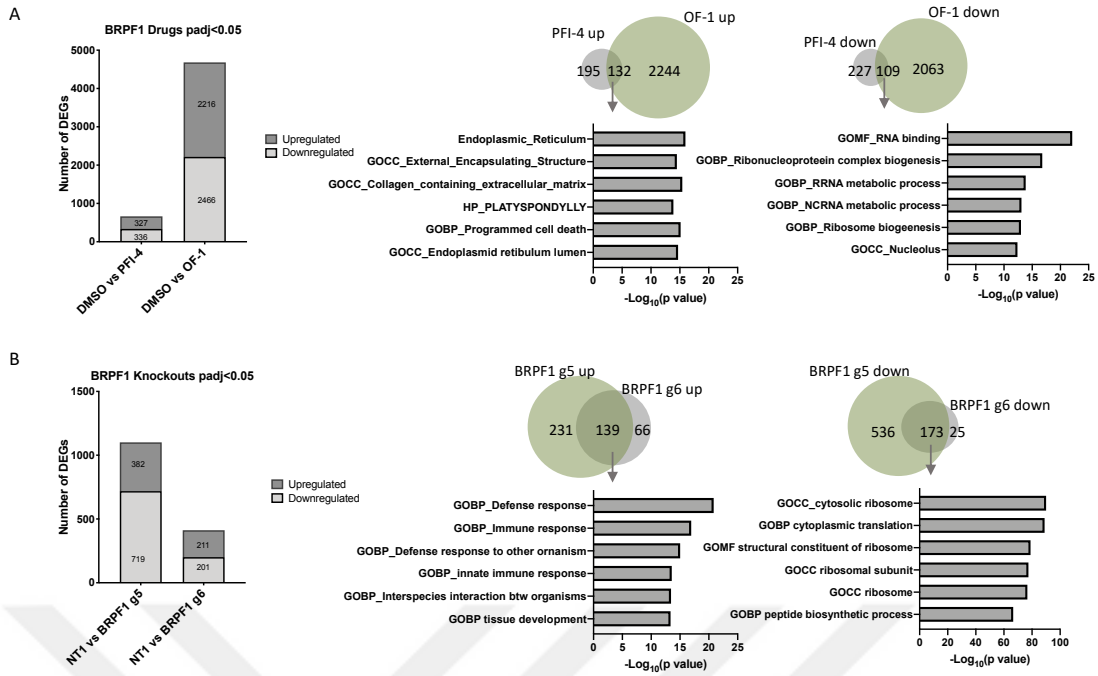

Figure 3.42: Transcriptome analysis of BRPF1 loss. A. DEGs in PFI-4 (5 µM) or OF-1 (5 µM) treated samples. Venn Diagrams of commonly upregulated and downregulated genes and biological processes that they overlap. **B.** DEGs in BRPF1 sgRNA #5 or #6 transduced samples. Venn Diagrams of commonly upregulated and downregulated genes and biological processes that they overlap.

Later, genes upregulated in T1-160 cells and downregulated upon knockout or drug treatment are analyzed together. For this, only p val <0.05 cutoff was applied without an LFC cutoff. Not the inhibitor treatment but the knockout of ABCB1 decreased the expression of ABCB1 in RNAseq (**Figure 3.43**).

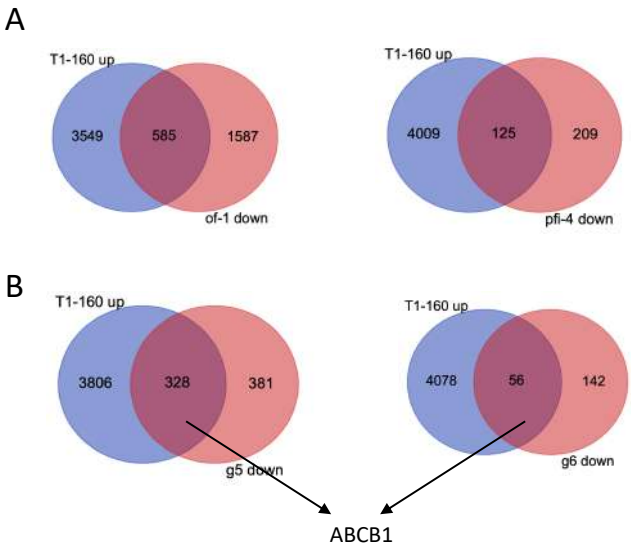

Figure 3.43: Downregulated genes upon inhibitor or knockout treatment. A. Comparison of upregulated genes in T1-160 and downregulated genes in inhibitor treated samples with p<0.05 cutoff. **B.** Comparison of upregulated genes in T1-160 and downregulated genes in BRPF1 knockout samples with p<0.05 cutoff.

Effect of BRPF1 loss on ABCB1 expression

To better understand the relationship between BRPF1 and multidrug resistance, we checked the expression of ABCB1 upon BRPF1 manipulation (**Figure 3.44**). We observed a small but significant and consistent decrease in ABCB1 mRNA expression upon PFI-4 and OF-1 treatment as well as upon RNAi silencing or knockout of BRPF1 with the most prominent effect observed in inhibitor treatment. Interestingly, we observed a significant decrease in ABCB1 mRNA expression in the same inhibitor treated samples that we sent to RNAseq with qPCR. The reason that we did not detect ABCB1 as a significantly downregulated gene might be an artifact of bioinformatic analysis of RNAseq experiment. These results suggested that BRPF1 might be regulating the ABCB1 expression either by direct binding to its promoter by BRPF1 or due to the decreased translational activity of the cells upon BRPF1 loss as seen in the RNA-seq results.

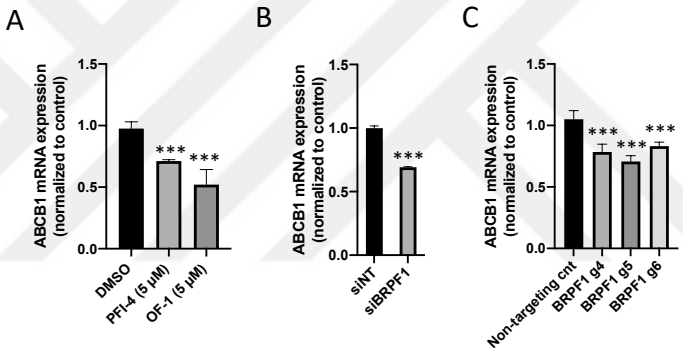

Figure 3.44: ABCB1 mRNA expression upon BRPF1 manipulation. A. T1-160 cells were treated with BRPF1 inhibitors PFI-4 and OF-1 for 72 hours. **B.** BRPF1 was silenced using siRNA and cells were collected 48 hours later than the transfection. **C.** ABCB1 mRNA levels was measured at day 12 post-transduction of three different sgRNAs.

Effect of BRPF1 on ABCB1 regulation

To differentiate the effect of BRPF1 on ABCB1, we performed a ChIP-qPCR experiment. Since BRPF1 antibody does not work in the chromatin immunoprecipitation, we first needed to clone BRPF1 into a backbone containing a tag that is suitable for pulldown. To be able to manipulate BRPF1 after overexpression, we decided to use dTAG system (**Figure 3.45A**) (Nabet et al., 2018). In this system, protein of interest is expressed as a chimera containing a mutant version of FKBP ($FKBP^{F36V}$). Chemically synthesized degrader molecules (dTAGs) are able to bind $FKBP^{F36V}$ causing it to dimerize with CRBN and recruit E3 ubiquitin ligase system. As a result, protein of interest is ubiquitinated and degraded. This system allows for both overexpression of the BRPF1

and also its degradation to draw conclusions by comparing the samples with each other in different assays. To this end, we cloned BRPF1 into pLEX305-c-dTAG plasmid containing FKBP^{F36V}and double-HA molecules that allows for pull-down of the BRPF1 (**Figure 3.45B**).

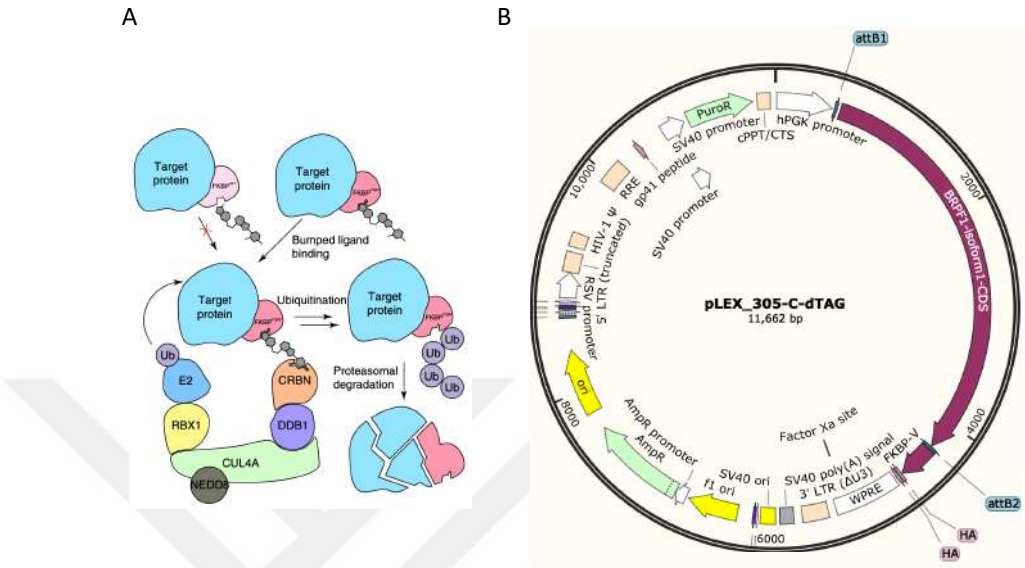

Figure 3.45: dTAG system and BRPF1-dTAG fusion protein. A. shematic of dTAG system. **B.** Plasmid map of pLEX305-c-dTAG system containing BRPF1 coding sequence.

To confirm BRPF1-dTAG fusion protein is expressed and can be degraded upon dTAG47 chemical treatment, we transduced T1-160 cells with lentiviruses containing BRPF1-dTAG plasmid and selected the transduced cells with puromycin. After selection, cells were treated with 100 nM of dTAG47 for 16 hours to allow for degradation. Following treatment, expression of fusion protein and its degradation was monitored by western blot (**Figure 3.46A**) and immunofluorescence staining with HA antibody (**Figure 3.46B**). Immunofluorescence staining was performed with the help of Nareg Pınarbaşı. In western blot, both BRPF1 and HA antibodies showed clear expression of BRPF1-dTAG fusion protein after nuclear fractionation. Immunofluorescence staining also detected the overexpressed BRPF1-dTAG fusion via HA staining as indicated by the green dots inside the cells. A study showed that BRPF1 is expressed as dot like structure in the cytoplasm when it is alone. However, when the other subunits such as MOZ/MORF, ING5 and EAF6 is expressed together, BRPF1 is translocated to the nucleus with its associated complex (Ullah et al., 2008). Upon dTAG47 treatment, BRPF1 loss was confirmed in both methods.

After confirming the BRPF1 overexpression and degradation, we performed a ChIP assay with HA antibody followed by qPCR in collaboration with Beyza Dedeoğlu

from Ceyda Açılan-Ayhan's laboratory (**Figure 3.46C**). As a positive control, we used RUNX2 acetylation where we see significant BRPF1 binding when compared to negative control. Fold enrichment in ABCB1 specific region was significantly higher than the positive control that indicates a clear binding of BRPF1 to ABCB1 promoter. These results suggest that BRPF1 directly binds to ABCB1 promoter to regulate the chemotherapy resistance of T1-160 cells explaining the re-sensitization of T1-160 cells to taxol upon BRPF1 loss.

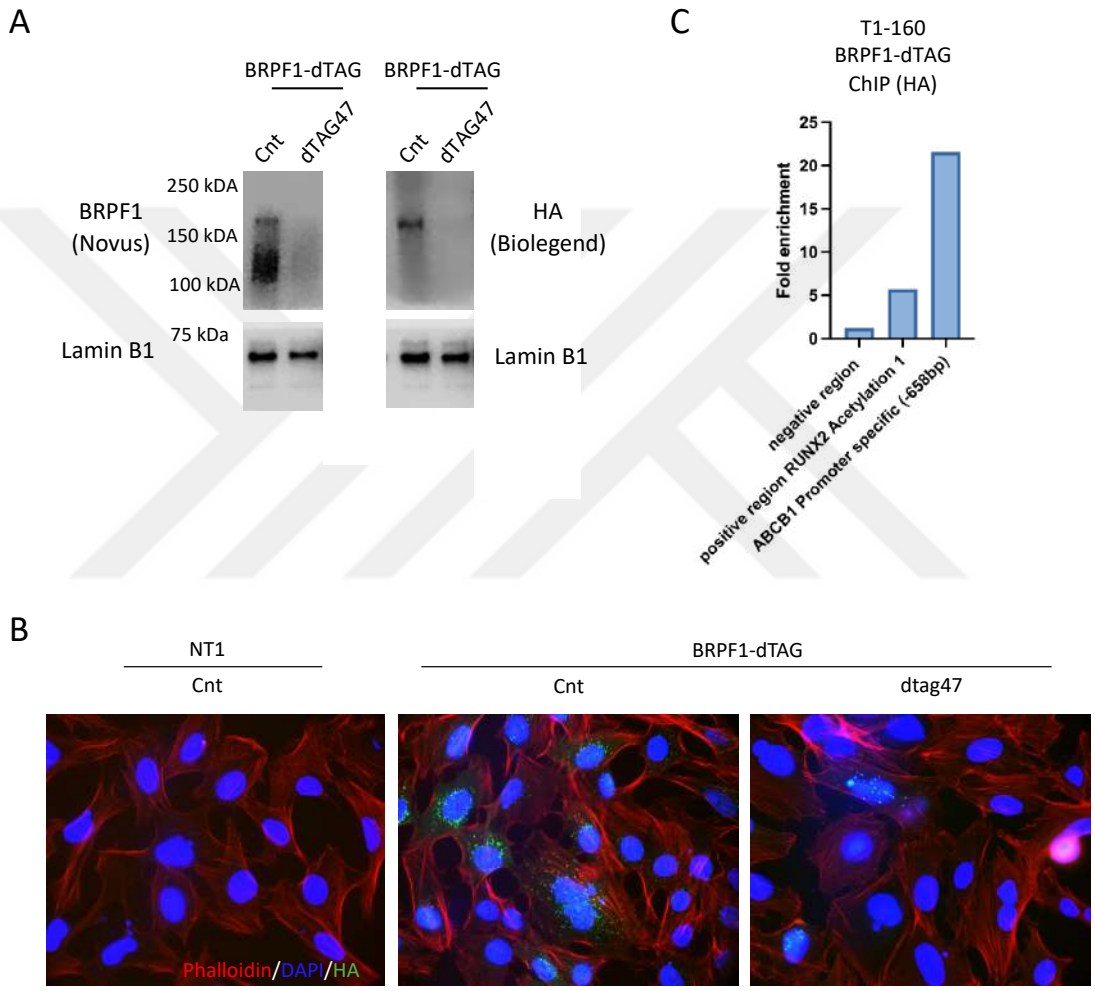

Figure 3.46: Confirmation of BRPF-dTAG fusion protein expression and ChIP-qPCR. A. Western blot showing BRPF1-dTAG overexpression and degradation with dTAG47 in T1-160 cells with two different antibodies (BRPF1 and HA) after nuclear fractionation. **B.** Immunofluorescence staining in T1-160 cells either expressing NT1 or BRPF1-dTAG with HA antibody. C. ChIP-qPCR analysis on T1-160 cells expressing BRPF1-dTAG.

Chapter 4

DISCUSSION

Triple-negative breast cancer (TNBC) is the most aggressive and recurrent type of breast cancer. Standard treatment of TNBC is with surgery followed by chemotherapy. Although TNBC is responsive to chemotherapy, overall survival of patients is worst when compared to other BC subtypes. This is due to the brain and lung metastasis and chemotherapy resistance in metastasized population. Development of epigenetic therapies gained momentum in the last decades since the role of epigenetics both in carcinogenesis and chemotherapy resistance is well established. HDAC and DNMT inhibitors were combined with cytotoxic chemotherapy however due to their broad effect and toxicity, more targeted epigenetic therapies are required.

In this thesis, we aimed to unravel chromatin-based vulnerabilities of naive and chemotherapy resistant TNBC cells. To this end, we generated a focused epigenetic knockout library (EPIKOL) and chemotherapy resistant TNBC cell lines. With functional genomics approach, we identified two novel targets in naïve TNBC cells as well as their taxol resistant counterparts.

In vitro EPIKOL screens in naïve TNBC cell lines reveals epigenetic vulnerabilities of TNBC cell fitness.

Through in vitro knockout screens, we demonstrated the efficiency of in-house generated epigenome-wide pooled CRISPR library (EPIKOL) (Yedier-Bayram et al., 2022). Unlike other currently available epigenome-targeting CRISPR libraries (Halaburkova et al., 2020; Henser-Brownhill et al., 2017; Li et al., 2020), EPIKOL has broader target distribution including chromatin remodelers, cofactors and structural subunits and greater number of sgRNAs per gene. This allows EPIKOL to interrogate the functions of epigenetic complexes as a whole. EPIKOL is available in two different backbones, pLentiCrisprv2 and LentiGuide, and has expected distribution of positive and negative controls in plasmid level as well as in transduced cells.

As a result of EPIKOL screens on three TNBC cell lines namely MDA-MB-231, SUM159PT and SUM149PT along with non-malignant control cell line HMLE allowed us to unravel TNBC specific cell fitness genes. Apart from well-known fitness-related genes in TNBC such as UHRF1 (Gao et al., 2017), PELP1 (Zhang et al., 2015) and

PRMT1 (Liu et al., 2019), we identified 12 additional genes that are not previously linked to TNBC fitness. Although they are not linked to TNBC, they are known as pan-cancer essential genes in Cancer Dependancy Map (*DepMap*) except ASH2L. Identification of previously known genes verified the performance of EPIKOL in revealing epigenetic vulnerabilities. In complex level, commonly depleted genes mainly belong to SWR, NUA4, RNA exosome, COMPASS, MLL, NSL and CAF-1 complexes.

Interestingly, EPIKOL screen revealed two genes commonly depleted in all TNBC cell lines, KANSL2 and KANSL3 belonging to the NSL complex (Radzisheuskaya et al., 2021). Moreover, catalytic subunit of NSL complex, KAT8 was found to be essential in two different TNBC cell lines. These genes did not cause any fitness defect in HMLE suggesting a TNBC specific effect. Earlier, NSL complex was linked to the H4K16Ac that is found in active enhancers and promoters causing chromatin relaxation (Sheikh et al., 2019; Su et al., 2016). The role of NSL complex in carcinogenesis is controversial. Downregulation of KAT8 and reduced H4K16Ac were previously associated with different cancer types, such as ovarian cancer (M. Cai et al., 2015), colorectal carcinoma (Cao et al., 2014), hepatocellular carcinoma (Zhang et al., 2014) and gastric cancer (Cao et al., 2014). In contrast, increased expression of KAT8 in non-small cell lung cancer results in poor survival (Chen et al., 2014). Analyses of 298 cases of primary breast carcinomas through immunohistochemistry indicated that KAT8 protein level was decreased in a subset of the cases (18%) indicating that the role of KAT8 might be different in breast cancer development than in other types of cancers (Pfister et al., 2008). However, a recent study from Radzisheuskaya *et al.* showed that KAT8 mainly regulates H4K5Ac and H5K8Ac as a member of NSL complex and this activity is critical for cancer cell survival. KAT8 is also found in MSL complex regulating H4K16Ac. They also proposed that complete loss of KAT8 is more detrimental for KAT8-low tumors as this would completely destroy the activity of NSL complex (Radzisheuskaya et al., 2021). To date, there was no study linking KAT8 and NSL complex activity to TNBC cell survival. As a result of EPIKOL screens, we showed that KAT8 together with the two structural subunits of NSL complex (KANSL2 and KANSL3), decrease TNBC cell fitness and induce apoptosis. Interestingly, neither of the MSL complex structural subunits were found essential.

In addition to NSL complex, significant depletion of SS18L2 was observed in all TNBC cell lines except HMLE. SS18L2 is one of the homologs of SS18, which is the member of ATP-dependent chromatin remodeling complex BAF (SWI/SNF) (de Bruijn

& Geurts van Kessel, 2006). Only limited number of studies about SS18L2 are found in the literature leaving it as an uncharacterized gene especially in cancer setting. Together with BAF47, SS18 regulates normal expression of genes at promoter or enhancers. However, in synovial sarcoma, an oncogenic fusion of SS18/SSX competitively binds to BAF complex causing eviction of BAF47 and directs BAF complex to activate bivalent genes (McBride et al., 2018). The role of SS18L2 is not known in cancers and there is no study showing the effect of this gene in TNBC. However, it is identified as a common essential in DepMap via CRISPR screens. Interestingly, there was no effect on RNAi screens suggesting that residual SS18L2 might be enough to execute the specific function. SS18L2 only contains SNH domain that is required for the protein-protein interactions but not the QPGY domain related to the transcriptional activation (de Bruijn & Geurts van Kessel, 2006). It is shown that SS18L2 binds to BAF complex possibly via its SNH domain (Alerasool et al., 2022).It is possible that BAF complex with SS18L2 localizes to oncogenic regions in TNBC. We showed that knockout of SS18L2 decreased TNBC cell survival, induced G2/M arrest and concomitantly induced apoptosis. Knockouts of SS18 or SS18L1 did not show any effect on TNBC cell fitness strengthening the novel interactions of SS18L2 in TNBC.

As an advantage of EPIKOL, previously published epigenome-wide knockout libraries did not include KANSL2, KANSL3 and SS18L2 targeting sgRNAs failing to identify effects of these genes in the cancer context.

Although EPIKOL works efficiently, newer technologies based on CRISPR-dCas9 system such as CRISPR interference (CRISPRi) and CRISPR activation (CRISPRa) are continuing to be developed. These systems utilize deactivated or dead Cas9 (dCas9) fused to an activator or repressor. Thus, one can perform gain-of-function experiments as well with physiologically relevant overexpression levels (Lo & Qi, 2017).

***In vivo* EPIKOL screen recapitulates the findings of *in vitro* screen.**

To test the performance of EPIKOL *in vivo*, we also performed a screen using MDA-MB-231$^{Cas9\text{-}Fluc}$ cells in Nude mice and compared the results of two different timepoints as week 2 and 4. As expected, overall depletion scores and number of depleted positive control genes increased from week 2 to week 4. 9 out of 10 commonly depleted genes from both timepoints of *in vivo* screen were shared with the TNBC *in vitro* screen. TFDP1 was identified as an *in vivo* specific cell fitness gene. These results indicate that EPIKOL efficiently works *in vivo* and can recapitulate the findings of in vitro screens.

This high correlation is encouraging however more in vivo specific genes would be identified if we were able to perform an orthotopic screen in mammary fat-pad. Also, decrease in a library coverage due to the decrease in cell viability after implantation to mice is a limitation. Since, we performed 1000x representation of the EPIKOL library in vivo screen, we believe that effect of this loss was neglegable in our screens. Interestingly, one of the significantly depleted genes *in vivo* was SS18L2. Individual knockout of SS18L2 gene markedly impaired tumor growth when compared to control confirming that SS18L2 is required for formation and growth of TNBC tumors. Alternatively, a breast cancer tissue microarray mainly containing TNBC tumors showed high percentage of positive cores for SS18L2 expression. Altogether, these data suggested that SS18L2 is required for proliferation and fitness of TNBC cell lines and tumors.

SS18L2 is required for G2/M transition in TNBC cells

To elucidate the transcriptomic changes that is caused by SS18L2 loss, we performed an RNA sequencing. Although the number of upregulated genes were significantly higher than the downregulated genes, they were not specifically enriched in any specific biological process. However, downregulated genes were significantly enriched in cell cycle related pathways indicating that SS18L2 might be important for the cell cycle progress. Our detailed analysis showed that DREAM complex members and genes that function during the late G2/M phase were significantly downregulated. It is known that MuvB core of DREAM complex activates late G2/M genes through its relationship with MYBL2 and FOXM1 genes both of which are downregulated upon SS18L2 knockout (Fischer et al., 2016; Sadasivam & DeCaprio, 2013). In light of these data, we hypothesized that SS18L2 might be an upstream regulator of the late G2/M genes. Functional assays such as PIP-FUCCI confirmed that when SS18L2 is lost, cells become arrested in G2/M phase of the cell cycle.

Taxol resistant TNBC cell lines showed characteristics of multidrug resistance.

Chemotherapy resistance in TNBC is commonly observed in clinic decreasing the overall survival rates of patients. Efforts on identifying specific molecular targets in TNBC is still ongoing. To be able to study epigenetic vulnerabilities of chemotherapy resistant cells, we generated taxol or doxorubicin resistant TNBC cell lines since they are the most commonly used chemotherapeutics in TNBC.

For generation of chemotherapy resistant cells, there are two options: clinically relevant models or high-level laboratory models (McDermott et al., 2014). Clinically relevant resistance models are generated by mimicking the doses and regimens of chemotherapeutics that is applied to the patients in clinic. These models are more valuable in terms of reflecting the mechanisms observed in patients however their fold resistance is very low rendering it hard to maintain in laboratory. High level laboratory models are generated with the dose-escalation method yielding increased fold resistance. These cells are more stable for prolonged durations of experiments in the laboratory (McDermott et al., 2014). In total, we generated 8 different chemotherapy resistant cells lines (six resistants to taxol, two resistants to doxorubicin) that are resistant to the folds of their initial IC50 or IC10 amounts of the drugs. These resistant cells exhibited the characteristics of chemotherapy resistant cells such as increased IC50 values (McDermott et al., 2014) and decreased growth rate (Moore et al., 2012). Even the two different resistant cells derived from the same parental cell line may differ significantly from each other (Tegze et al., 2012). We observed a similar result in our resistant cells as understood from the colony formation assays, growth rates and transcriptomic changes. Number of differentially expressed genes upon becoming resistant was different in each cell line. In T1-160 cells, cell adhesion related pathways were positively enriched while pathways related with oxidative phosphorylation were significantly negatively enriched. It is reported that some paclitaxel resistant cells have altered mitochondrial dynamics resulting in a shift from oxidative phosphorylation to glycolysis (Zhou et al., 2020). Increase in aerobic glycolysis and glucose uptake has been linked to chemotherapy resistance in breast cancer (Desbats et al., 2020; Ruprecht et al., 2017). In T2-450 cells, inflammatory response related pathways were significantly positively enriched upon becoming resistant in line with the literature (Jones et al., 2016; Vyas et al., 2014).

Cross-resistance to other chemotherapeutics is also observed in our resistant cells as a well-known characteristic of multidrug resistance (Wu et al., 2014). Indeed, transcriptome analysis showed that ABCB1 was the most upregulated gene in taxol resistant SUM159PT cell lines. The link between ABCB1 overexpression and breast cancer chemotherapy resistance is extensively studied (Holohan et al., 2013; Kuo, 2007; Nemcova-Furstova et al., 2016). Other ABC transporters that are highly associated with taxol resistance such as ABCC1, ABCC3 and ABCG2 were not elevated in our resistant cells (Wu et al., 2014). SUM159PT taxol resistant cells were highly dependent on ABCB1 since the knockout resulted in complete sensitization of the cell to taxol. In most cases,

copy number alterations of ABCB1 was also reported (Genovese et al., 2017). However increase in copy numbers did not solely explain the very high expressions of ABCB1 suggesting that there are additional mechanisms contributing such as stabilization of mRNA or epigenetic regulation (Yabuki et al., 2007). Indeed, growing our resistant cells in a drug-free environment for at least 1 month (holiday) resulted in re-sensitization to taxol and decrease in ABCB1 expression to the parental cell levels suggesting an epigenetic control.

To better understand the temporal changes during resistance development, single-cell barcoding or single-cell RNAseq techniques would allow for deeper analysis (Tang et al., 2009; Zilionis et al., 2017). It would be very helpful to understand if ABCB1 upregulation is an early event or if it is due to the selection of poised cells or random cells with high expression of ABCB1.

Epigenetic focused screens identified BRPF1 as a possible target in taxol resistant cells

To delineate the epigenetic regulation of chemotherapy resistance in TNBC, we performed EPIKOL screens in the absence and presence of chemotherapeutic agents. As an advantage of EPIKOL, presence of context-specific positive controls such as drug-resistance related genes served as an internal control during the resistant cell screen analysis. In T1-160 cells, both ABCB1 and ABCG2 strongly depleted in taxol treated group when compared to DMSO control group. Several candidate genes including KMT2A and MEN1 showed strong depletions in competition assays in the presence of taxol. As a complementary approach, we also performed an epigenetic probe library screen in SUM159PT taxol resistant cells. Interestingly, in both types of screens, BRPF1 was the only common hit. BRPF1 is a bromodomain containing epigenetic reader that belongs to BRD family (Perez-Salvia & Esteller, 2017). BRPF1 is an essential gene during embryonic development and recently linked to the progression of hepatocellular carcinoma (Cheng et al., 2021; Klein et al., 2014). However, there is no study that shows an association between BRPF1 and taxol resistance.

BRPF1 knockout and silencing with siRNA sensitized T1-160 cells to taxol treatment with no effect in control samples. In T2-450 cells, BRPF1 loss impaired cell growth both in control and taxol treated samples indicating that BRPF1 acts as an essential gene rather than a sensitizer. This result also shows that T1-160 and T2-450 cells developed resistance via distinct molecular mechanisms. No effect was observed in naïve

parental cells upon BRPF1 loss suggesting that it has taxol resistance specific effects. BRPF2 and BRPF3 did not exert similar effects in any of the resistant cells.

BRPF1 inhibition or loss caused significant downregulation of ribosome biogenesis, RNA binding, rRNA processing related pathways. A study showed that deficiency of RUNX1, one of the known targets of BRPF1, decreases ribosome biogenesis and confers stress resistance (X. Cai et al., 2015; Ullah et al., 2008). It is possible that the effect that we observed upon BRPF1 knockout is due to the decreased expression of RUNX1 in the cells. However, downregulation of ribosome related genes in our cells reverted the resistance rather than supporting it. One hypothesis might be that the decreased ribosomal biogenesis lead to decreased protein synthesis especially the ABCB1 that is desperately needed by the taxol resistant cells. Indeed, downregulation in the mRNA levels of ABCB1 was observed both in BRPF1 knockout or BRPF1 inhibitor treated T1-160 samples. Our preliminary results on chromatin immunoprecipitation assay with the pulldown of HA-tagged BRPF1 protein demonstrated significant fold enrichment of BRPF1 in ABCB1 promoter. Collectively, these results showed that BRPF1 regulates taxol resistance via the maintenance of ribosome biogenesis and protein translation and thereby sustains the expression of ABCB1.

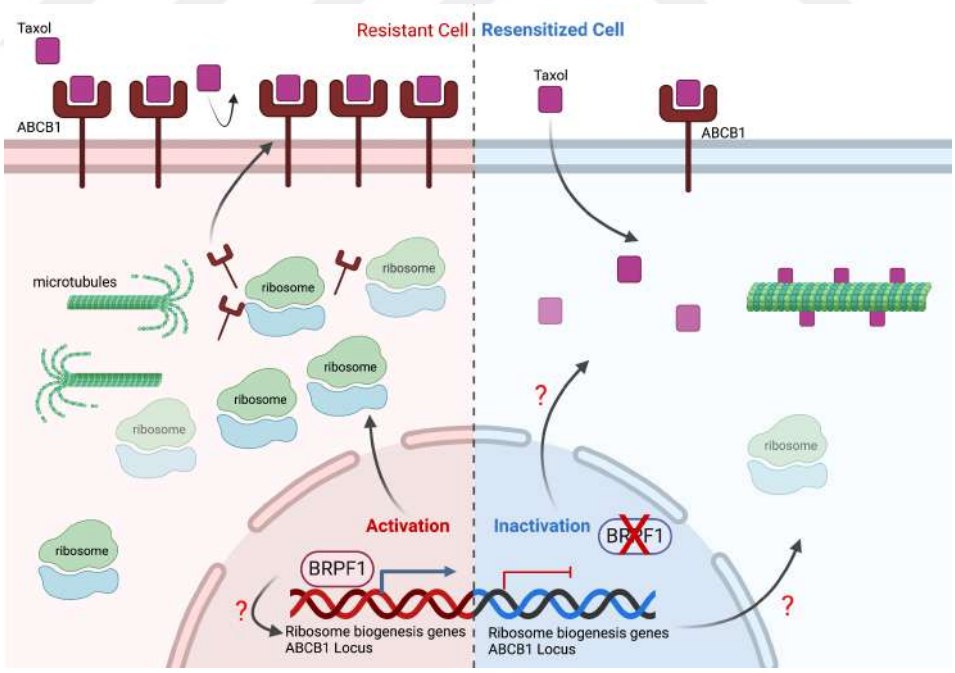

Figure 4.1: Proposed model of chemotherapy resistance regulation by BRPF1. In resistant cells, BRPF1 possibly binds to ribosome biogenesis related genes and increases translation rate by indirectly increasing ABCB1 expression. BRPF1 also binds to ABCB1 promoter and increase gene expression. If BRPF1 is knocked out or silenced, ribosome biogenesis decreases, and it cannot bind to ABCB1 promoter thus resulting in a decrease in ABCB1 expression and re-sensitization of resistant cells. Figure created in biorender.com

Chapter 5

APPENDIX

RNAseq and EPIKOL screens in other chemoresistant cells of TNBC

To understand the epigenetic regulators of chemotherapy resistance more broadly, we generated other taxol and doxorubicin resistant TNBC cell lines in addition to SUM159PT taxol resistant cells (**Figure 3.18, Figure 3.19**). In each cell type, one taxol resistant or one doxorubicin resistant cell were selected for further functional experiments. MDA-MB-231 60xIC10 taxol resistant cells (MDA-TaxR) were maintained in 21 nM taxol and SUM149PT 700xIC10 taxol resistant cells (SUM149-TaxR) were maintained in 22.4 nM taxol. SUM159PT 16xIC10 doxorubicin resistant cells (SUM159-DoxR) were maintained in 332 nM of doxorubicin. To reveal the transcriptomic changes upon becoming resistance, we performed RNA-seq with these cell lines. **Figure 5.1A** shows the number of DEGs in each cell line when the LFC>|-2| and pval<0.001 cutoff was applied. There were many upregulated and downregulated genes in all cell lines with smallest number in MDA-TaxR cells. After GSEA analysis with all genes without a cutoff, waterfall plots showed number of significantly enriched pathways in each cell line (**Figure 5.1B**). In line with the small number of DEGs in MDA-TaxR cells, only 1 gene set was significantly positively enriched. In other resistant cell types (SUM149-TaxR and SUM159-DoxR), number of significantly negatively enriched pathways was more than the positively enriched ones although the number of upregulated genes was more than the downregulated genes. Later, we performed an overlap analysis with only the most changed genes limiting their number to 500 at maximum and using MSigDB GO biological pathway gene sets (**Figure 5.1C**). In these cell lines, DEGs overlapped with different gene sets without an enrichment of a particular biological process.

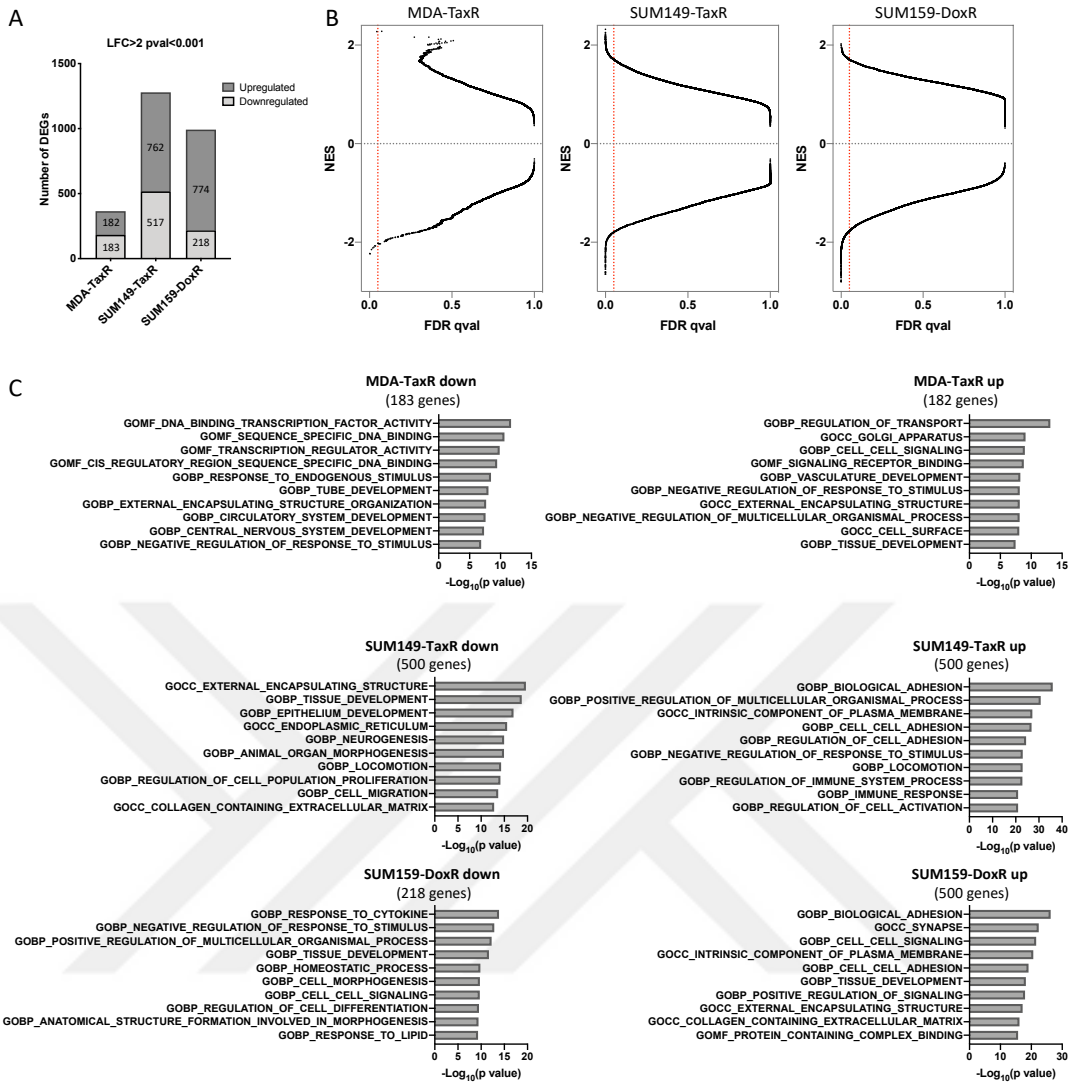

Figure 5.1: Transcriptome analysis of other chemotherapy resistant cells. A. Number of differentially expressed genes (DEGs) in all cell lines. **B.** GSEA plots showing negatively or positively enriched gene sets when all genes were analyzed together in ranked list format without a cutoff. Red dashed line indicates FDR qval<0.05 **C.** Overlap analysis of cells using MSigDB GO gene sets with the genes in LFC>|-2| and p<0.001 cutoff.

Interestingly, ABCB1 was not significantly upregulated in any of these resistant cell lines (**Figure 5.2**). This result may indicate that upregulation of ABCB1 is not an early event in chemotherapy resistance development since these cells are not as resistant as the SUM159PT taxol resistant cells. This also increases the likelihood that the ABCB1 is epigenetically regulated as an adaptation event in the later courses of resistance generation. Barcoding the cells while resistance generation or checking the copy number and expression of ABCB1 at specific time points during this process might help us to understand the actual mechanism.

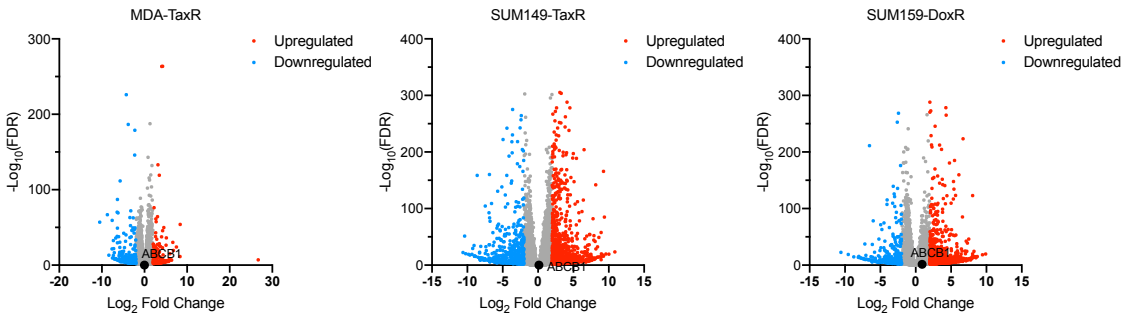

Figure 5.2: Volcano plots showing DEGs on other resistant cell lines. Location of ABCB1 is labeled as a black dot in each plot

Ultimately, we performed EPIKOL screens in these resistant cell lines to understand the epigenetic mechanisms underlying their resistance. For that, all cell lines were cultured in the maintenance dose of the drug that they are resistant. As control, a group of cells were treated with DMSO. NGS results of drug treated samples were compared to DMSO control group and depleted genes were identified (**Figure 5.3A,B, Figure 5.4**).

Depletion ratios was higher in MDA-MB-231 cell line when compared to other cells. Importantly, BRPF1 was also depleted in MDA-MB-231 taxol resistant cells in the presence of taxol indicating that the role of BRPF1 in regulating taxol resistance is not cell line specific. However, we did not observe BRPF1 depletion in SUM149PT taxol resistant cells. When the EPIKOL screen results of three taxol resistant cell line was analyzed together, we did not observe commonly depleted genes in all three cell lines (**Figure 5.3C**). However, several genes were identified as commonly depleted in at least two cell lines. MEN1, KMT2D, GATAD1 and BRPF1 was significantly depleted in MDA-MB-231 and SUM159PT taxol resistant cells. ARNTL was depleted in SUM149PT and SUM159PT taxol resistant cells. KMT2B, SNAI2, PCGF3, AURKA, CDK2 was significantly depleted in MDA-MB-231 and SUM149PT taxol resistant cells.

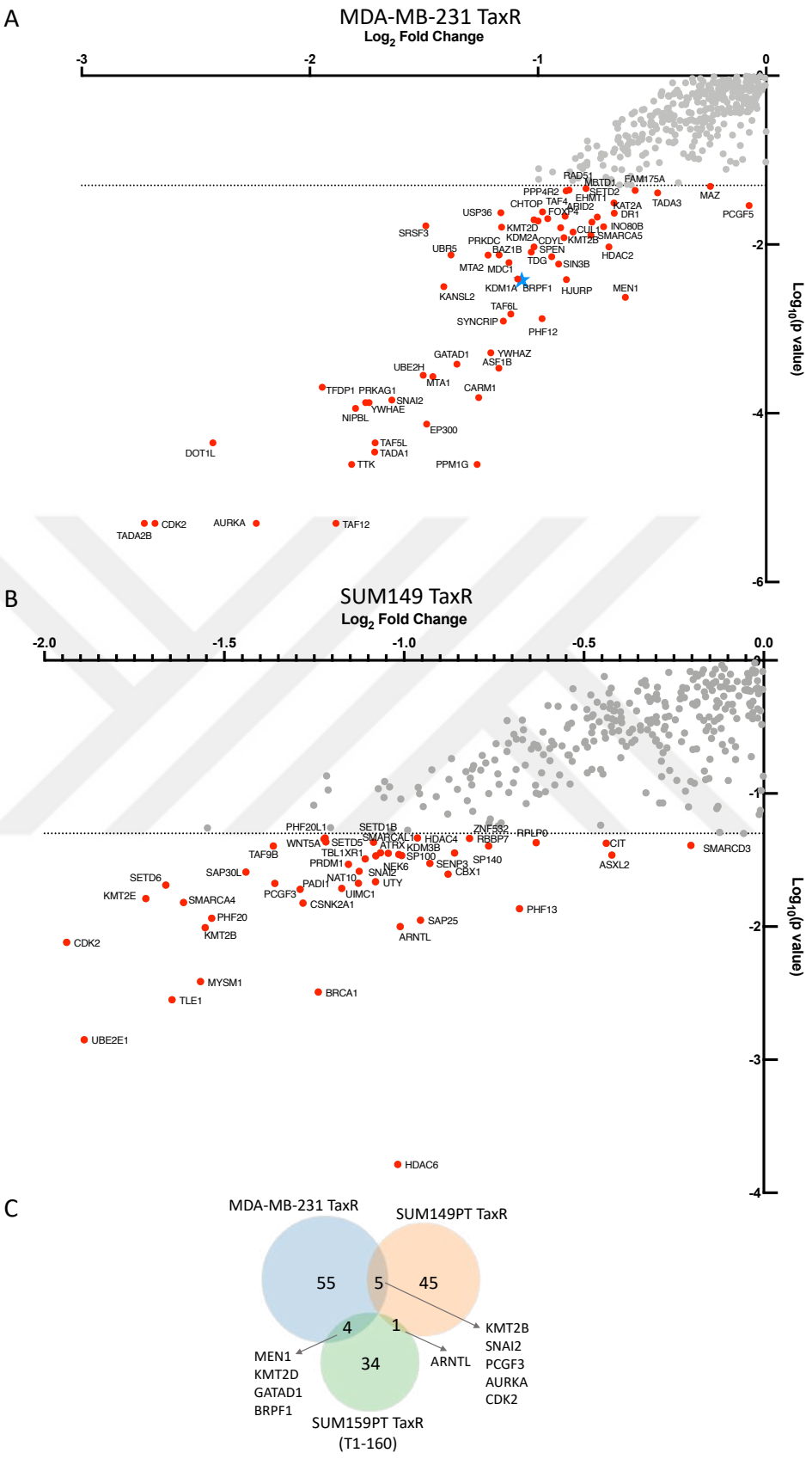

Figure 5.3: EPIKOL screens in other resistant cells. For EPIKOL screens MDA-MB-231 60xIC10 resistant cells **(A)** and SUM149PT 700xIC10 resistant cells **(B)** were used. Each cell type either treated with the chemotherapeutic agent with the dose they were

maintained in or with DMSO as control. After 14-16 population doublings, NGS results of drug treated samples were compared to DMSO treated controls. Volcano plot shows Log_2 Fold changes of depleted genes and corresponding p-values in taxol treated T1-160 samples when compared to DMSO. Venn diagram of the commonly depleted genes ($p<0.05$) in three TNBC cell lines resistant to taxol.

As a positive control, ABCC1 which is a drug transporter was the most significantly depleted gene in SUM159PT doxorubicin resistant cells.

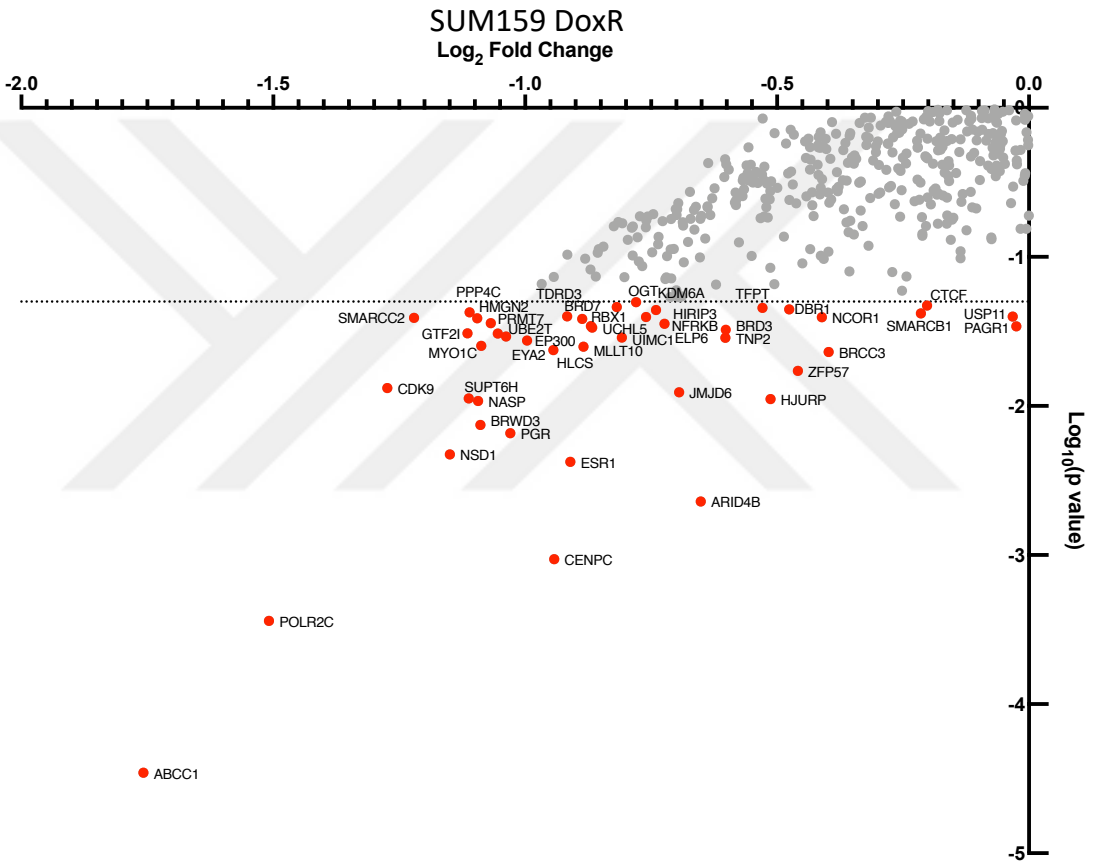

Figure 5.4: EPIKOL screen in SUM159PT 16xIC10 resistant cells.

After selection of candidate genes in SUM159PT T1-160 cells for validation experiments via competition experiment, T1-160-Cas9 stable cells were labeled with either H2B-eGFP or H2B-mCherry viruses. Then mCherry+ cells were transduced with NT1, eGFP+ cells were transduced with sgRNA of interest and cells were mixed in a 1:1 ratio. However, as shown in **Figure 3.31**, eGFP+ cells gained a random proliferative advantage during the experiment and their ratio increased from 50% to 65-70% in -Tax samples. Therefore, T1-160-Cas9 cells were transduced again with new H2B-eGFP and

H2B-mCherry and experiment was repeated with a smaller set of candidate genes (**Figure 5.5**). Although depletion ratios of GFP+ cells were different from the previous experiment, same genes were depleted in both experiments.

		Day 0		Day 5		Day 10		Day 15		Day 25	
		- Tax	+ Tax	- Tax	+ Tax	- Tax	+ Tax	- Tax	+ Tax	- Tax	+ Tax
1st Group	gatad1 g1	50	50	46	47	44	30	41	28	38	28
	gatad1 g2	50	50	45	45	45	26	42	24	41	12
	KMT2A g1	50	50	48	47	49	33	48	29	47	22
	KMT2A g2	50	50	50	46	52	37	49	36	50	28
	men1 g1	50	50	51	52	48	48	48	49	53	50
	men1 g2	50	50	48	50	46	40	44	42	48	39
	brd8 g1	50	50	45	47	45	41	42	36	43	37
	brd8 g2	50	50	44	49	43	42	41	35	42	26
	ppp2ca g1	50	50	44	45	46	41	43	40	44	43
	ppp2ca g2	50	50	44	44	45	35	42	33	42	32
	CHD8 g1	50	50	46	47	44	35	40	27	34	13
	CHD8 g2	50	50	46	47	45	34	41	29	37	13
	brpf1 g4	50	50	45	49	45	44	42	41	36	34
	brpf1 g5	50	50	46	49	46	42	42	38	42	34
	brpf1 g6	50	50	46	50	48	43	45	39	47	35
	jade3 g1	50	50	47	48	49	44	47	43	52	47
	jade3 g2	50	50	47	53	48	54	45	53	48	61
	meaf6 g1	50	50	47	50	52	46	50	45	55	45
	meaf6 g2	50	50	46	48	48	39	46	37	50	34
	ing5 g1	50	50	49	51	54	50	51	47	58	50
	ing5 g2	50	50	48	50	53	50	51	46	57	48
2nd Group	ing3 g1	50	50	41	52	26	30	25	25	18	35
	ing3 g2	50	50	44	48	41	37	37	34	39	28
	rbbp7 g1	50	50	47	47	50	38	45	35	46	35
	rbbp7 g2	50	50	46	47	46	31	42	28	40	25
	prmt1 g1	50	50	42	47	40	35	37	35	40	32
	prmt1 g2	50	50	31	45	11	13	13	13	11	9
	paxip1 g1	50	50	43	47	34	33	31	27	20	18
	paxip1 g2	50	50	46	51	45	49	41	47	40	49
	ABCB1 g2	50	50	49	44	52	18	48	17	54	13
	RPL11 g2	50	50	21	42	15	18	16	12	13	18
	NT1 mix	50	50	48	51	52	51	49	46	53	42

Figure 5.5: Second dual color competition assay with candidate genes from T1-160 EPIKOL screen.

It is known that drug resistance and epithelial-mesenchymal transition (EMT) are closely linked (Shibue & Weinberg, 2017). Therefore, we wondered the EMT profiles of SUM159PT taxol resistant cells and performed western blot analysis with a panel of EMT related antibodies (**Figure 5.6A**). We observed a slightly induced EMT on resistant cells when compared to parental with an increase in Zeb1, Slug, Snail and Fibronectin. Tumor initiation abilities of breast cancer cell lines can be measured via mammosphere formation assay (**Figure 5.6B**). We used Integrin-β4-high (159hi) and low (159lo) cells as positive controls for sphere formation assay (Bierie et al., 2017). Interestingly, taxol resistant cells had decreased ability to form spheres when compared to parental cells. It is known in the literature that extensive EMT activation decreases the tumor initiation capacity (Shibue & Weinberg, 2017). Since SUM159PT cells are mesenchymal in origin, further activation of EMT upon becoming resistant might have killed the ability of tumor initiation.

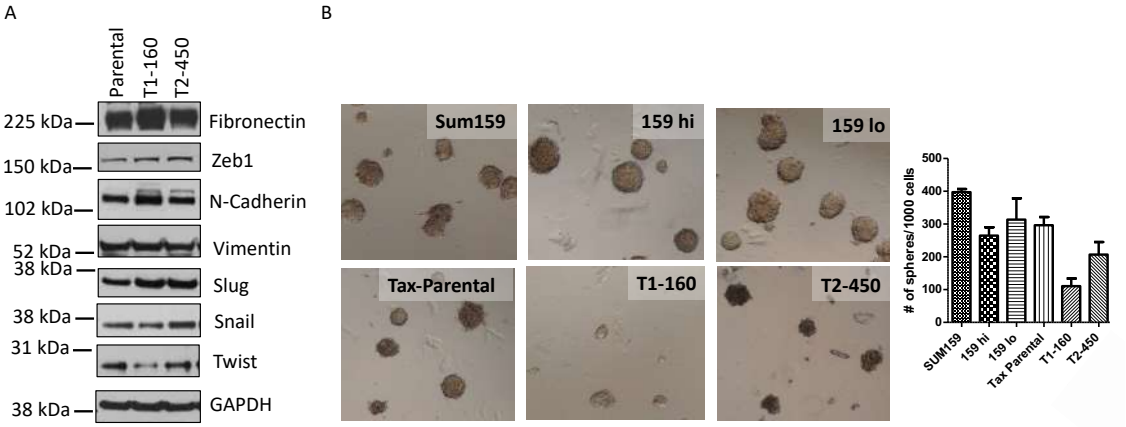

Figure 5.6: EMT profiles of SUM159PT taxol resistant cells. A. Western blot analysis of EMT related proteins. **B.** Mammosphere formation assay on SUM159PT taxol resistant cells.

Chapter 6
FUTURE DIRECTIONS

In this thesis we identified novel epigenetic modifiers, members of SS18L2 and NSL complex, as cell fitness regulators in TNBC. We validated their effect on cell viability with functional assay. Since SS18L2 is an uncharacterized gene with limited information in the literature, it would be valuable to study SS18L2 in greater detail. We plan to perform proximity labeling followed by mass-spectrometry to reveal the interacting partners of SS18L2 in TNBC. While doing this, we also need to perform the same analysis for its close homologs SS18 and SS18L1 to differentiate SS18L2 interactors from others. For this, we plan to use BioID approach.

After finding interacting partners of SS18L2 in TNBC, it would be interesting to see where this complex binds to DNA and what it regulates. Since SS18L2 might be competing with SS18 and SS18L1 to bind to BAF complex as suggested by a novel paper (Alerasool et al., 2022), specific effect of SS18L2 might be due to the changes in DNA binding pattern of BAF complex rather than a differential complex formation by SS18L2. To uncover this, we need to perform ChIP-seq analysis with SS18L2 as well as SS18 and SS18L1. These two experiments would unravel many unknown things about SS18L2s role in TNBC cell fitness.

In the second part of this thesis, we generated chemotherapy resistant TNBC cell lines. However, we only focused on the experiments that we performed on SUM159PT taxol resistant cells. RNAseq and EPIKOL screen results on other resistant cells await for detailed analysis. There were some commonly depleted genes in EPIKOL screens of two different taxol resistant cell lines. Validation of the effect of those genes on overcoming chemotherapy resistance might propose a broader mechanism.

In the third part of this thesis, we identified BRPF1 as a novel regulator of taxol resistance. Although we showed it regulates ribosome biogenesis via RNAseq and ABCB1 expression via ChIP-qPCR, further experiments are needed. We plan to perform ChIPseq analysis to see if BRPF1 really binds to ribosome biogenesis related genes directly or if it is an indirect effect. ChIPseq analysis is also required to understand if BRPF1 binds only to ABCB1 or if it binds to other members of ABC transporter family acting as a master regulator of multidrug resistance.

Lastly, it would be extremely valuable to validate our findings about chemotherapy resistance in matched naïve and chemotherapy resistant TNBC patient samples.

BIBLIOGRAPHY

Alerasool, N., Leng, H., Lin, Z. Y., Gingras, A. C., & Taipale, M. (2022, Feb 3). Identification and functional characterization of transcriptional activators in human cells. *Mol Cell, 82*(3), 677-695 e677. https://doi.org/10.1016/j.molcel.2021.12.008

Alfert, A., Moreno, N., & Kerl, K. (2019, Mar 21). The BAF complex in development and disease. *Epigenetics Chromatin, 12*(1), 19. https://doi.org/10.1186/s13072-019-0264-y

Allis, C. D., & Jenuwein, T. (2016, Aug). The molecular hallmarks of epigenetic control. *Nat Rev Genet, 17*(8), 487-500. https://doi.org/10.1038/nrg.2016.59

Arrigoni, E., Galimberti, S., Petrini, M., Danesi, R., & Di Paolo, A. (2016, Dec). ATP-binding cassette transmembrane transporters and their epigenetic control in cancer: an overview. *Expert Opin Drug Metab Toxicol, 12*(12), 1419-1432. https://doi.org/10.1080/17425255.2016.1215423

Bai, X., Ni, J., Beretov, J., Graham, P., & Li, Y. (2021, Jan 28). Triple-negative breast cancer therapeutic resistance: Where is the Achilles' heel? *Cancer Lett, 497*, 100-111. https://doi.org/10.1016/j.canlet.2020.10.016

Banito, A., Li, X., Laporte, A. N., Roe, J. S., Sanchez-Vega, F., Huang, C. H., Dancsok, A. R., Hatzi, K., Chen, C. C., Tschaharganeh, D. F., Chandwani, R., Tasdemir, N., Jones, K. B., Capecchi, M. R., Vakoc, C. R., Schultz, N., Ladanyi, M., Nielsen, T. O., & Lowe, S. W. (2018, Aug 13). The SS18-SSX Oncoprotein Hijacks KDM2B-PRC1.1 to Drive Synovial Sarcoma. *Cancer Cell, 34*(2), 346-348. https://doi.org/10.1016/j.ccell.2018.07.006

Bhattacharya, A., Fushimi, A., Yamashita, N., Hagiwara, M., Morimoto, Y., Rajabi, H., Long, M. D., Abdulla, M., Ahmad, R., Street, K., Liu, S., Liu, T., & Kufe, D. (2022, Apr 1). MUC1-C Dictates JUN and BAF-Mediated Chromatin Remodeling at Enhancer Signatures in Cancer Stem Cells. *Mol Cancer Res, 20*(4), 556-567. https://doi.org/10.1158/1541-7786.MCR-21-0672

Bianchini, G., De Angelis, C., Licata, L., & Gianni, L. (2022, Feb). Treatment landscape of triple-negative breast cancer - expanded options, evolving needs. *Nat Rev Clin Oncol, 19*(2), 91-113. https://doi.org/10.1038/s41571-021-00565-2

Bierie, B., Pierce, S. E., Kroeger, C., Stover, D. G., Pattabiraman, D. R., Thiru, P., Liu Donaher, J., Reinhardt, F., Chaffer, C. L., Keckesova, Z., & Weinberg, R. A. (2017, Mar 21). Integrin-beta4 identifies cancer stem cell-enriched populations of partially mesenchymal carcinoma cells. *Proc Natl Acad Sci U S A, 114*(12), E2337-E2346. https://doi.org/10.1073/pnas.1618298114

Biswas, S., & Rao, C. M. (2018, Oct 15). Epigenetic tools (The Writers, The Readers and The Erasers) and their implications in cancer therapy. *Eur J Pharmacol, 837*, 8-24. https://doi.org/10.1016/j.ejphar.2018.08.021

Black, J. C., Van Rechem, C., & Whetstine, J. R. (2012, Nov 30). Histone lysine methylation dynamics: establishment, regulation, and biological impact. *Mol Cell, 48*(4), 491-507. https://doi.org/10.1016/j.molcel.2012.11.006

Branham, M. T., Marzese, D. M., Laurito, S. R., Gago, F. E., Orozco, J. I., Tello, O. M., Vargas-Roig, L. M., & Roque, M. (2012, Jul 2). Methylation profile of triple-negative breast carcinomas. *Oncogenesis, 1*, e17. https://doi.org/10.1038/oncsis.2012.17

Breslow, D. K., Hoogendoorn, S., Kopp, A. R., Morgens, D. W., Vu, B. K., Kennedy, M. C., Han, K., Li, A., Hess, G. T., Bassik, M. C., Chen, J. K., & Nachury, M. V. (2018, Mar). A CRISPR-based screen for Hedgehog signaling provides insights into ciliary function and ciliopathies. *Nat Genet, 50*(3), 460-471. https://doi.org/10.1038/s41588-018-0054-7

Britton, K. M., Eyre, R., Harvey, I. J., Stemke-Hale, K., Browell, D., Lennard, T. W. J., & Meeson, A. P. (2012, Oct 1). Breast cancer, side population cells and ABCG2 expression. *Cancer Lett, 323*(1), 97-105. https://doi.org/10.1016/j.canlet.2012.03.041

Burstein, M. D., Tsimelzon, A., Poage, G. M., Covington, K. R., Contreras, A., Fuqua, S. A., Savage, M. I., Osborne, C. K., Hilsenbeck, S. G., Chang, J. C., Mills, G. B., Lau, C. C., & Brown, P. H. (2015, Apr 1). Comprehensive genomic analysis identifies novel subtypes and targets of triple-negative breast cancer. *Clin Cancer Res, 21*(7), 1688-1698. https://doi.org/10.1158/1078-0432.CCR-14-0432

Cai, M., Hu, Z., Liu, J., Gao, J., Tan, M., Zhang, D., Zhu, L., Liu, S., Hou, R., & Lin, B. (2015, Feb). Expression of hMOF in different ovarian tissues and its effects on ovarian cancer prognosis. *Oncol Rep, 33*(2), 685-692. https://doi.org/10.3892/or.2014.3649

Cai, X., Gao, L., Teng, L., Ge, J., Oo, Z. M., Kumar, A. R., Gilliland, D. G., Mason, P. J., Tan, K., & Speck, N. A. (2015, Aug 6). Runx1 Deficiency Decreases Ribosome Biogenesis and Confers Stress Resistance to Hematopoietic Stem and Progenitor Cells. *Cell Stem Cell, 17*(2), 165-177. https://doi.org/10.1016/j.stem.2015.06.002

Cao, L., Zhu, L., Yang, J., Su, J., Ni, J., Du, Y., Liu, D., Wang, Y., Wang, F., Jin, J., & Cai, Y. (2014, Apr). Correlation of low expression of hMOF with

clinicopathological features of colorectal carcinoma, gastric cancer and renal cell carcinoma. *Int J Oncol, 44*(4), 1207-1214. https://doi.org/10.3892/ijo.2014.2266

Chalakur-Ramireddy, N. K. R., & Pakala, S. B. (2018, Feb 28). Combined drug therapeutic strategies for the effective treatment of Triple Negative Breast Cancer. *Biosci Rep, 38*(1). https://doi.org/10.1042/BSR20171357

Chen, J., Bell, J., Lau, B. T., Whittaker, T., Stapleton, D., & Ji, H. P. (2019, May 10). A functional CRISPR/Cas9 screen identifies kinases that modulate FGFR inhibitor response in gastric cancer. *Oncogenesis, 8*(5), 33. https://doi.org/10.1038/s41389-019-0145-z

Chen, S., Sanjana, N. E., Zheng, K., Shalem, O., Lee, K., Shi, X., Scott, D. A., Song, J., Pan, J. Q., Weissleder, R., Lee, H., Zhang, F., & Sharp, P. A. (2015, Mar 12). Genome-wide CRISPR screen in a mouse model of tumor growth and metastasis. *Cell, 160*(6), 1246-1260. https://doi.org/10.1016/j.cell.2015.02.038

Chen, Z., Ye, X., Tang, N., Shen, S., Li, Z., Niu, X., Lu, S., & Xu, L. (2014, Jul). The histone acetylranseferase hMOF acetylates Nrf2 and regulates anti-drug responses in human non-small cell lung cancer. *Br J Pharmacol, 171*(13), 3196-3211. https://doi.org/10.1111/bph.12661

Cheng, C. L., Tsang, F. H., Wei, L., Chen, M., Chin, D. W., Shen, J., Law, C. T., Lee, D., Wong, C. C., Ng, I. O., & Wong, C. M. (2021, Jul 20). Bromodomain-containing protein BRPF1 is a therapeutic target for liver cancer. *Commun Biol, 4*(1), 888. https://doi.org/10.1038/s42003-021-02405-6

Clark, J., Rocques, P. J., Crew, A. J., Gill, S., Shipley, J., Chan, A. M., Gusterson, B. A., & Cooper, C. S. (1994, Aug). Identification of novel genes, SYT and SSX, involved in the t(X;18)(p11.2;q11.2) translocation found in human synovial sarcoma. *Nat Genet, 7*(4), 502-508. https://doi.org/10.1038/ng0894-502

Cui, Z., Xie, M., Wu, Z., & Shi, Y. (2018, Apr 22). Relationship Between Histone Deacetylase 3 (HDAC3) and Breast Cancer. *Med Sci Monit, 24*, 2456-2464. https://doi.org/10.12659/msm.906576

Dawson, M. A., Kouzarides, T., & Huntly, B. J. (2012, Aug 16). Targeting epigenetic readers in cancer. *N Engl J Med, 367*(7), 647-657. https://doi.org/10.1056/NEJMra1112635

de Bruijn, D. R., & Geurts van Kessel, A. (2006). Common origin of the human synovial sarcoma associated SS18 and SS18L1 gene loci. *Cytogenet Genome Res, 112*(3-4), 222-226. https://doi.org/10.1159/000089874

de Bruijn, D. R., Kater-Baats, E., Eleveld, M., Merkx, G., & Geurts Van Kessel, A. (2001). Mapping and characterization of the mouse and human SS18 genes, two human SS18-like genes and a mouse Ss18 pseudogene.

Cytogenet Cell Genet, 92(3-4), 310-319. https://doi.org/10.1159/000056920

De Laurentiis, M., Cianniello, D., Caputo, R., Stanzione, B., Arpino, G., Cinieri, S., Lorusso, V., & De Placido, S. (2010, Nov). Treatment of triple negative breast cancer (TNBC): current options and future perspectives. *Cancer Treat Rev, 36 Suppl 3*, S80-86. https://doi.org/10.1016/S0305-7372(10)70025-6

Dean, M. (2009, Mar). ABC transporters, drug resistance, and cancer stem cells. *J Mammary Gland Biol Neoplasia, 14*(1), 3-9. https://doi.org/10.1007/s10911-009-9109-9

Deblois, G., Tonekaboni, S. A. M., Grillo, G., Martinez, C., Kao, Y. I., Tai, F., Ettayebi, I., Fortier, A. M., Savage, P., Fedor, A. N., Liu, X., Guilhamon, P., Lima-Fernandes, E., Murison, A., Kuasne, H., Ba-Alawi, W., Cescon, D. W., Arrowsmith, C. H., De Carvalho, D. D., Haibe-Kains, B., Locasale, J. W., Park, M., & Lupien, M. (2020, Sep). Epigenetic Switch-Induced Viral Mimicry Evasion in Chemotherapy-Resistant Breast Cancer. *Cancer Discov, 10*(9), 1312-1329. https://doi.org/10.1158/2159-8290.CD-19-1493

DepMap. Retrieved 3rd May from www.depmap.org

Desbats, M. A., Giacomini, I., Prayer-Galetti, T., & Montopoli, M. (2020). Metabolic Plasticity in Chemotherapy Resistance. *Front Oncol, 10*, 281. https://doi.org/10.3389/fonc.2020.00281

Dobin, A., Davis, C. A., Schlesinger, F., Drenkow, J., Zaleski, C., Jha, S., Batut, P., Chaisson, M., & Gingeras, T. R. (2013, Jan 1). STAR: ultrafast universal RNA-seq aligner. *Bioinformatics, 29*(1), 15-21. https://doi.org/10.1093/bioinformatics/bts635

Doench, J. G., Fusi, N., Sullender, M., Hegde, M., Vaimberg, E. W., Donovan, K. F., Smith, I., Tothova, Z., Wilen, C., Orchard, R., Virgin, H. W., Listgarten, J., & Root, D. E. (2016, Feb). Optimized sgRNA design to maximize activity and minimize off-target effects of CRISPR-Cas9. *Nat Biotechnol, 34*(2), 184-191. https://doi.org/10.1038/nbt.3437

Doudna, J. A., & Charpentier, E. (2014, Nov 28). Genome editing. The new frontier of genome engineering with CRISPR-Cas9. *Science, 346*(6213), 1258096. https://doi.org/10.1126/science.1258096

Eliyatkin, N., Yalcin, E., Zengel, B., Aktas, S., & Vardar, E. (2015, Apr). Molecular Classification of Breast Carcinoma: From Traditional, Old-Fashioned Way to A New Age, and A New Way. *J Breast Health, 11*(2), 59-66. https://doi.org/10.5152/tjbh.2015.1669

Esteller, M. (2008, Mar 13). Epigenetics in cancer. *N Engl J Med, 358*(11), 1148-1159. https://doi.org/10.1056/NEJMra072067

Evers, B., Jastrzebski, K., Heijmans, J. P., Grernrum, W., Beijersbergen, R. L., &

Bernards, R. (2016, Jun). CRISPR knockout screening outperforms shRNA and CRISPRi in identifying essential genes. *Nat Biotechnol, 34*(6), 631-633. https://doi.org/10.1038/nbt.3536

Fischer, M., Grossmann, P., Padi, M., & DeCaprio, J. A. (2016, Jul 27). Integration of TP53, DREAM, MMB-FOXM1 and RB-E2F target gene analyses identifies cell cycle gene regulatory networks. *Nucleic Acids Res, 44*(13), 6070-6086. https://doi.org/10.1093/nar/gkw523

Foulkes, W. D., Smith, I. E., & Reis-Filho, J. S. (2010, Nov 11). Triple-negative breast cancer. *N Engl J Med, 363*(20), 1938-1948. https://doi.org/10.1056/NEJMra1001389

Fusella, F., Secli, L., Busso, E., Krepelova, A., Moiso, E., Rocca, S., Conti, L., Annaratone, L., Rubinetto, C., Mello-Grand, M., Singh, V., Chiorino, G., Silengo, L., Altruda, F., Turco, E., Morotti, A., Oliviero, S., Castellano, I., Cavallo, F., Provero, P., Tarone, G., & Brancaccio, M. (2017, Nov 21). The IKK/NF-kappaB signaling pathway requires Morgana to drive breast cancer metastasis. *Nat Commun, 8*(1), 1636. https://doi.org/10.1038/s41467-017-01829-1

Gao, S. P., Sun, H. F., Li, L. D., Fu, W. Y., & Jin, W. (2017). UHRF1 promotes breast cancer progression by suppressing KLF17 expression by hypermethylating its promoter. *Am J Cancer Res, 7*(7), 1554-1565. https://www.ncbi.nlm.nih.gov/pubmed/28744404

Gayatri, S., & Bedford, M. T. (2014, Aug). Readers of histone methylarginine marks. *Biochim Biophys Acta, 1839*(8), 702-710. https://doi.org/10.1016/j.bbagrm.2014.02.015

Genovese, I., Ilari, A., Assaraf, Y. G., Fazi, F., & Colotti, G. (2017, May). Not only P-glycoprotein: Amplification of the ABCB1-containing chromosome region 7q21 confers multidrug resistance upon cancer cells by coordinated overexpression of an assortment of resistance-related proteins. *Drug Resist Updat, 32*, 23-46. https://doi.org/10.1016/j.drup.2017.10.003

Gomez-Miragaya, J., Moran, S., Calleja-Cervantes, M. E., Collado-Sole, A., Pare, L., Gomez, A., Serra, V., Dobrolecki, L. E., Lewis, M. T., Diaz-Lagares, A., Eroles, P., Prat, A., Esteller, M., & Gonzalez-Suarez, E. (2019, Oct). The Altered Transcriptome and DNA Methylation Profiles of Docetaxel Resistance in Breast Cancer PDX Models. *Mol Cancer Res, 17*(10), 2063-2076. https://doi.org/10.1158/1541-7786.MCR-19-0040

Grant, G. D., Kedziora, K. M., Limas, J. C., Cook, J. G., & Purvis, J. E. (2018). Accurate delineation of cell cycle phase transitions in living cells with PIP-FUCCI. *Cell Cycle, 17*(21-22), 2496-2516. https://doi.org/10.1080/15384101.2018.1547001

Grosselin, K., Durand, A., Marsolier, J., Poitou, A., Marangoni, E., Nemati, F., Dahmani, A., Lameiras, S., Reyal, F., Frenoy, O., Pousse, Y., Reichen, M., Woolfe, A., Brenan, C., Griffiths, A. D., Vallot, C., & Gerard, A. (2019, Jun).

High-throughput single-cell ChIP-seq identifies heterogeneity of chromatin states in breast cancer. *Nat Genet, 51*(6), 1060-1066. https://doi.org/10.1038/s41588-019-0424-9

Guestini, F., Ono, K., Miyashita, M., Ishida, T., Ohuchi, N., Nakagawa, S., Hirakawa, H., Tamaki, K., Ohi, Y., Rai, Y., Sagara, Y., Sasano, H., & McNamara, K. M. (2019, Jan). Impact of Topoisomerase IIalpha, PTEN, ABCC1/MRP1, and KI67 on triple-negative breast cancer patients treated with neoadjuvant chemotherapy. *Breast Cancer Res Treat, 173*(2), 275-288. https://doi.org/10.1007/s10549-018-4985-6

Gupta, G. K., Collier, A. L., Lee, D., Hoefer, R. A., Zheleva, V., Siewertsz van Reesema, L. L., Tang-Tan, A. M., Guye, M. L., Chang, D. Z., Winston, J. S., Samli, B., Jansen, R. J., Petricoin, E. F., Goetz, M. P., Bear, H. D., & Tang, A. H. (2020, Aug 24). Perspectives on Triple-Negative Breast Cancer: Current Treatment Strategies, Unmet Needs, and Potential Targets for Future Therapies. *Cancers (Basel), 12*(9). https://doi.org/10.3390/cancers12092392

Halaburkova, A., Cahais, V., Novoloaca, A., Araujo, M., Khoueiry, R., Ghantous, A., & Herceg, Z. (2020, Oct). Pan-cancer multi-omics analysis and orthogonal experimental assessment of epigenetic driver genes. *Genome Res, 30*(10), 1517-1532. https://doi.org/10.1101/gr.268292.120

Hart, T., Chandrashekhar, M., Aregger, M., Steinhart, Z., Brown, K. R., MacLeod, G., Mis, M., Zimmermann, M., Fradet-Turcotte, A., Sun, S., Mero, P., Dirks, P., Sidhu, S., Roth, F. P., Rissland, O. S., Durocher, D., Angers, S., & Moffat, J. (2015, Dec 3). High-Resolution CRISPR Screens Reveal Fitness Genes and Genotype-Specific Cancer Liabilities. *Cell, 163*(6), 1515-1526. https://doi.org/10.1016/j.cell.2015.11.015

Hayakawa, T., & Nakayama, J. (2011). Physiological roles of class I HDAC complex and histone demethylase. *J Biomed Biotechnol, 2011*, 129383. https://doi.org/10.1155/2011/129383

Heigwer, F., Kerr, G., & Boutros, M. (2014, Feb). E-CRISP: fast CRISPR target site identification. *Nat Methods, 11*(2), 122-123. https://doi.org/10.1038/nmeth.2812

Henser-Brownhill, T., Monserrat, J., & Scaffidi, P. (2017). Generation of an arrayed CRISPR-Cas9 library targeting epigenetic regulators: from high-content screens to in vivo assays. *Epigenetics, 12*(12), 1065-1075. https://doi.org/10.1080/15592294.2017.1395121

Holohan, C., Van Schaeybroeck, S., Longley, D. B., & Johnston, P. G. (2013, Oct). Cancer drug resistance: an evolving paradigm. *Nat Rev Cancer, 13*(10), 714-726. https://doi.org/10.1038/nrc3599

Hon, G. C., Hawkins, R. D., & Ren, B. (2009, Oct 15). Predictive chromatin signatures in the mammalian genome. *Hum Mol Genet, 18*(R2), R195-201. https://doi.org/10.1093/hmg/ddp409

Howard, F. M., & Olopade, O. I. (2021, Jan-Feb 01). Epidemiology of Triple-Negative Breast Cancer: A Review. *Cancer J, 27*(1), 8-16. https://doi.org/10.1097/PPO.0000000000000500

Huo, H., Magro, P. G., Pietsch, E. C., Patel, B. B., & Scotto, K. W. (2010, Nov 1). Histone methyltransferase MLL1 regulates MDR1 transcription and chemoresistance. *Cancer Res, 70*(21), 8726-8735. https://doi.org/10.1158/0008-5472.CAN-10-0755

Jiang, F., & Doudna, J. A. (2017, May 22). CRISPR-Cas9 Structures and Mechanisms. *Annu Rev Biophys, 46*, 505-529. https://doi.org/10.1146/annurev-biophys-062215-010822

Jinek, M., Chylinski, K., Fonfara, I., Hauer, M., Doudna, J. A., & Charpentier, E. (2012, Aug 17). A programmable dual-RNA-guided DNA endonuclease in adaptive bacterial immunity. *Science, 337*(6096), 816-821. https://doi.org/10.1126/science.1225829

Jones, V. S., Huang, R. Y., Chen, L. P., Chen, Z. S., Fu, L., & Huang, R. P. (2016, Apr). Cytokines in cancer drug resistance: Cues to new therapeutic strategies. *Biochim Biophys Acta, 1865*(2), 255-265. https://doi.org/10.1016/j.bbcan.2016.03.005

Kadoch, C., & Crabtree, G. R. (2013, Mar 28). Reversible disruption of mSWI/SNF (BAF) complexes by the SS18-SSX oncogenic fusion in synovial sarcoma. *Cell, 153*(1), 71-85. https://doi.org/10.1016/j.cell.2013.02.036

Kadoch, C., Hargreaves, D. C., Hodges, C., Elias, L., Ho, L., Ranish, J., & Crabtree, G. R. (2013, Jun). Proteomic and bioinformatic analysis of mammalian SWI/SNF complexes identifies extensive roles in human malignancy. *Nat Genet, 45*(6), 592-601. https://doi.org/10.1038/ng.2628

Kensler, K. H., Sankar, V. N., Wang, J., Zhang, X., Rubadue, C. A., Baker, G. M., Parker, J. S., Hoadley, K. A., Stancu, A. L., Pyle, M. E., Collins, L. C., Hunter, D. J., Eliassen, A. H., Hankinson, S. E., Tamimi, R. M., & Heng, Y. J. (2019, Apr). PAM50 Molecular Intrinsic Subtypes in the Nurses' Health Study Cohorts. *Cancer Epidemiol Biomarkers Prev, 28*(4), 798-806. https://doi.org/10.1158/1055-9965.EPI-18-0863

Kim, C., Gao, R., Sei, E., Brandt, R., Hartman, J., Hatschek, T., Crosetto, N., Foukakis, T., & Navin, N. E. (2018, May 3). Chemoresistance Evolution in Triple-Negative Breast Cancer Delineated by Single-Cell Sequencing. *Cell, 173*(4), 879-893 e813. https://doi.org/10.1016/j.cell.2018.03.041

Klein, B. J., Lalonde, M. E., Cote, J., Yang, X. J., & Kutateladze, T. G. (2014, Feb). Crosstalk between epigenetic readers regulates the MOZ/MORF HAT complexes. *Epigenetics, 9*(2), 186-193. https://doi.org/10.4161/epi.26792

Kumar, P., & Aggarwal, R. (2016, Feb). An overview of triple-negative breast

cancer. *Arch Gynecol Obstet, 293*(2), 247-269. https://doi.org/10.1007/s00404-015-3859-y

Kuo, M. T. (2007). Roles of multidrug resistance genes in breast cancer chemoresistance. *Adv Exp Med Biol, 608*, 23-30. https://doi.org/10.1007/978-0-387-74039-3_2

Kurata, J. S., & Lin, R. J. (2018, Jul). MicroRNA-focused CRISPR-Cas9 library screen reveals fitness-associated miRNAs. *RNA, 24*(7), 966-981. https://doi.org/10.1261/rna.066282.118

Lefort, S., Joffre, C., Kieffer, Y., Givel, A. M., Bourachot, B., Zago, G., Bieche, I., Dubois, T., Meseure, D., Vincent-Salomon, A., Camonis, J., & Mechta-Grigoriou, F. (2014). Inhibition of autophagy as a new means of improving chemotherapy efficiency in high-LC3B triple-negative breast cancers. *Autophagy, 10*(12), 2122-2142. https://doi.org/10.4161/15548627.2014.981788

Lehmann, B. D., Bauer, J. A., Chen, X., Sanders, M. E., Chakravarthy, A. B., Shyr, Y., & Pietenpol, J. A. (2011, Jul). Identification of human triple-negative breast cancer subtypes and preclinical models for selection of targeted therapies. *J Clin Invest, 121*(7), 2750-2767. https://doi.org/10.1172/JCI45014

Lehmann, B. D., Colaprico, A., Silva, T. C., Chen, J., An, H., Ban, Y., Huang, H., Wang, L., James, J. L., Balko, J. M., Gonzalez-Ericsson, P. I., Sanders, M. E., Zhang, B., Pietenpol, J. A., & Chen, X. S. (2021, Nov 1). Multi-omics analysis identifies therapeutic vulnerabilities in triple-negative breast cancer subtypes. *Nat Commun, 12*(1), 6276. https://doi.org/10.1038/s41467-021-26502-6

Lehmann, B. D., Jovanovic, B., Chen, X., Estrada, M. V., Johnson, K. N., Shyr, Y., Moses, H. L., Sanders, M. E., & Pietenpol, J. A. (2016). Refinement of Triple-Negative Breast Cancer Molecular Subtypes: Implications for Neoadjuvant Chemotherapy Selection. *PLoS One, 11*(6), e0157368. https://doi.org/10.1371/journal.pone.0157368

Li, E., Bestor, T. H., & Jaenisch, R. (1992, Jun 12). Targeted mutation of the DNA methyltransferase gene results in embryonic lethality. *Cell, 69*(6), 915-926. https://doi.org/10.1016/0092-8674(92)90611-f

Li, F., Huang, Q., Luster, T. A., Hu, H., Zhang, H., Ng, W. L., Khodadadi-Jamayran, A., Wang, W., Chen, T., Deng, J., Ranieri, M., Fang, Z., Pyon, V., Dowling, C. M., Bagdatlioglu, E., Almonte, C., Labbe, K., Silver, H., Rabin, A. R., Jani, K., Tsirigos, A., Papagiannakopoulos, T., Hammerman, P. S., Velcheti, V., Freeman, G. J., Qi, J., Miller, G., & Wong, K. K. (2020, Feb). In Vivo Epigenetic CRISPR Screen Identifies Asf1a as an Immunotherapeutic Target in Kras-Mutant Lung Adenocarcinoma. *Cancer Discov, 10*(2), 270-287. https://doi.org/10.1158/2159-8290.CD-19-0780

Li, G., Wang, D., Ma, W., An, K., Liu, Z., Wang, X., Yang, C., Du, F., Han, X., Chang, S., Yu, H., Zhang, Z., Zhao, Z., Zhang, Y., Wang, J., & Sun, Y. (2018, Jun). Transcriptomic and epigenetic analysis of breast cancer stem cells. *Epigenomics, 10*(6), 765-783. https://doi.org/10.2217/epi-2018-0008

Li, W., Xu, H., Xiao, T., Cong, L., Love, M. I., Zhang, F., Irizarry, R. A., Liu, J. S., Brown, M., & Liu, X. S. (2014). MAGeCK enables robust identification of essential genes from genome-scale CRISPR/Cas9 knockout screens. *Genome Biol, 15*(12), 554. https://doi.org/10.1186/s13059-014-0554-4

Lim, S., Janzer, A., Becker, A., Zimmer, A., Schule, R., Buettner, R., & Kirfel, J. (2010, Mar). Lysine-specific demethylase 1 (LSD1) is highly expressed in ER-negative breast cancers and a biomarker predicting aggressive biology. *Carcinogenesis, 31*(3), 512-520. https://doi.org/10.1093/carcin/bgp324

Liu, L. M., Sun, W. Z., Fan, X. Z., Xu, Y. L., Cheng, M. B., & Zhang, Y. (2019, Jun 1). Methylation of C/EBPalpha by PRMT1 Inhibits Its Tumor-Suppressive Function in Breast Cancer. *Cancer Res, 79*(11), 2865-2877. https://doi.org/10.1158/0008-5472.CAN-18-3211

Lo, A., & Qi, L. (2017). Genetic and epigenetic control of gene expression by CRISPR-Cas systems. *F1000Res, 6*. https://doi.org/10.12688/f1000research.11113.1

Love, M. I., Huber, W., & Anders, S. (2014). Moderated estimation of fold change and dispersion for RNA-seq data with DESeq2. *Genome Biol, 15*(12), 550. https://doi.org/10.1186/s13059-014-0550-8

Lyons, T. G. (2019, Nov 21). Targeted Therapies for Triple-Negative Breast Cancer. *Curr Treat Options Oncol, 20*(11), 82. https://doi.org/10.1007/s11864-019-0682-x

Ma, F., Li, H., Wang, H., Shi, X., Fan, Y., Ding, X., Lin, C., Zhan, Q., Qian, H., & Xu, B. (2014, Oct 28). Enriched CD44(+)/CD24(-) population drives the aggressive phenotypes presented in triple-negative breast cancer (TNBC). *Cancer Lett, 353*(2), 153-159. https://doi.org/10.1016/j.canlet.2014.06.022

Ma, H., Tu, L. C., Naseri, A., Huisman, M., Zhang, S., Grunwald, D., & Pederson, T. (2016, Aug 29). CRISPR-Cas9 nuclear dynamics and target recognition in living cells. *J Cell Biol, 214*(5), 529-537. https://doi.org/10.1083/jcb.201604115

Malfatti, M. C., Gerratana, L., Dalla, E., Isola, M., Damante, G., Di Loreto, C., Puglisi, F., & Tell, G. (2019, Jul 15). APE1 and NPM1 protect cancer cells from platinum compounds cytotoxicity and their expression pattern has a prognostic value in TNBC. *J Exp Clin Cancer Res, 38*(1), 309. https://doi.org/10.1186/s13046-019-1294-9

Manguso, R. T., Pope, H. W., Zimmer, M. D., Brown, F. D., Yates, K. B., Miller, B. C., Collins, N. B., Bi, K., LaFleur, M. W., Juneja, V. R., Weiss, S. A., Lo, J.,

Fisher, D. E., Miao, D., Van Allen, E., Root, D. E., Sharpe, A. H., Doench, J. G., & Haining, W. N. (2017, Jul 27). In vivo CRISPR screening identifies Ptpn2 as a cancer immunotherapy target. *Nature, 547*(7664), 413-418. https://doi.org/10.1038/nature23270

Martinez-Useros, J., Martin-Galan, M., Florez-Cespedes, M., & Garcia-Foncillas, J. (2021, Jun 27). Epigenetics of Most Aggressive Solid Tumors: Pathways, Targets and Treatments. *Cancers (Basel), 13*(13). https://doi.org/10.3390/cancers13133209

Masliah-Planchon, J., Bieche, I., Guinebretiere, J. M., Bourdeaut, F., & Delattre, O. (2015). SWI/SNF chromatin remodeling and human malignancies. *Annu Rev Pathol, 10*, 145-171. https://doi.org/10.1146/annurev-pathol-012414-040445

McBride, M. J., Pulice, J. L., Beird, H. C., Ingram, D. R., D'Avino, A. R., Shern, J. F., Charville, G. W., Hornick, J. L., Nakayama, R. T., Garcia-Rivera, E. M., Araujo, D. M., Wang, W. L., Tsai, J. W., Yeagley, M., Wagner, A. J., Futreal, P. A., Khan, J., Lazar, A. J., & Kadoch, C. (2018, Jun 11). The SS18-SSX Fusion Oncoprotein Hijacks BAF Complex Targeting and Function to Drive Synovial Sarcoma. *Cancer Cell, 33*(6), 1128-1141 e1127. https://doi.org/10.1016/j.ccell.2018.05.002

McDermott, M., Eustace, A. J., Busschots, S., Breen, L., Crown, J., Clynes, M., O'Donovan, N., & Stordal, B. (2014). In vitro Development of Chemotherapy and Targeted Therapy Drug-Resistant Cancer Cell Lines: A Practical Guide with Case Studies. *Front Oncol, 4*, 40. https://doi.org/10.3389/fonc.2014.00040

Medvedeva, Y. A., Lennartsson, A., Ehsani, R., Kulakovskiy, I. V., Vorontsov, I. E., Panahandeh, P., Khimulya, G., Kasukawa, T., Consortium, F., & Drablos, F. (2015). EpiFactors: a comprehensive database of human epigenetic factors and complexes. *Database (Oxford), 2015*, bav067. https://doi.org/10.1093/database/bav067

Mehanna, J., Haddad, F. G., Eid, R., Lambertini, M., & Kourie, H. R. (2019). Triple-negative breast cancer: current perspective on the evolving therapeutic landscape. *Int J Womens Health, 11*, 431-437. https://doi.org/10.2147/IJWH.S178349

Moore, N., Houghton, J., & Lyle, S. (2012, Jul 1). Slow-cycling therapy-resistant cancer cells. *Stem Cells Dev, 21*(10), 1822-1830. https://doi.org/10.1089/scd.2011.0477

Musselman, C. A., Khorasanizadeh, S., & Kutateladze, T. G. (2014, Aug). Towards understanding methyllysine readout. *Biochim Biophys Acta, 1839*(8), 686-693. https://doi.org/10.1016/j.bbagrm.2014.04.001

Musselman, C. A., Lalonde, M. E., Cote, J., & Kutateladze, T. G. (2012, Dec). Perceiving the epigenetic landscape through histone readers. *Nat Struct Mol Biol, 19*(12), 1218-1227. https://doi.org/10.1038/nsmb.2436

Nabet, B., Roberts, J. M., Buckley, D. L., Paulk, J., Dastjerdi, S., Yang, A., Leggett, A. L., Erb, M. A., Lawlor, M. A., Souza, A., Scott, T. G., Vittori, S., Perry, J. A., Qi, J., Winter, G. E., Wong, K. K., Gray, N. S., & Bradner, J. E. (2018, May). The dTAG system for immediate and target-specific protein degradation. *Nat Chem Biol, 14*(5), 431-441. https://doi.org/10.1038/s41589-018-0021-8

Nedeljkovic, M., & Damjanovic, A. (2019, Aug 22). Mechanisms of Chemotherapy Resistance in Triple-Negative Breast Cancer-How We Can Rise to the Challenge. *Cells, 8*(9). https://doi.org/10.3390/cells8090957

Nemcova-Furstova, V., Kopperova, D., Balusikova, K., Ehrlichova, M., Brynychova, V., Vaclavikova, R., Daniel, P., Soucek, P., & Kovar, J. (2016, Nov 1). Characterization of acquired paclitaxel resistance of breast cancer cells and involvement of ABC transporters. *Toxicol Appl Pharmacol, 310*, 215-228. https://doi.org/10.1016/j.taap.2016.09.020

O'Connor, R., O'Leary, M., Ballot, J., Collins, C. D., Kinsella, P., Mager, D. E., Arnold, R. D., O'Driscoll, L., Larkin, A., Kennedy, S., Fennelly, D., Clynes, M., & Crown, J. (2007, Jan). A phase I clinical and pharmacokinetic study of the multi-drug resistance protein-1 (MRP-1) inhibitor sulindac, in combination with epirubicin in patients with advanced cancer. *Cancer Chemother Pharmacol, 59*(1), 79-87. https://doi.org/10.1007/s00280-006-0240-7

Park, S. Y., Lee, H. E., Li, H., Shipitsin, M., Gelman, R., & Polyak, K. (2010, Feb 1). Heterogeneity for stem cell-related markers according to tumor subtype and histologic stage in breast cancer. *Clin Cancer Res, 16*(3), 876-887. https://doi.org/10.1158/1078-0432.CCR-09-1532

Patro, R., Duggal, G., Love, M. I., Irizarry, R. A., & Kingsford, C. (2017, Apr). Salmon provides fast and bias-aware quantification of transcript expression. *Nat Methods, 14*(4), 417-419. https://doi.org/10.1038/nmeth.4197

Perez-Salvia, M., & Esteller, M. (2017, May 4). Bromodomain inhibitors and cancer therapy: From structures to applications. *Epigenetics, 12*(5), 323-339. https://doi.org/10.1080/15592294.2016.1265710

Perou, C. M., Sorlie, T., Eisen, M. B., van de Rijn, M., Jeffrey, S. S., Rees, C. A., Pollack, J. R., Ross, D. T., Johnsen, H., Akslen, L. A., Fluge, O., Pergamenschikov, A., Williams, C., Zhu, S. X., Lonning, P. E., Borresen-Dale, A. L., Brown, P. O., & Botstein, D. (2000, Aug 17). Molecular portraits of human breast tumours. *Nature, 406*(6797), 747-752. https://doi.org/10.1038/35021093

Pfister, S., Rea, S., Taipale, M., Mendrzyk, F., Straub, B., Ittrich, C., Thuerigen, O., Sinn, H. P., Akhtar, A., & Lichter, P. (2008, Mar 15). The histone acetyltransferase hMOF is frequently downregulated in primary breast carcinoma and medulloblastoma and constitutes a biomarker for clinical

outcome in medulloblastoma. *Int J Cancer, 122*(6), 1207-1213. https://doi.org/10.1002/ijc.23283

Poggio, F., Bruzzone, M., Ceppi, M., Ponde, N. F., La Valle, G., Del Mastro, L., de Azambuja, E., & Lambertini, M. (2018, Jul 1). Platinum-based neoadjuvant chemotherapy in triple-negative breast cancer: a systematic review and meta-analysis. *Ann Oncol, 29*(7), 1497-1508. https://doi.org/10.1093/annonc/mdy127

Pogoda, K., Niwinska, A., Murawska, M., & Pienkowski, T. (2013, Mar). Analysis of pattern, time and risk factors influencing recurrence in triple-negative breast cancer patients. *Med Oncol, 30*(1), 388. https://doi.org/10.1007/s12032-012-0388-4

Radzisheuskaya, A., Shliaha, P. V., Grinev, V. V., Shlyueva, D., Damhofer, H., Koche, R., Gorshkov, V., Kovalchuk, S., Zhan, Y., Rodriguez, K. L., Johnstone, A. L., Keogh, M. C., Hendrickson, R. C., Jensen, O. N., & Helin, K. (2021, Apr 15). Complex-dependent histone acetyltransferase activity of KAT8 determines its role in transcription and cellular homeostasis. *Mol Cell, 81*(8), 1749-1765 e1748. https://doi.org/10.1016/j.molcel.2021.02.012

Ruprecht, B., Zaal, E. A., Zecha, J., Wu, W., Berkers, C. R., Kuster, B., & Lemeer, S. (2017, Apr 15). Lapatinib Resistance in Breast Cancer Cells Is Accompanied by Phosphorylation-Mediated Reprogramming of Glycolysis. *Cancer Res, 77*(8), 1842-1853. https://doi.org/10.1158/0008-5472.CAN-16-2976

Sadasivam, S., & DeCaprio, J. A. (2013, Aug). The DREAM complex: master coordinator of cell cycle-dependent gene expression. *Nat Rev Cancer, 13*(8), 585-595. https://doi.org/10.1038/nrc3556

Sanjana, N. E., Shalem, O., & Zhang, F. (2014, Aug). Improved vectors and genome-wide libraries for CRISPR screening. *Nat Methods, 11*(8), 783-784. https://doi.org/10.1038/nmeth.3047

Sanson, K. R., Hanna, R. E., Hegde, M., Donovan, K. F., Strand, C., Sullender, M. E., Vaimberg, E. W., Goodale, A., Root, D. E., Piccioni, F., & Doench, J. G. (2018, Dec 21). Optimized libraries for CRISPR-Cas9 genetic screens with multiple modalities. *Nat Commun, 9*(1), 5416. https://doi.org/10.1038/s41467-018-07901-8

Sarmiento-Salinas, F. L., Delgado-Magallon, A., Montes-Alvarado, J. B., Ramirez-Ramirez, D., Flores-Alonso, J. C., Cortes-Hernandez, P., Reyes-Leyva, J., Herrera-Camacho, I., Anaya-Ruiz, M., Pelayo, R., Millan-Perez-Pena, L., & Maycotte, P. (2019). Breast Cancer Subtypes Present a Differential Production of Reactive Oxygen Species (ROS) and Susceptibility to Antioxidant Treatment. *Front Oncol, 9*, 480. https://doi.org/10.3389/fonc.2019.00480

Shahbazian, M. D., & Grunstein, M. (2007). Functions of site-specific histone

acetylation and deacetylation. *Annu Rev Biochem, 76*, 75-100. https://doi.org/10.1146/annurev.biochem.76.052705.162114

Shalem, O., Sanjana, N. E., Hartenian, E., Shi, X., Scott, D. A., Mikkelson, T., Heckl, D., Ebert, B. L., Root, D. E., Doench, J. G., & Zhang, F. (2014, Jan 3). Genome-scale CRISPR-Cas9 knockout screening in human cells. *Science, 343*(6166), 84-87. https://doi.org/10.1126/science.1247005

Sheikh, B. N., Guhathakurta, S., & Akhtar, A. (2019, Jul). The non-specific lethal (NSL) complex at the crossroads of transcriptional control and cellular homeostasis. *EMBO Rep, 20*(7), e47630. https://doi.org/10.15252/embr.201847630

Shibata, M., & Hoque, M. O. (2019, May 27). Targeting Cancer Stem Cells: A Strategy for Effective Eradication of Cancer. *Cancers (Basel), 11*(5). https://doi.org/10.3390/cancers11050732

Shibue, T., & Weinberg, R. A. (2017, Oct). EMT, CSCs, and drug resistance: the mechanistic link and clinical implications. *Nat Rev Clin Oncol, 14*(10), 611-629. https://doi.org/10.1038/nrclinonc.2017.44

Shu, S., Lin, C. Y., He, H. H., Witwicki, R. M., Tabassum, D. P., Roberts, J. M., Janiszewska, M., Huh, S. J., Liang, Y., Ryan, J., Doherty, E., Mohammed, H., Guo, H., Stover, D. G., Ekram, M. B., Brown, J., D'Santos, C., Krop, I. E., Dillon, D., McKeown, M., Ott, C., Qi, J., Ni, M., Rao, P. K., Duarte, M., Wu, S. Y., Chiang, C. M., Anders, L., Young, R. A., Winer, E., Letai, A., Barry, W. T., Carroll, J. S., Long, H., Brown, M., Liu, X. S., Meyer, C. A., Bradner, J. E., & Polyak, K. (2016, Jan 21). Response and resistance to BET bromodomain inhibitors in triple-negative breast cancer. *Nature, 529*(7586), 413-417. https://doi.org/10.1038/nature16508

Siegel, R. L., Miller, K. D., Fuchs, H. E., & Jemal, A. (2021, Jan). Cancer Statistics, 2021. *CA Cancer J Clin, 71*(1), 7-33. https://doi.org/10.3322/caac.21654

Stemmer, M., Thumberger, T., Del Sol Keyer, M., Wittbrodt, J., & Mateo, J. L. (2015). CCTop: An Intuitive, Flexible and Reliable CRISPR/Cas9 Target Prediction Tool. *PLoS One, 10*(4), e0124633. https://doi.org/10.1371/journal.pone.0124633

Stirzaker, C., Zotenko, E., Song, J. Z., Qu, W., Nair, S. S., Locke, W. J., Stone, A., Armstong, N. J., Robinson, M. D., Dobrovic, A., Avery-Kiejda, K. A., Peters, K. M., French, J. D., Stein, S., Korbie, D. J., Trau, M., Forbes, J. F., Scott, R. J., Brown, M. A., Francis, G. D., & Clark, S. J. (2015, Feb 2). Methylome sequencing in triple-negative breast cancer reveals distinct methylation clusters with prognostic value. *Nat Commun, 6*, 5899. https://doi.org/10.1038/ncomms6899

Strahl, B. D., & Allis, C. D. (2000, Jan 6). The language of covalent histone modifications. *Nature, 403*(6765), 41-45. https://doi.org/10.1038/47412

Su, D., Feng, X., Colic, M., Wang, Y., Zhang, C., Wang, C., Tang, M., Hart, T., &

Chen, J. (2020, Mar). CRISPR/CAS9-based DNA damage response screens reveal gene-drug interactions. *DNA Repair (Amst), 87*, 102803. https://doi.org/10.1016/j.dnarep.2020.102803

Su, J., Wang, F., Cai, Y., & Jin, J. (2016, Jan 14). The Functional Analysis of Histone Acetyltransferase MOF in Tumorigenesis. *Int J Mol Sci, 17*(1). https://doi.org/10.3390/ijms17010099

Subramanian, A., Kuehn, H., Gould, J., Tamayo, P., & Mesirov, J. P. (2007, Dec 1). GSEA-P: a desktop application for Gene Set Enrichment Analysis. *Bioinformatics, 23*(23), 3251-3253. https://doi.org/10.1093/bioinformatics/btm369

Szlachta, K., Kuscu, C., Tufan, T., Adair, S. J., Shang, S., Michaels, A. D., Mullen, M. G., Fischer, N. L., Yang, J., Liu, L., Trivedi, P., Stelow, E. B., Stukenberg, P. T., Parsons, J. T., Bauer, T. W., & Adli, M. (2018, Oct 15). CRISPR knockout screening identifies combinatorial drug targets in pancreatic cancer and models cellular drug response. *Nat Commun, 9*(1), 4275. https://doi.org/10.1038/s41467-018-06676-2

Tang, F., Barbacioru, C., Wang, Y., Nordman, E., Lee, C., Xu, N., Wang, X., Bodeau, J., Tuch, B. B., Siddiqui, A., Lao, K., & Surani, M. A. (2009, May). mRNA-Seq whole-transcriptome analysis of a single cell. *Nat Methods, 6*(5), 377-382. https://doi.org/10.1038/nmeth.1315

Tarumoto, Y., Lu, B., Somerville, T. D. D., Huang, Y. H., Milazzo, J. P., Wu, X. S., Klingbeil, O., El Demerdash, O., Shi, J., & Vakoc, C. R. (2018, Mar 15). LKB1, Salt-Inducible Kinases, and MEF2C Are Linked Dependencies in Acute Myeloid Leukemia. *Mol Cell, 69*(6), 1017-1027 e1016. https://doi.org/10.1016/j.molcel.2018.02.011

Tegze, B., Szallasi, Z., Haltrich, I., Penzvalto, Z., Toth, Z., Liko, I., & Gyorffy, B. (2012). Parallel evolution under chemotherapy pressure in 29 breast cancer cell lines results in dissimilar mechanisms of resistance. *PLoS One, 7*(2), e30804. https://doi.org/10.1371/journal.pone.0030804

Temian, D. C., Pop, L. A., Irimie, A. I., & Berindan-Neagoe, I. (2018, Sep). The Epigenetics of Triple-Negative and Basal-Like Breast Cancer: Current Knowledge. *J Breast Cancer, 21*(3), 233-243. https://doi.org/10.4048/jbc.2018.21.e41

Thomas, T., & Voss, A. K. (2007, Mar 15). The diverse biological roles of MYST histone acetyltransferase family proteins. *Cell Cycle, 6*(6), 696-704. https://doi.org/10.4161/cc.6.6.4013

Thorn, C. F., Oshiro, C., Marsh, S., Hernandez-Boussard, T., McLeod, H., Klein, T. E., & Altman, R. B. (2011, Jul). Doxorubicin pathways: pharmacodynamics and adverse effects. *Pharmacogenet Genomics, 21*(7), 440-446. https://doi.org/10.1097/FPC.0b013e32833ffb56

Tong, J. T. W., Harris, P. W. R., Brimble, M. A., & Kavianinia, I. (2021, Sep 27).

An Insight into FDA Approved Antibody-Drug Conjugates for Cancer Therapy. *Molecules, 26*(19). https://doi.org/10.3390/molecules26195847

Ullah, M., Pelletier, N., Xiao, L., Zhao, S. P., Wang, K., Degerny, C., Tahmasebi, S., Cayrou, C., Doyon, Y., Goh, S. L., Champagne, N., Cote, J., & Yang, X. J. (2008, Nov). Molecular architecture of quartet MOZ/MORF histone acetyltransferase complexes. *Mol Cell Biol, 28*(22), 6828-6843. https://doi.org/10.1128/MCB.01297-08

Vagia, E., Mahalingam, D., & Cristofanilli, M. (2020, Apr 8). The Landscape of Targeted Therapies in TNBC. *Cancers (Basel), 12*(4). https://doi.org/10.3390/cancers12040916

Vetting, M. W., LP, S. d. C., Yu, M., Hegde, S. S., Magnet, S., Roderick, S. L., & Blanchard, J. S. (2005, Jan 1). Structure and functions of the GNAT superfamily of acetyltransferases. *Arch Biochem Biophys, 433*(1), 212-226. https://doi.org/10.1016/j.abb.2004.09.003

Vinet, M., Suresh, S., Maire, V., Monchecourt, C., Nemati, F., Lesage, L., Pierre, F., Ye, M., Lescure, A., Brisson, A., Meseure, D., Nicolas, A., Rigaill, G., Marangoni, E., Del Nery, E., Roman-Roman, S., & Dubois, T. (2019, May). Protein arginine methyltransferase 5: A novel therapeutic target for triple-negative breast cancers. *Cancer Med, 8*(5), 2414-2428. https://doi.org/10.1002/cam4.2114

Vyas, D., Laput, G., & Vyas, A. K. (2014). Chemotherapy-enhanced inflammation may lead to the failure of therapy and metastasis. *Onco Targets Ther, 7*, 1015-1023. https://doi.org/10.2147/OTT.S60114

Waks, A. G., & Winer, E. P. (2019, Jan 22). Breast Cancer Treatment: A Review. *JAMA, 321*(3), 288-300. https://doi.org/10.1001/jama.2018.19323

Wang, T., Birsoy, K., Hughes, N. W., Krupczak, K. M., Post, Y., Wei, J. J., Lander, E. S., & Sabatini, D. M. (2015, Nov 27). Identification and characterization of essential genes in the human genome. *Science, 350*(6264), 1096-1101. https://doi.org/10.1126/science.aac7041

Wang, T., Wei, J. J., Sabatini, D. M., & Lander, E. S. (2014, Jan 3). Genetic screens in human cells using the CRISPR-Cas9 system. *Science, 343*(6166), 80-84. https://doi.org/10.1126/science.1246981

Wu, Q., Sharma, S., Cui, H., LeBlanc, S. E., Zhang, H., Muthuswami, R., Nickerson, J. A., & Imbalzano, A. N. (2016, May 10). Targeting the chromatin remodeling enzyme BRG1 increases the efficacy of chemotherapy drugs in breast cancer cells. *Oncotarget, 7*(19), 27158-27175. https://doi.org/10.18632/oncotarget.8384

Wu, Q., Yang, Z., Nie, Y., Shi, Y., & Fan, D. (2014, Jun 1). Multi-drug resistance in cancer chemotherapeutics: mechanisms and lab approaches. *Cancer Lett, 347*(2), 159-166. https://doi.org/10.1016/j.canlet.2014.03.013

Yabuki, N., Sakata, K., Yamasaki, T., Terashima, H., Mio, T., Miyazaki, Y., Fujii, T., & Kitada, K. (2007, Feb). Gene amplification and expression in lung cancer cells with acquired paclitaxel resistance. *Cancer Genet Cytogenet, 173*(1), 1-9. https://doi.org/10.1016/j.cancergencyto.2006.07.020

Yan, K., Rousseau, J., Machol, K., Cross, L. A., Agre, K. E., Gibson, C. F., Goverde, A., Engleman, K. L., Verdin, H., De Baere, E., Potocki, L., Zhou, D., Cadieux-Dion, M., Bellus, G. A., Wagner, M. D., Hale, R. J., Esber, N., Riley, A. F., Solomon, B. D., Cho, M. T., McWalter, K., Eyal, R., Hainlen, M. K., Mendelsohn, B. A., Porter, H. M., Lanpher, B. C., Lewis, A. M., Savatt, J., Thiffault, I., Callewaert, B., Campeau, P. M., & Yang, X. J. (2020, Jan). Deficient histone H3 propionylation by BRPF1-KAT6 complexes in neurodevelopmental disorders and cancer. *Sci Adv, 6*(4), eaax0021. https://doi.org/10.1126/sciadv.aax0021

Yang, X. J. (2015, Aug). MOZ and MORF acetyltransferases: Molecular interaction, animal development and human disease. *Biochim Biophys Acta, 1853*(8), 1818-1826. https://doi.org/10.1016/j.bbamcr.2015.04.014

Yang, X. J., & Ullah, M. (2007, Aug 13). MOZ and MORF, two large MYSTic HATs in normal and cancer stem cells. *Oncogene, 26*(37), 5408-5419. https://doi.org/10.1038/sj.onc.1210609

Yedier-Bayram, O., Gokbayrak, B., Kayabolen, A., Aksu, A. C., Cavga, A. D., Cingoz, A., Kala, E. Y., Karabiyik, G., Gunsay, R., Esin, B., Morova, T., Uyulur, F., Syed, H., Philpott, M., Cribbs, A. P., Kung, S. H. Y., Lack, N. A., Onder, T. T., & Bagci-Onder, T. (2022, Aug 16). EPIKOL, a chromatin-focused CRISPR/Cas9-based screening platform, to identify cancer-specific epigenetic vulnerabilities. *Cell Death Dis, 13*(8), 710. https://doi.org/10.1038/s41419-022-05146-4

Yersal, O., & Barutca, S. (2014, Aug 10). Biological subtypes of breast cancer: Prognostic and therapeutic implications. *World J Clin Oncol, 5*(3), 412-424. https://doi.org/10.5306/wjco.v5.i3.412

Yin, L., Duan, J. J., Bian, X. W., & Yu, S. C. (2020, Jun 9). Triple-negative breast cancer molecular subtyping and treatment progress. *Breast Cancer Res, 22*(1), 61. https://doi.org/10.1186/s13058-020-01296-5

You, L., Yan, K., Zou, J., Zhao, H., Bertos, N. R., Park, M., Wang, E., & Yang, X. J. (2015, May 1). The chromatin regulator Brpf1 regulates embryo development and cell proliferation. *J Biol Chem, 290*(18), 11349-11364. https://doi.org/10.1074/jbc.M115.643189

You, L., Zou, J., Zhao, H., Bertos, N. R., Park, M., Wang, E., & Yang, X. J. (2015, Mar 13). Deficiency of the chromatin regulator BRPF1 causes abnormal brain development. *J Biol Chem, 290*(11), 7114-7129. https://doi.org/10.1074/jbc.M114.635250

Yu, K. D., Ye, F. G., He, M., Fan, L., Ma, D., Mo, M., Wu, J., Liu, G. Y., Di, G. H., Zeng, X. H., He, P. Q., Wu, K. J., Hou, Y. F., Wang, J., Wang, C., Zhuang,

Z. G., Song, C. G., Lin, X. Y., Toss, A., Ricci, F., Shen, Z. Z., & Shao, Z. M. (2020, Sep 1). Effect of Adjuvant Paclitaxel and Carboplatin on Survival in Women With Triple-Negative Breast Cancer: A Phase 3 Randomized Clinical Trial. *JAMA Oncol, 6*(9), 1390-1396. https://doi.org/10.1001/jamaoncol.2020.2965

Zhang, J., Liu, H., Pan, H., Yang, Y., Huang, G., Yang, Y., Zhou, W. P., & Pan, Z. Y. (2014, Sep 26). The histone acetyltransferase hMOF suppresses hepatocellular carcinoma growth. *Biochem Biophys Res Commun, 452*(3), 575-580. https://doi.org/10.1016/j.bbrc.2014.08.122

Zhang, Y., Dai, J., McNamara, K. M., Bai, B., Shi, M., Chan, M. S., Liu, M., Sasano, H., Wang, X., Li, X., Liu, L., Ma, Y., Cao, S., Xing, Y., Zhao, B., Song, Y., & Wang, L. (2015, Oct 15). Prognostic significance of proline, glutamic acid, leucine rich protein 1 (PELP1) in triple-negative breast cancer: a retrospective study on 129 cases. *BMC Cancer, 15*, 699. https://doi.org/10.1186/s12885-015-1694-y

Zhou, X., Li, R., Chen, R., & Liu, J. (2020, Mar 4). Altered Mitochondrial Dynamics, Biogenesis, and Functions in the Paclitaxel-Resistant Lung Adenocarcinoma Cell Line A549/Taxol. *Med Sci Monit, 26*, e918216. https://doi.org/10.12659/MSM.918216

Zilionis, R., Nainys, J., Veres, A., Savova, V., Zemmour, D., Klein, A. M., & Mazutis, L. (2017, Jan). Single-cell barcoding and sequencing using droplet microfluidics. *Nat Protoc, 12*(1), 44-73. https://doi.org/10.1038/nprot.2016.154

Zolota, V., Tzelepi, V., Piperigkou, Z., Kourea, H., Papakonstantinou, E., Argentou Mu, I., & Karamanos, N. K. (2021, Feb 9). Epigenetic Alterations in Triple-Negative Breast Cancer-The Critical Role of Extracellular Matrix. *Cancers (Basel), 13*(4). https://doi.org/10.3390/cancers13040713